REPUBLIC OF TURKEY
YILDIZ TECHNICAL UNIVERSITY
GRADUATE SCHOOL OF NATURAL AND APPLIED SCIENCES

REDUCTION OF GRAPHENE OXIDE BY NATURAL PRODUCTS AND PRODUCTION OF REDUCED GRAPHENE OXIDE-HYDROXYAPATITE COMPOSITES

ELİF ÖZTÜRK

MSc. THESIS
DEPARTMENT OF CHEMICAL ENGINEERING
PROGRAM OF CHEMICAL ENGINEERING

ADVISER
PROF. DR. BELMA ÖZBEK

İSTANBUL, 2015

REPUBLIC OF TURKEY

YILDIZ TECHNICAL UNIVERSITY

GRADUATE SCHOOL OF NATURAL AND APPLIED SCIENCES

REDUCTION OF GRAPHENE OXIDE BY NATURAL PRODUCTS AND PRODUCTION OF REDUCED GRAPHENE OXIDE-HYDROXYAPATITE COMPOSITES

A thesis submitted by Elif ÖZTÜRK in partial fulfillment of the requirements for the degree of **MASTER OF SCIENCE** is approved by the committee on 29.07.2015 in Department of Chemical Engineering, Program of Chemical Engineering.

Thesis Adviser

Prof. Dr. Belma ÖZBEK

Yıldız Technical University

Approved By the Examining Committee

Prof. Dr. Belma ÖZBEK

Yıldız Technical University _____

Prof. Dr. Dilek KAZAN

Marmara University _____

Assist. Prof. Dr. Elçin DEMİRHAN YILMAZ

Yıldız Technical University _____

This research has been supported by Yıldız Technical University Scientific Research Project Coordination Department. Project Number: 2015-07-01-YL01.

ACKNOWLEDGEMENTS

The writing of this dissertation has been one of the most significant challenges in my academic career. I would never have been completed this work without the guidance of my supervisor, help from friends and support from my family.

First and foremost, I would like to express my sincerest gratitude to my supervisor, Prof. Dr. Belma ÖZBEK who has offered her unreserved help, insight and continuous guidance. She provided me with every bit of her assistance, knowledge and expertise when I needed. In the meantime, she gave me the freedom to study on whatever I wanted, at the same time continuing to contribute valuable feedback and advice. Her patience, endless knowledge and kindness have always encouraged me to carry out this study.

I would like to thank Assist. Prof. Dr. Elçin DEMİRHAN YILMAZ, Prof. Dr. Cengiz KAYA and Prof. Dr. Hikmet YÜKSELİCİ for their contributions to my study. I gratefully acknowledge the members of my Master committee for their time and valuable feedback on a preliminary version of this thesis.

Many thanks to my friends and colleagues, Research Assistant Sinem ŞİMŞEK, Research Assistant Meral YILDIRIM and Research Assistant Şule ÜNAL who inspired my all effort despite the enormous work pressures we were facing together. Especially Sinem always discussed me with new ideas and expanded my horizon.

I would like to thank the Department of Science and Technology Application and Research Center at the Yıldız Technical University especially Ali Can ZAMAN, Yusuf KAHRAMAN and Özlem YAĞCI for their substantial efforts in the study.

I would like to thank my best friends Esma PİŞKİN and Semra TAŞ for all the great times that we have shared for over twelve years. We always walk in our way arm in arm and shoulder to shoulder in either bad or good day.

I would also like to thank my mother and three brothers. They were always supporting and motivating me. Without them, this thesis would never have been written. I dedicate this thesis to the memory of my father Sait ÖZTÜRK whose role in my life was, remains and immense. This is the last word acknowledgement I have saved for my dear boyfriend Erkut ER who has been with me all these years and has made them the best years of my life.

July, 2015

Elif ÖZTÜRK

TABLE OF CONTENTS

LIST OF SYMBOLS

n	Mole
P	Pressure
T	Temperature
$\propto$	The lattice vacancy in the OH position

LIST OF ABBREVIATIONS

AFM	Atomic Force Microscope
AM	Additive Manufacturing
ARGO	Reduced Graphene Oxide by *Achillea nobilis* extract
ATR	Attenuated Total Reflection
CNT	Carbon Nanotube
CT	Charge Transfer
CVD	Chemical Vapor Decomposition
DLS	Dynamic Light Scattering
DMF	N,N-dimethlyformamide
ECL	Electrochemiluminescence
ECM	Extracellular Matrix
EDA	Ethylenediamine
EDAX	Energy-dispersive X-ray Spectroscopy
EG	Ethylene Glycol
EPD	Electrophoretic Deposition
FLG	Few-Layer Graphene
FTIR	Fourier-Transform Infrared Spectrometer
F-CNT	Functionalized Carbon Nanotube
GFN	Graphene Family Nanomaterial
GND	Graphene Dot
GNR	Graphene Nanoribbon
GNS	Graphene Nanosheet
GO	Graphene Oxide
HA	Hydroxyapatite
HAp	Ultrathin Plate-Like Hydroxyapatite
HFCVD	Hot Filament Chemical Deposition Vapor System
HIP	Hot Isostatic Pressing
IR	Infrared Region
ITO	Indium tin oxide
LARGO	Reduced Graphene Oxide by *Lavandula agnustifolia* extract
LNRGO	Reduced Graphene Oxide by *Laurus nobilis* extract
MB	Methylene Blue
MG	Malachite Green
MRGO	Reduced Graphene Oxide by *Melissa officinalis* extract
nHA	Hydroxyapatite Nano-tube
nHAp	Nanocrystalline Hydroxyapatite
oCNT	Oxidized Carbon Nanotubes
OCP	Open Circuit Potential

OHA	Oxyapatite
OHAP	Oxyhydroxyapatite
PMMA	Poly(methyl methacrylate)
PVDF	Polyvinylidene Fluoride
RGO	Reduced Graphene Oxide
RGON	Reduced Graphene Oxide Nanosheet
RRGO	Reduced Graphene Oxide by *Rosae caninae* extract
SBF	Synthetic Body Fluid
SEM	Scanning Electron Microscope
SiC	Silicon Carbide
SPS	Spark Plasma Sintering
SRGO	Reduced Graphene Oxide by *Salvia officinalis* extract
TEM	Transmission Electron Microscope
TG/DTA	Thermogravimetric/Differential Thermal Analyzer
TOC	Total Organic Carbon
UV	Ultraviolet Region
UV-Vis	Ultraviolet-Visible Spectrophotometer
XPS	X-Ray Photoelectron Spectroscopy
XRD	X-Ray Powder Diffraction

LIST OF FIGURES

LIST OF TABLES

ABSTRACT

REDUCTION OF GRAPHENE OXIDE BY NATURAL PRODUCTS AND PRODUCTION OF REDUCED GRAPHENE OXIDE-HYDROXYAPATITE COMPOSITES

Elif ÖZTÜRK

Department of Chemical Engineering

MSc. Thesis

Adviser: Prof. Dr. Belma ÖZBEK

Beside the well-known 3-D allotropes of carbon; like graphite and diamond, recently 0-D fullerenes and 1-D carbon nanotubes have been discovered; and the studies are focused on these allotropes. Graphene has been experimentally studied for over 40 years. Novoselov and Geim, synthesized graphene by a Scotch-tape method which includes mechanical exfoliation of graphite to single-layer graphene; and single-layer graphene was identified by a basic microscope in 2004. The discovery of this 2-D allotrope of carbon was awarded by Nobel Prize in physics in 2010.

Graphene is a honeycomb lattice structure of one atom thick layer and comprises σ bonds between sp^2 carbon atoms. This two dimensional sp^2 carbon network structure makes it the thinnest and strongest material among others. Graphene has unique properties such as extremely high surface area to mass ratio (theoretically 2,630 m^2g^{-1}), excellent thermal conductivity (~5,000 $Wm^{-1}K^{-1}$, 10 times better than copper), optical transparency (~ 97.7 %).

On the other hand, hydroxyapatite [HA: $Ca_{10}(PO_4)_6(OH)_2$], one of the bioactive materials, is a basic calcium phospate mineral. It is also major inorganic constituent of bones and teeth tissues. It has applications in orthopedic, dental and maxillofacial fields due to its binding potential to bone tissue, promotion ability of bone repair and excellent biocompatibility. However, it shows poor mechanical properties like low fracture toughness and high elastic modulus; and these properties makes them unsuitable for major load bearing applications.

In the present study, it was focused on developing mechanically stronger HA composites by using green reduced graphene oxide (RGO) reinforcement to strengthen the negative features of HA. To our knowledge, there are no previous studies reported in the literature about production of green RGO-HA composites. For this purpose, graphene oxide was synthesized by Hummer's method; and this synthesized graphene oxide was reduced by applying plant-based method. In this method, *Achillea nobilis* (yarrow), *Laurus nobilis* (daphne), *Lavandula agnustifolia* (lavandula), *Rosae caninae* (rose hip), *Salvia officinalis* (salvia) and *Melissa officinalis* (melisa) extracts were used due to their rich chemical content such as flavonoids, ascorbic acid, pectins acting as reducing agents. The plant-based method has certain advantages over chemical-based methods such as being non-toxic, economic and usable for bio-applications. Therefore, the plant extract that showed the highest reduction efficiency among others was determined and the reduced graphene oxide by this plant extract was used as the second material to HA. The RGO-HA composites were produced via precipitation method at different concentrations of RGO in HA, 0.25, 0.5, 1 and 2% (wt) while pure HA was also produced for comparison. The samples were characterized by Ultraviolet-Visible Spectroscopy, Fourier Transform-Infrared Spectroscopy, X-Ray Powder Diffraction, Scanning Electron Microscope, Transmission Electron Microscope and Thermogravimetric Analysis. The mechanical properties of the samples have been evaluated by Universal Testing Machine.

As a result, *Melissa officinalis* extract showed the optimum reduction efficiency on graphene oxide with the extraction conditions by sonication at temperature of 80°C for 2 h. Therefore, the reduced graphene oxide by *Melissa* extract (MRGO) sample was used as second material to HA. Furthermore, the characterization results showed that pure HA and RGO-HA composites were produced successfully and the mechanical properties of pure HA were improved with RGO reinforcement. Compared to pure HA, the compressive strength values increased 77.44%, 156.05%, 220.25% and 231.51% for 0.25, 0.5, 1, 2% (wt) RGO-HA composites, respectively. Thus, the produced RGO-HA composites would be open up for various future biotechnological applications such as bone tissue engineering and etc.

Keywords: Composites, Graphene Oxide, Green Reduction, Hydroxyapatite, Characterization, Optimal Conditions

ÖZET

GRAFEN OKSİTİN DOĞAL KAYNAKLI ÜRÜNLER İLE İNDİRGENMESİ VE İNDİRGENMİŞ GRAFEN OKSİT-HİDROKSİAPATİT KOMPOZİTLERİN ÜRETİLMESİ

Elif ÖZTÜRK

Kimya Mühendisliği Anabilim Dalı

Yüksek Lisans Tezi

Tez Danışmanı: Prof. Dr. Belma ÖZBEK

Karbonun çok bilinen 3 boyutlu elmas ve grafit gibi allotroplarının yanında son dönemde 0 boyutlu fulleren ve 1 boyutlu karbon nanotüp allotropları da bulunmuş ve araştırmalar bu allotroplar üzerine yoğunlaşmıştır. Grafen 40 yıldan fazla süredir deneysel olarak sentezlenmeye çalışılmıştır. Novoselov ve Geim 2004 yılında ilk kez, grafiti bir selobant üzerine tekrar tekrar yapıştırma ile grafiti katmanlarına ayırarak tek katmanlı grafen sentezlemişler ve basit bir optik mikroskop ile bu tek katmanlı grafeni gözlemlemişlerdir. Karbonun keşfedilen bu 2 boyutlu allotropu 2010 yılında fizik dalında Nobel ile ödüllendirilmiştir.

Grafen bal peteği şeklinde örülü tek atom kalınlığındadır ve sp^2 karbon atomları arasında σ bağları içerir. Bu 2 boyutlu sp^2 karbon bağ yapısı ile yeryüzünde bilinen en sağlam ve en ince malzeme olma özelliği taşımaktadır. Grafen kütle oranına göre oldukça geniş spesifik yüzey alanına (teorik olarak, 2,630 m^2g^{-1}), oldukça yüksek termal iletkenliğe (~5,000 $Wm^{-1}K^{-1}$, bakırdan 10 kat daha yüksek) ve optik geçirgenliğe (~ %97.7) sahiptir.

Diğer yandan, temel bir kalsiyum fosfat minerali olan hidroksiapatit (HA: $Ca_{10}(PO_4)_6(OH)_2$) biyoaktif malzemelerden biridir ve aynı zamanda kemik ve diş dokusunun major inorganik bileşeni olarak bilinmektedir. Kemik dokusuna bağlanma potansiyeli, kemik onarımını destekleme özelliği ve biyouyumluluğu ile diş, çene ve ortopedik alanlarda kullanım alanı bulmaktadır. Ancak düşük kırılma tokluğu, yüksek elastik modulü gibi zayıf mekanik özellikler gösterdiğinden yük dayanımı gerektiren uygulamalarda kullanımı oldukça sınırlıdır.

Bu çalışmada, bitkisel olarak indirgenmiş grafen oksit (RGO) kullanılarak hidroksiapatitin negatif özelliklerinin güçlendirilmesine yönelik mekanik dayanımı arttırılmış HA kompozitlerinin geliştirilmesi amaçlanmıştır. Bildiğimiz üzere, daha önce bitkisel olarak indirgenmiş grafen oksit-hidroksiapatit (RGO-HA) kompozitlerinin üretimi literatürde yer almamaktadır. Bu kapsamda, grafen oksit Hummers' yöntemi ile sentezlenmiş ve sentezlenen grafen oksit bitkisel metot uygulanarak ile indirgenmiştir. Bu metotta flavonoid, askorbik asit, pektin gibi indirgeyici ajan olarak görev yapan kimyasallarca zengin olan *Achillea nobilis* (civan perçemi), *Laurus nobilis* (defne), *Lavandula agnustifolia* (lavanta), *Rosae caninae* (kuşburnu), *Salvia officinalis* (adaçayı) ve *Melissa officinalis* (melisa) bitkilerinin ekstreleri kullanılmıştır. Bitki kaynaklı indirgeme metodunun; kimyasal metota göre toksik olmaması, ekonomik ve biyo-uygulamalarda kullanılabilir olması gibi önemli üstünlükleri bulunmaktadır. Bu nedenle, bu 6 bitki arasından grafen oksitin indirgenmesinde en yüksek verimi sağlayan bitki ekstresi seçilmiş ve bu bitki ekstresi ile indirgenen grafen oksit HA'ya ikinci malzeme olarak katkılandırılmıştır. Böylelikle, HA içerisinde farklı RGO konsantrasyonlarında (% ağırlıkça, 0.25, 0.5, 1 ve 2) RGO-HA kompozitleri ve aynı zamanda kıyaslama için saf HA presipitasyon yöntemi ile üretilmiştir. Bu örnekler, Ultraviyole-Görünür Spektroskopi, Fourier Dönüşümlü Kızılötesi Spektroskopi, X-Ray Toz Difraksiyonu, Taramalı Elektron Mikroskopu, Geçirimli Elektron Mikroskopu ve Termogravimetrik analizler ile karakterize edilmiştir. Örneklerin mekanik özellikleri ise Evrensel Test Cihazı ile ölçülmüştür.

Sonuç olarak, 2 saat süresince 80°C sıcaklıkta sonikasyon ile gerçekleştirilen ekstraksiyon koşullarında *Melissa officinalis* ekstresi grafen oksit üzerinde optimum indirgeme verimi göstermiştir. Bu nedenle *Melissa officinalis* ekstresi ile indirgenen grafen oksit (MRGO), HA kompozitleri için ikinci malzeme olarak kullanılmıştır. Bununla birlikte, gerçekleştirilen karakterizasyon testleri kompozitlerin başarılı bir şekilde üretildiğini ve HA yapısına RGO katkılandırılmasının HA'nın mekanik özelliklerini iyileştirdiğini göstermiştir. Saf HA ile kıyaslandığında, basınç dayanımı değerleri ağırlıkça % 0.25, 0.5, 1 ve 2 RGO-HA kompozitleri için sırasıyla %77.44, 156.05, 220.25 ve 231.51 artış göstermiştir. Üretilen RGO-HA kompozitlerinin kemik dokusu mühendisliği gibi gelecekte çeşitli biyoteknolojik uygulamalarda kullanım alanı bulması mümkün olacaktır.

Anahtar Kelimeler: Kompozit, Grafen Oksit, Bitkisel İndirgeme, Hidroksiapatit, Karakterizasyon, Optimum Koşullar

CHAPTER 1

INTRODUCTION

1.1 Literature Review

New-found nanomaterials are attracted great attention in recent years regarding to their unique structures and properties. Therefore, the development of nanomaterial research plays a significant role in various fields such as biochemistry, material science and physics. Hereby, carbon nanomaterials have been studied extensively since their discoveries.

Carbon-based materials like graphite, diamond, fullerenes and nanotubes have found large application area such as electronics, medical devices, sensors and tissue engineering. The discovery of graphene in 2004, added a new member to these carbon nanomaterials. Graphene is a sp^2 bonded carbon atoms in a hexagonal lattice structure. Long range π-conjugation in this structure yields to excellent mechanical, thermal and electrical properties. However, the hydrophobicity and agglomeration tendency of graphene are restricting its applications. Therefore, its composite with a second material may prevent its restacking of graphene layers but also shows cooperative contributions to the properties of graphene based nanocomposites. Correspondingly, graphene and inorganic composites hold promise for many applications. Regarding to this, it is reported that graphene composites with inorganic nanomaterials exhibit unique characters and improved functionalities due to synergistic effects between graphene and the inorganic compound [1].

Hydroxyapatite, [HA: $Ca_{10}(PO_4)_6(OH)_2$] is the major component of bones and teeth. Synthetic HA possesses excellent biocompatibility and unique bioactivity. It has applications in orthopedic, dental and maxillofacial fields. Unfortunately, HA shows low strength and toughness with brittle nature which makes it unsuitable for load bearing applications. Hence, it is required to combine HA with a mechanically strong material like graphene while keeping its bioactivity by producing it with green reduction method.

1.2 Objective of the Thesis

Chemical reduction of graphene oxide is the most common method which includes exfoliation of graphite to graphene oxide and reduction of graphene oxide to graphene by reducing agents like hydrazine and its derivatives. Although, this method provides cost effectiveness and bulk production, the toxic nature of reducing agents restricting its applications in bio-related sciences. On the other hand, synthesis of metal nanoparticles using plants is an alternative and cost effective way to produce large scale metal nanoparticles [2]. The main objectives of the present study were given as below:

- to reduce graphene oxide by using various natural products instead of chemically toxic reducing agents and
- to produce reduced graphene oxide- hydroxyapatite (RGO-HA) composites for tissue engineering applications.

1.3 Hypothesis

The combination of a carbon nanomaterial with an inorganic matrix may lead to obtain the composites with the functional characteristics of two matrix. Therefore, graphene reinforcement in hydroxyapatite matrix may provide mechanically stronger hydroxyapatite composites. The investigation of mechanically stronger hydroxyapatite composites may generate a useful application of these composites as scaffold material for later studies.

CHAPTER 2

GRAPHENE

Beside the well-known three-dimensional (3-D) allotropes of carbon; like graphite and diamond, recently zero-dimensional (0-D) fullerens and one-dimensional (1-D) carbon nanotubes (CNTs) have been discovered; and the studies are focused on these allotropes (Figure 2.1). Graphene as a two-dimensional (2-D) allotrope of carbon was synthesized in 2004 and this discovery won the 2010 Nobel Prize in physics. Novoselov and Geim, synthesized graphene by a Scotch-tape method which includes mechanical exfoliation of graphite to single-layer graphene; and identified this single-layer structure by a basic microscope [3].

Graphene is a single or few layer of sp^2 hybridized carbon atoms arranged in a hexagonal lattice structure. Each carbon atoms in this lattice has four valence electrons; the first three are used to form covalent sp^2 bonds while the final p_z electron makes up the π bonds and the half-filled band permit electrons to move freely [4]. This special atomic arrangement of graphene leads a continuous layer of delocalized electrons and rigid covalent bonds [4].This structure allows dispersing phonons efficiently and gives it the ability to withstand a great deal of stretching making it the strongest material ever known [4].

Graphene's extended and conjugated network absorbs a great deal of light regarding to its aromatic macromolecule structure without a band gap [4]. As the electrons in graphene behave like massless relativistic particles, it shows significant properties such as quantum Hall effect and the absence of localization [5]. As graphene has demonstrated a variety of extraordinary properties, there is no doubt that graphene and its derivatives have risen as a shining star in scientific researches for future applications.

		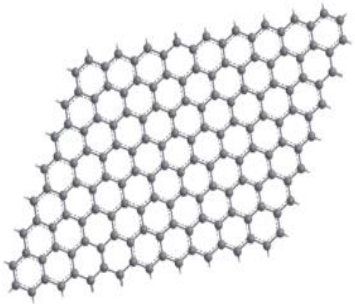
Fulleren (0D) Smalley et al. (1985) [6] Nobel Prize (1996)	Carbon Nanotube (1D) Lijima et al. (1991) [7]	Graphene (2D) Geim et al. (2004) [8] Nobel Prize (2010)

Figure 2.1 Three major types of sp^2 nanocarbons including fullerene, carbon nanotube and graphene [9]

2.1 History of Graphene

Graphite was first used 6000 years ago by Marican in Europe [10] to decorate pottery and the research for an isolated-single layer of graphite dates back to the 1960s, when surprisingly higher basal-plane conductivity of graphite intercalation compounds were discovered compared to that of the original graphite. While this discovery had drawn much interest by scientific community that might lead to lighter, cheaper substitute for existing metal conductors, the cause of the high conductivity of graphite intercalation compounds needed to be solved for future applications [5].

The research for obtaining thin graphite or graphene layers has grown slowly in late 20^{th} century with the hope to observe superior electrical properties. In the graphite intercalation systems, isolated graphene layers were obtained in a three-dimensional matrix by inserting large molecules between atomic planes. The subsequent removal of the large molecules from atomic planes generated a mixture of stacked or scrolled graphene layers with no control of the structure. According to both theoretical calculations and experimental observations, it was generally believed that 2-D materials did not exist without a 3-D base [5].

The calculations showed that a graphene sheet thermodynamically unstable if its size was less than about 20 nm [graphene is the least stable structure until about 6000 atoms and becomes the most stable one only for sizes larger than 24,000 carbon atoms (graphite)] [5].

Various attempts were made to synthesize graphene including the same method for the growth of carbon nanotubes, chemical vapor decomposition (CVD) on metal substrates or thermal decomposition on silicon carbide (SiC). However, only a few layers of graphene produced instead of monolayer graphene. Even so, these studies clarified the high-charge mobility of a few layer graphene and the optimized CVD method has been a major technique.

In year 2004, monolayer graphene was first isolated by Geim and Novoselov [8] by peeling graphite with an adhesive tape till monolayer is obtained. This approach enabled to obtain high quality graphene with size in hundreds of microns. Since then, graphene has attracted much attention and its properties have been investigated.

Nowadays, it is possible to control graphene layers on substrates, functionalize graphene or produce graphene derivatives. As different graphene family materials exhibit markedly different physicochemical properties and surface functionalities, it is possible to use these materials in wide range of applications [11].

2.2 Graphene Family Nanomaterials (GFNs)

Although the term of "graphene" actually refers to a 2-D monolayer of carbon atoms, it also comprises other forms of graphene comprising single layer or few layer (2-10 graphene layers) graphene, graphene oxide (GO), reduced graphene oxide (RGO), graphene nanosheets, ultrafine graphite (more than 10 sheets but below 100 nm in thickness), graphene nanoribbons (GNRs) and graphene dots (GNDs) [12]. These structures were presented in Figure 2.2.

Owing to the inert chemical property and the difficulty in defect-free graphene production, GO and RGO not only compensate for the drawbacks of graphene but also bring about new properties. One of the main advantages of the GO derivatives is the dispersion ability in aqueous solution, thus broadening their usage in biological applications. RGO can be considered as a transitional material between graphene and GO and offers both aqueous solubility and partial recovery of the conjugate system in carbon network [13].

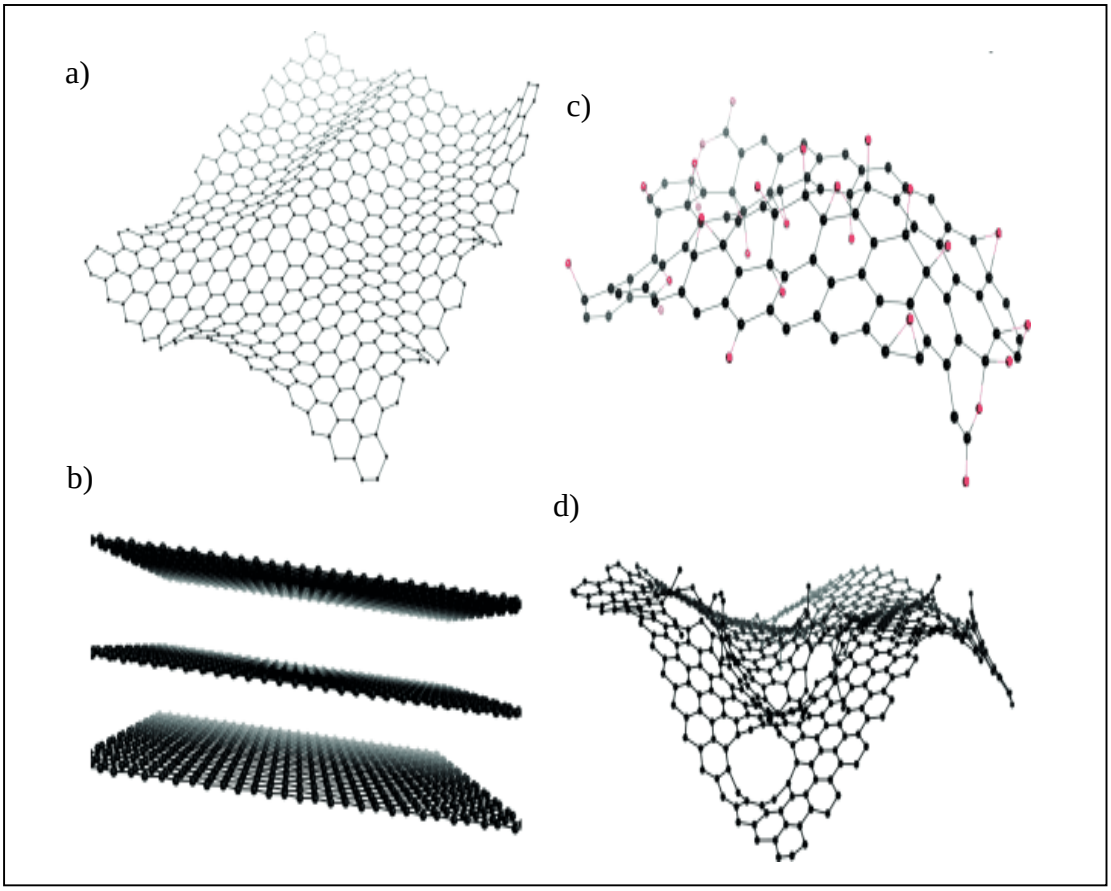

Figure 2.2 Representative chemical structures of some of the members of GFNs: a) graphene, b) few-layer graphene, c) graphene oxide (oxygen atoms are in red) and d) reduced graphene oxide [12]

Cutting graphene sheets into narrow strips yields GNRs. GNRs can be thought of as planar analogues of CNTs with band gaps depending upon the ribbon width [14]. The properties of GNRs depend strongly on both the crystallographic orientation of their edges and the width of the GNR [15]. The actual atomic structures of the edges also have important effects on the properties of GNRs [15].

Furthermore, as the 0-D form of graphene, GNDs also exists but has been much less studied compared to other forms. GNDs can potentially range in size from molecular to semi-infinite 2-D structures and thus, their electronic structures vary from having discrete molecular levels to being band-like. Using GNDs in different dimensions leads to the potential of spanning the range of electronic and magnetic properties from molecular-like to 2-D like [16]. Within each of these forms a variety of structures are possible for wide range of applications. The description of all these forms and well understanding of properties for each forms are mandatory to elucidate their effects.

2.3 Properties of Graphene

2.3.1 Morphology and Structure of Graphene

Carbon is a versatile element that it can either display as a hard diamond or soft graphite depending on its atom arrangements. The flat and tightly bonded carbon arrangement gives graphene many unusual characteristics, including the status of strongest material in the world. The hexagonal lattice of graphene consists triangular two sub-lattices of carbon atoms which are tied to its three nearest neighbors via strong σ bonds that is stable under a rotation of 120° around any atom [17-19] (Figure 2.3). The σ bonds results the sp^2 hybridization for three valence electrons and the fourth one is in π orbital that contributes to a delocalized electron networks [18].

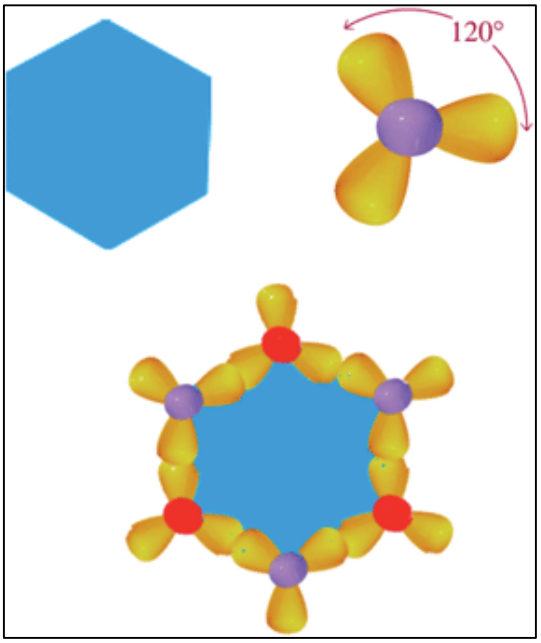

Figure 2.3 Construction of the graphene lattice. One may observe that the six carbon atoms make up two families—the purple and red positions—which can replace each other by simple translations, while no red atom can replace a purple atom only by a translation operation [15]

The hybridized orbitals are in trigonal planar geometry. This is the reason why each carbon atom has three nearest neighbors [15]. Each p_z orbital overlaps with neighbor carbon atoms to form π-bonds which lead to delocalized π bands like in benzene, naphthalene and other aromatic molecules [15]. Thus, graphene can be thought as the extreme size of planar aromatic molecules [15]. The covalent σ bonds in graphene are shorter than the C-C bonds in diamond and lead to extremely high mechanical strength.

Band structure calculations show an unusual electronic structure for the honeycomb lattice [15]. Thus, graphene is called as a zero-band gap semiconductor or semimetal. Electrons in graphene behave like massless relativistic particles that contribute very special properties like quantum Hall effect and the absence of localization [5]. Along with all these properties and very thin atom thickness (0.345 nm) of graphene enable it to break so many records in terms of strength, electricity and heat conduction [20].

2.3.2 Mechanical Properties

After carbon nanotube, graphene has been reported as the strongest material in the universe with an intrinsic tensile strength of 130 GPa and a Young modulus of 1 TPa. Monolayer graphene shows the highest intrinsic strength with stiffness similar to graphite [5]. The elastic properties and intrinsic breaking strength of monolayer graphene was measured by nanoindentation in an atomic force microscope (AFM) [21] (Figure 2.4). The stiffness was reported as 300 – 400 N/m with a breaking strength of 42 N/m.

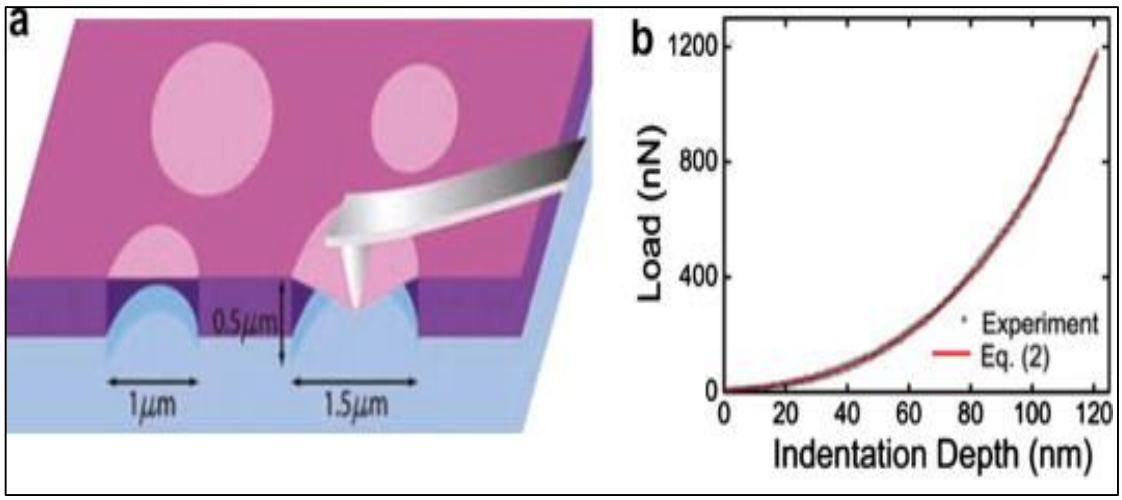

Figure 2.4 Mechanical properties (a) Schematic of AFM nanoindentation on suspended graphene, (b) Loading/unloading curve for device in (a) with modeling comparison (red line) [19]

2.3.3 Optical Properties

The optical transparency of graphene has been measured as ~ 97.7% using a xenon lamb light source in the visible range (250 -1200 nm) and the transmittance linearly decreases with the number of layers for n-layer graphene [22]. For 2-nm thickness, the transmittance is higher than 95% and for 10-nm thickness the transmittance is higher than 70% [19]. A deviation from this behavior has been found for incident photons with energy lower than

0.5 eV regarding to the finite temperature and a doping-induced chemical potential shift of the charge-neutrality (Dirac) point [17].

2.3.4 Thermal Properties

The thermal conduction in a monolayer graphene was tested with the help of confocal micro-Raman spectroscopy. It is measured as 5,300 W/mK for a monolayer graphene from the dependence of the Raman *G* peak frequency on the excitation laser power [23].

2.3.5 Electronic Properties

The electronic properties of graphene have received much attention due to its extremely high nature of charge carriers which behave as massless relativistic particles (Dirac fermions) [5]. Although there is nothing relativistic about the electrons moving around the carbon atoms, their interaction with the periodic potential of the honeycomb lattice of graphene gives rise to quasiparticles, called massless Dirac fermions [24]. The high electronic conductivity in graphene is related to low defect density in its crystal lattice [5]. Defects generally acts as scattering sites and inhibit charge transport by limiting the electron mean free path [5].

2.4 Synthesis of Graphene

Since graphene production is difficult due to its agglomeration and restacking tendency, various synthesis methods have been improved to produce graphene and its derivatives. These methods are classified as top down and bottom up approaches [25]. While the top down methods comprise to degrade the stacked layer of graphite, the bottom up method comprises to synthesize graphene from other carbon containing groups [25]. Top down approach is based on overcoming the interlayer van der Waals forces and separating these layers without damaging the layers [25].

For bottom up approach, it is based on constructing graphene from other carbon sources. Despite its feasibility to produce large graphene films from polymers and small molecules, it is generally required high temperatures to obtain high level of graphitization [25], [26]. Taking all advantages and disadvantages of these synthesis methods into account, it is still an important issue to develop new processing routes for efficient synthesis of large-scale graphene.

2.4.1 Top-down Methods

2.4.1.1 Mechanical Exfoliation

The interlayer van der Waals interaction energy of graphene is about 2 eV/nm^2 and a weak force about 300 nN/μm^2 is required to exfoliate graphite [19]. This force can be applied even with an adhesive tape as experienced before [27], [28]. This micromechanical cleavage method was used to mechanically split graphite into atomic layers by a 'Scotch tape'. To date several mechanical exfoliation techniques have been reported such as exfoliating graphite by using a micro-cantilever with keeping constant the pressure and shearing force [29]. Although this method is a simple, economic process and provides to obtain defect free, un-oxidized graphene, it is limited to thinning the graphite crystal below thickness of ~10 nm and not suitable for large scale production [19]. Optical images of micromechanically exfoliated graphene with various layer forms are shown in Figure 2.5.

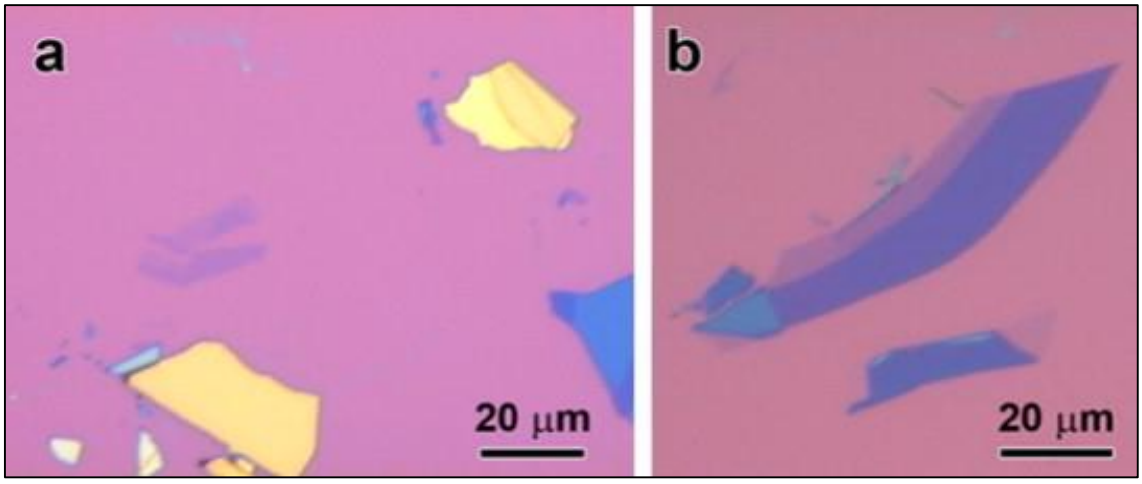

Figure 2.5 Micromechanically exfoliated graphene. Optical images of (a) thin graphite and (b) few-layer graphene (FLG) and single-layer graphene (lighter purple contrast) on a ~300 nm SiO_2 layer, Yellow-like color indicates thicker samples (~100 s of nm) while bluish and lighter contrast indicates thinner samples[19]

2.4.1.2 Exfoliation of Graphite Oxide

Graphene can be produced in liquid phase from graphite by thermal or oxidation technique followed by reduction reaction. In oxidation technique, the heavy oxidation of natural graphite by concentrated acids and strong oxidants leads to graphite oxide. The Hummers' method is the most common process to produce graphite oxide. Graphite oxide is exfoliated by thermal treatments or sonication to graphene oxide. Graphene oxide

composes oxygen-containing groups such as epoxide, hydroxyl, carbonyl and carboxyl and these groups makes graphite oxide hydrophilic by weaken the van der Waals interactions [30]. The hydrophilicity allows water to intercalate between the layers and disperse them as individuals [31].

Wherefore graphene oxide is electrically insulating due to its disrupted sp^2 bonding network, it is exposed to reduction reaction to restore the π-network. The reduction reaction can be performed through chemical, thermal or electrochemical reactions. As the most common reduction method, chemical reduction is carried out by extremely strong reducing agents such as hydrazine, hydroquinone and sodium borohydride which have highly hazardous and toxic nature [32], [33]. As the second method, instead of using a chemical reductant, it is possible to cut off the oxygen functionalities by heating graphite oxide in a furnace [34]. The high temperature gas leads to extremely high pressure onto the stacked layers and approximately 30% of the mass of graphite oxide is lost during this process [34].

Therefore vacancies and defects occurred on the plane and they affect the electronic and mechanical properties of the product. Finally, the third method is based on removing oxygen functionalities by electrochemically. After depositing thin films of graphene oxide on glass, plastic or other substrates, electrodes are placed at opposite ends of the film implementing linear sweep voltammetry [34]. Although this route appears to be effective, scalability is required. Typical optical images for this process were shown in Figure 2.6.

The most important advantages of the chemical exfoliation method are the low-cost and large-scale production. Also, this method enables to deposit the monolayer graphene on any substrate with simple processing.

2.4.1.3 Arc Discharge

Arc discharge method includes synthesizing few layer graphene flakes from graphite electrodes by using direct current under a mixture atmosphere of hydrogen and helium. The presence of hydrogen gas minimizes the nanotubes and other carbon structures formation [35]. It is possible to obtain large scale graphene using arc evaporation of graphite rod in air [24]. This method also has been widely used to synthesis carbon nanotubes and fullerenes. A schematic illustration was shown in Figure 2.7.

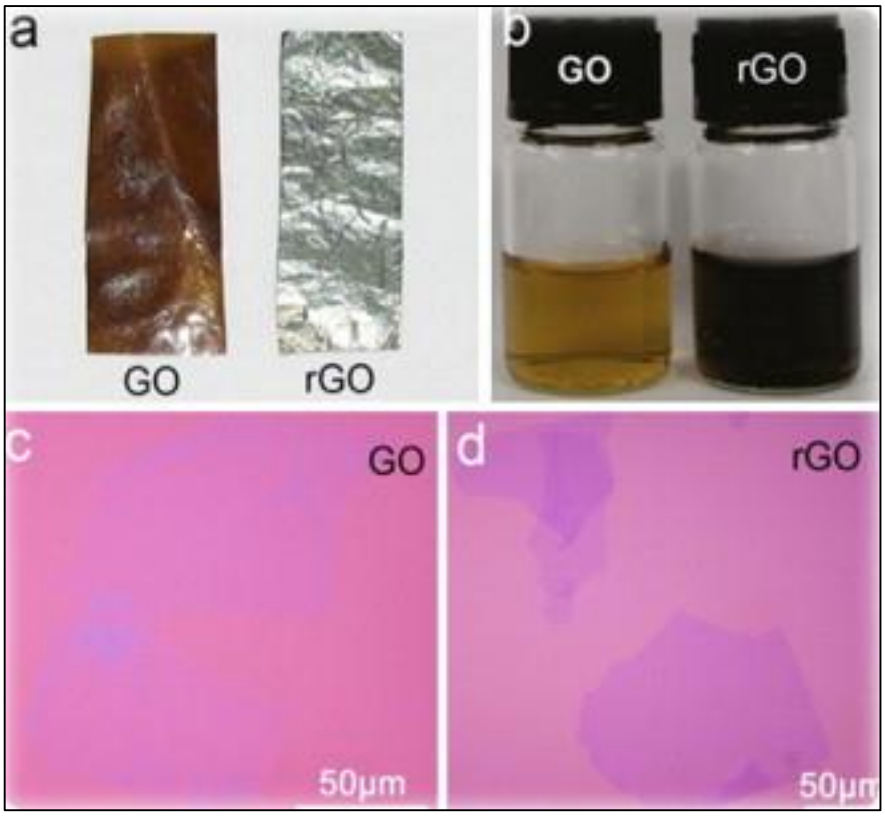

Figure 2.6 Typical optical images of (a) a GO film and RGO film, (b) GO solution and RGO solution (c, d) GO and RGO sheets on a 300 nm SiO_2/Si substrate [36]

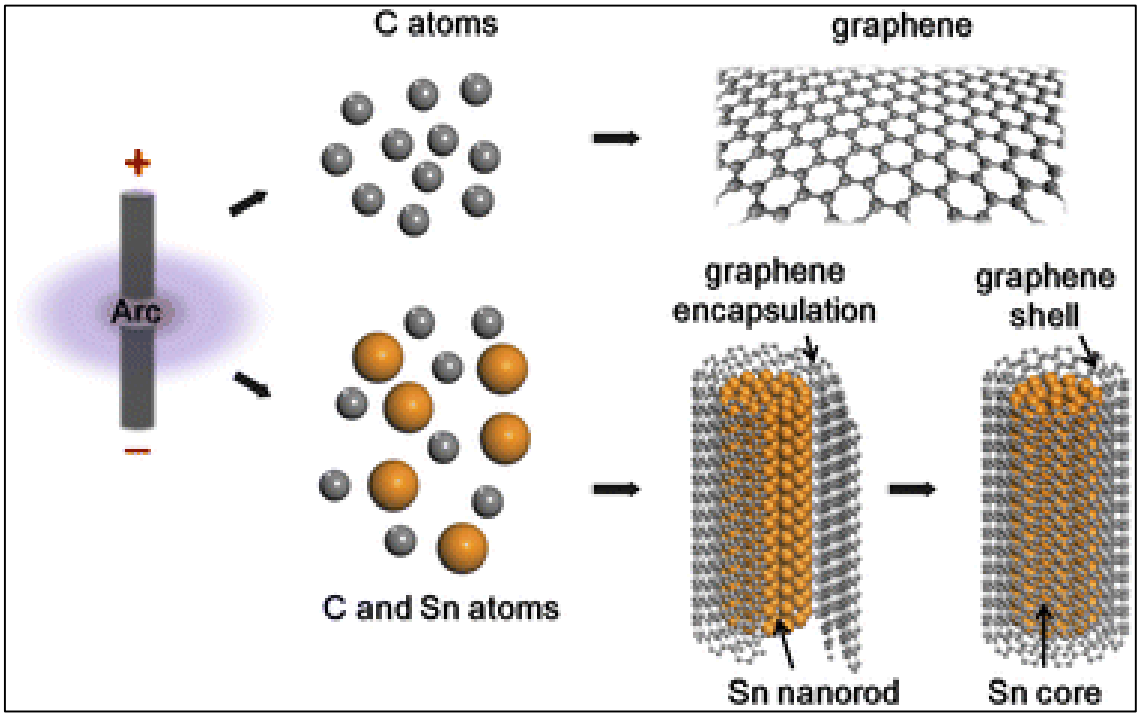

Figure 2.7 Schematic arc-discharge synthesis of graphene and graphene-encapsulated tin nanorod [37]

2.4.1.4 Unzipping Carbon Nanotubes

Since carbon nanotubes are described as cylindrical forms of graphene sheets and synthesis methods have been well developed, graphene can be synthesized by unzipping carbon nanotubes using strong oxidizing agents or by physical methods such as laser irradiation and plasma etching [25]. This method represents a novel strategy to obtain smooth edges and controllable widths graphene nanoribbons at extremely high yields. These nanoribbons are considered as quasi one dimensional materials and unzipping process occurs via C-C bond fission which leads to irregular cutting [25]. Pd metal nanoparticles were reported as the catalyst for unzipping process (Figure 2.8) [38].

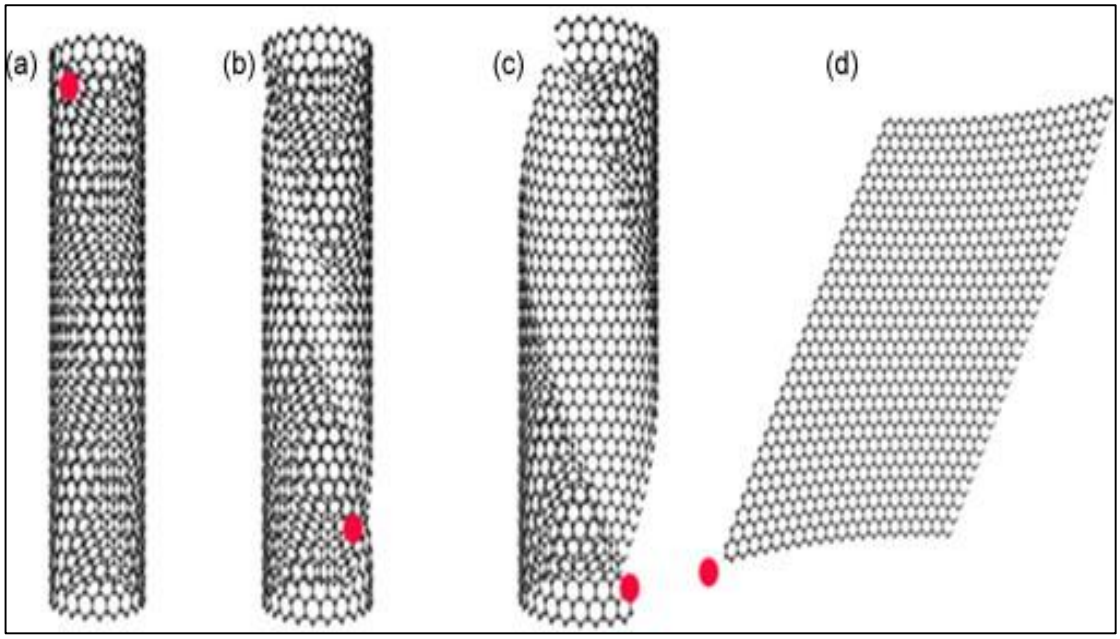

Figure 2.8 Schematic representation of the different unzipping steps of the pristine carbon nanotube decorated with palladium nanoparticles to form a graphene nanoribbon. The unzipping process was expected to follow the helicoidal organization of defects in carbon nanotube structures [38]

2.4.2 Bottom-up Methods

2.4.2.1 Chemical Vapor Deposition (CVD)

Chemical vapor deposition is a thermal method where hydrocarbons are exposed to a heated metal surface under vacuum and it has been widely used to produce graphene films [39-41]. This method can be performed by proceeding surface catalyzed or segregation methods depending on the metal [25].

For surface catalyzed reactions, the metal catalyzes hydrogen loss and the graphene formation occurs at the metal surface. For segregation, regarding to lower solubility of carbon in metals at low temperatures dissolved carbon in the bulk metal diffuses to the metal surface upon cooling [25]. The dissolved carbon amount and cooling rates are the important factors on the number of graphene layers.

As stated by Munoz and Gomez-Aleixandre (2013) [42] in their study, the CVD (Figure 2.9) process is carried out by the following steps;

1. Transport of reactants by forced convection.
2. Thermal activation. Homogeneous gas reaction with particles and powder production should be avoided in graphene synthesis, controlling the kinetic parameters (P,T,n).
3. Transport of reactants by gas diffusion from the main gas stream through the boundary layer.
4. Adsorption of reactants on the substrate surface.
5. Dissolution and bulk diffusion of species depending on the solubility and physical properties of the substrate.
6. Thermal activation-mediated-surface processes, including chemical decomposition (catalytic), reaction, surface migration to attachment sites (such as atomic-level steps), incorporation, and other heterogeneous surface reactions. Growth of the film.
7. Desorption of by-products from the surface.
8. Transport of by-products by diffusion through the boundary layer and back to the main gas stream.
9. Transport of by-products by forced convection away from the deposition region [42].

Recently, high quality of large area graphene growth on catalytic metal substrates becomes an interesting topic of material science. Hereby, graphene growth has been studied on a variety of metal substrates such as Cu [13], Ni [43], Ru [44], Ir [45], Pt [46], Co [47], Au [48], Pd [49]. Nevertheless, the high quality of grown graphene has been obtained on Cu(111) regarding to its hexagonal lattice. During the graphene growth on Cu(111), graphene growth became well controlled with domain boundaries atomically connected [42].

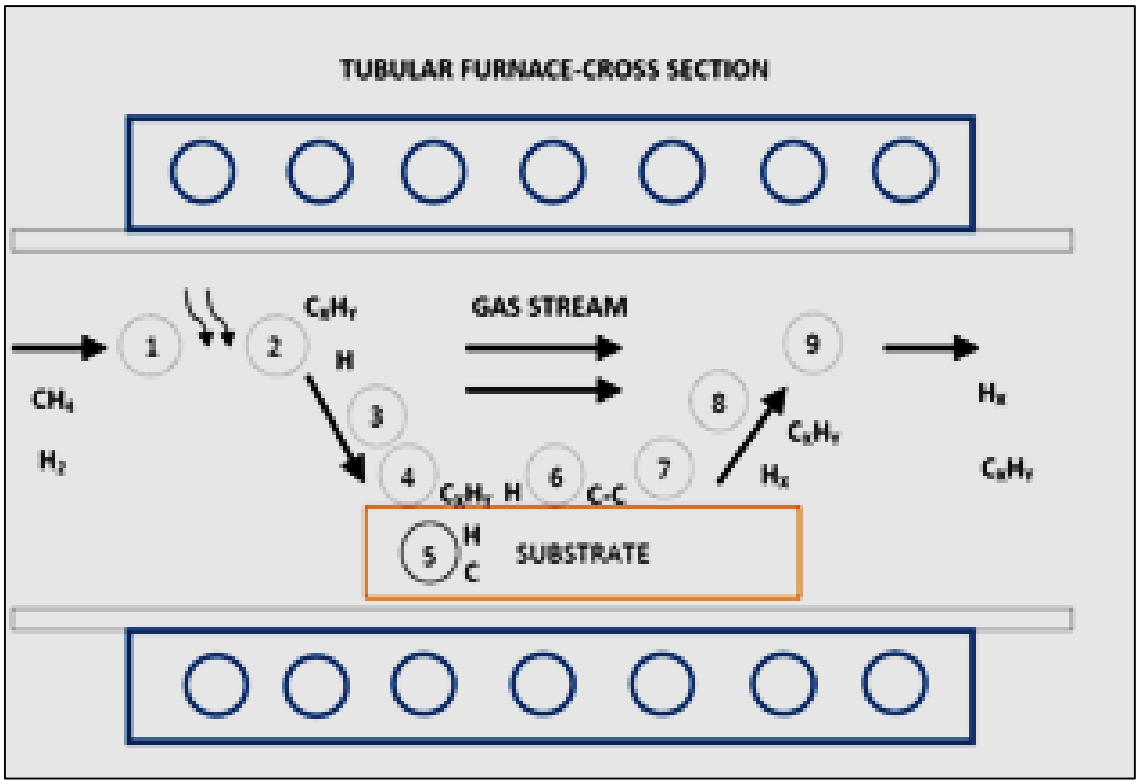

Figure 2.9 Schematic diagram of thermal CVD processes in the case of graphene from CH_4/H_2 mixtures [42]

Among all the strategies to produce graphene, CVD method is inexpensive and produces large-area graphene. Even so, controlled synthesis of graphene with large area still needs to be developed and low temperature graphene growth would reduce cost and enable the direct growth on flexible polymer-based substrates [50]. Recently, high quality of large area graphene has been synthesized via CVD method using polycrystalline nickel films and copper foils [51], [52].

2.4.2.2 Epitaxial Growth

One of the popular methods for graphene growth is thermal decomposition of the surface of a monocrystal silicon carbide (SiC). Silicon carbide is a crystalline compound of silicon and carbon and the surface of a monocrystal SiC is terminated with silicon atoms one side while the other side is terminated with carbon atoms [53]. When silicon carbide is heated to high temperatures in the range of 1200-1600°C in vacuum, it preferentially evaporates and pure crystalline graphite-like layers are left behind. A schematic illustration of epitaxy process was represented by Tetlow et al. (2014) [54].

As shown in Figure 2.10, E indicates the hydrocarbon molecules which deposited on the surface and these molecules undergo decomposition via a series of dehydrogenation reactions giving rise to various C_xH_y species shown as E_d, and H atoms. The new species are all able to diffuse across the surface. Smaller carbon species M and D form and diffuse on the surface, aggregating into larger clusters C. H atoms of the original molecule migrate on the surface, and form H_2 molecules that evaporate from the surface. Finally, some of the species like M and D, or even their bigger clusters C, may attach to the island G at its edge.

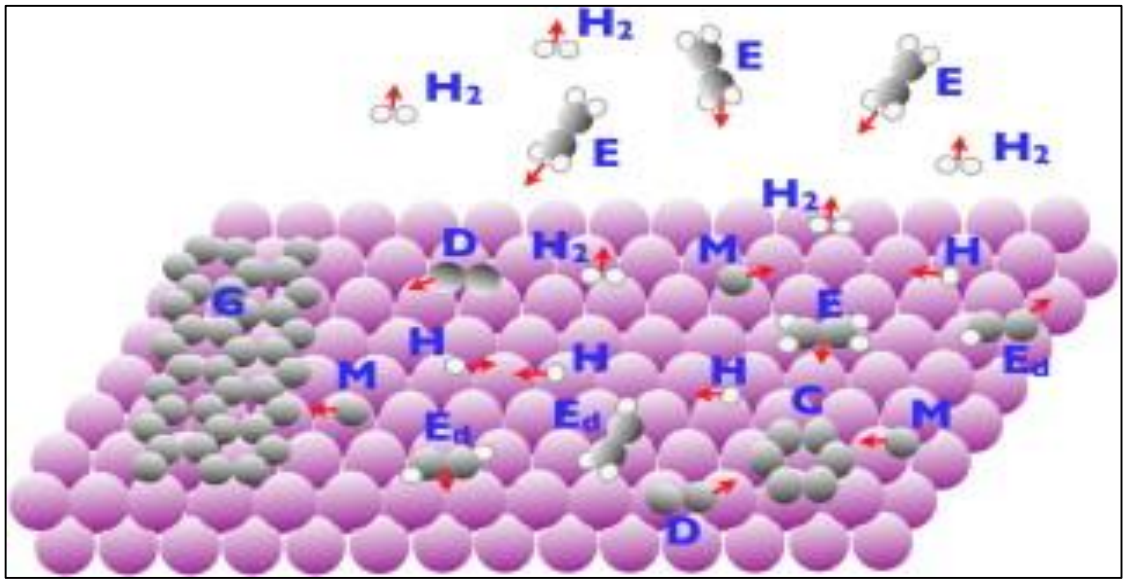

Figure 2.10 Schematic representation of fundamental processes during epitaxy [54]

Other processes (not shown) are also possible based on e.g. diffusion of atoms along the edge of an island, nucleation of second- and higher layers on the islands, downward movement of atoms adsorbed on top of islands to lower layers, and the break up, or dissolution, of islands [54].

In this process, the atoms at the surface form a hexagonal structure so graphene is grown epitaxially. When properly passivated, the SiC substrate does not show any interaction with the graphene layer. These epitaxially grown graphene is suitable for the most demanding electronics applications as it can be considered an insulator at room temperature [55]. Besides that, this process allows to synthesize high quality and large-area graphene. However, to control the thickness of graphene layers and crystal size is limited and needs to be improved. Other issues that restrict to use of this method are the high cost of the single crystal SiC substrate, specialized equipment requirement, high temperature, ultrahigh vacuum or inert atmosphere.

2.5 Applications of Graphene

2.5.1 Electrochemical Applications

In electrochemical applications, GOs and RGOs are more preferred rather than pristine graphene due to its high dispersibility in water and organic solvents and its wide range of reactive surface-bound functional groups [56]. Additionally, GO-based materials exhibit a moderate conductivity depending on the extent of reduction and they also have high chemical stability and excellent electrochemical properties [56].

To date, GO-based materials have been used in GO-based electrodes for electrochemical applications consisting of electrocatalysis, electrochemiluminescence, electrochemical sensors, immunoassays, DNA sensors and others [56]. In electrocatalysis studies, GO has been investigated as a support for the dispersion of precious metal nanoparticles to improve their electrocatalytic activities in fuel cells [57-60].

For electrochemiluminescence (ECL) applications, even though GO sheets cannot generate ECL effect on its own, it exhibits ECL effect by anchoring different luminophore moieties to the GO-based electrodes. Hereby, GO sheets not only supports ECL-based sensors in accelerating electron transfer between the lumophores and the electrode, they also increase the surface area and porosity of the sensor platform to make coreactant diffusion faster for the ECL-based sensors [56].

For electrochemical sensors, GO-based materials are most promising materials due to higher specific surface area and surface to bulk-ratio of GO. Since GO is decorated with oxygen functional groups and every atom can be considered as a surface atom, electron transport through these ultrathin materials can be highly sensitive to adsorbed molecules [56]. GO-based materials can present high selectivity by enhancing gas adsorption or promoting specific chemical reactions at the GO-based electrodes through controlling the surface defect sites [56].

Immunosensors and DNA sensors have currently tremendous interest in the application of electrochemical sensors. In the case of immunosensors, GO-based materials enable the detection of ultralow amounts of analytes by enhancing detection sensitivity [30]. For DNA sensors, GO has been reported as a sensitive building block with excellent sensitivity and used for signal enhancement in target DNA for hybridization [61]. GO-DNA based sensors makes possible to detect DNA, proteins and other molecules with

high selectivity and low cost [62].

2.5.2 Energy Applications

Compared to conventional energy materials, graphene exhibits unusual size- and surface-dependent properties that enhance energy-conversion performance [63]. In this view, graphene has been used as transparent conductive electrodes or active cells in solar cells, counter electrodes in dye-sensitized solar cells, electrocatalysis for oxygen reduction in fuel cells, high performance electrodes in supercapacitors and lithium ion batteries [64].

In solar cell applications, as a transparent electrode graphene sheets with good transparency and low sheet resistance offers an alternative to indium tin oxide (ITO). ITO has been widely used but it is toxic, costly and suffers from brittleness [64]. The application of graphene in solar cells creates a window for inducing wide ranges (from UV to far IR regions) of photon energy inside the solar cells, exhibits higher charge transfer (CT) kinetics at the interface of electrochemical hybrid cells [65]. It also manufactures a flexible device with robust architecture and provides greater heat dissipation [65].

In supercapacitor applications, it is significant to use electrode materials with good conductivity and large specific surface area such as activated carbon, CNTs, carbon nanofibers and graphene sheets. Among all, graphene has good conductivity, low cost and mass production. Also aggregated graphene sheets exhibits an open-pore structure that allows the easy access of electrolyte ions to form electric double layers [21]. To exploit from all these advantages of graphene, graphene-metal oxide supercapacitors, graphene-conducting polymer supercapacitors and graphene-CNT supercapacitors have been reported for higher energy density and electrochemical stability [21].

In lithium-ion batteries, regarding to its good life cycle performance and high coulombic efficiency, graphite is the commercialized anode. However, its specific capacity is limited and it forms an intercalation compound of LiC_6. Compared to graphite, graphene has larger surface area and more edge sites for anchoring other electroactive materials [64]. Recent studies showed that the addition of graphene to transition metal oxide supports the specific capacity of the electrodes at high discharge rate and enhance the electrochemical stability for longer cycles [5].

2.5.3 Biomedical Applications

Among various applications, graphene-family nanomaterials have attracted ever-increasing interests in biomedical applications over the last three years. It has been reported in many studies ([66], [67]) that graphene is a promising material to replace existing materials and devices used as drug delivery vehicles, tissue engineered scaffolds and grafts etc.

In drug delivery systems, GO is more widely used than pristine graphene regarding to the epoxy, hydroxyl and carboxylic functional groups in its structure. These functional groups allow wide range of reactions and functionalization opportunities [11]. They also facilitate conjugation with various systems such as proteins, biomolecules, DNA and others [68]. The exploration of GO-based drug delivery expands from anticancer drugs to other drugs for non-cancer diseases treatments [68]. Many aromatic drug molecules can be physically adsorbed on the polyaromatic graphene surface by ϖ-ϖ stacking which usually takes place in the aqueous phase for less water-soluble drugs [9].

Although GO is water soluble, it is not stable in physiological solutions and causes dose-dependent toxicity both *in vitro* and *in vivo* [69]. In contrast, nanographene with biocompatible materials exhibits excellent stability in in the presence of high concentration salts and proteins and appears to be less toxic *in vivo* and *in vitro* [9]. The *in vivo* biodistribution of graphene is also highly dependent on its surface chemistry [9]. Ultra-high drug loading efficiency was achieved for polyethylene glycol-nanographene surface regarding to the extremely large surface area of graphene [70].

In tissue engineering applications, it is very important to develop scaffolds similar to extracellular matrix (ECM) which can enable cells to enhance adhesion, proliferation and differentiation for tissue regeneration [71]. Carbon nanomaterials provide similar microenvironment to ECM in terms of chemical composition and physical structure making them a potential candidate for the development of artificial scaffolds [71].

Among all, graphene with good biocompatibility, chemical inertness and special surface structure can provide a specialized surface structure for cell culture and its mechanical properties like high elasticity, flexibility and adaptability to flat or irregular surfaces are suitable for cell culture [72]. It has been reported that graphene support the adhesion and proliferation of mammalian cells, human osteoblasts and fibroblasts [71].

A graphene/chitosan film has been investigated as scaffold material and the work indicates that graphene-based film does not hamper the proliferation of human mesenchymal stem cells and accelerates their specific differentiation into bone cells [73]. The research of graphene-based scaffold materials are relatively new direction for tissue engineering and mechanical and electrical properties of graphene can be useful for development of scaffold properties with fine-tuned for target tissues.

CHAPTER 3

HYDROXYAPATITE

The term of "apatite" refers to a general formula of compounds in the form of $M_{10}(XO_4)_6Z_2$, where M^{2+} is a metal and species XO_4^{3-} and Z^- are anions. The particular name of an apatite depends on the elements or radicals, M, Z and X. In this context, hydroxyapatite [HA: $Ca_{10}(PO_4)_6(OH)_2$] has the molecular structure of apatite, where M is calcium, X is phosphorus and Z is the hydroxyl radical. This structure is known as stoichiometric hydroxyapatite which has 1.67 Ca/P atomic ratio. It contains 39% Ca, 18.5% P and 3.38% of OH in weight [74].

3.1 Properties of Hydroxyapatite

3.1.1 Morphology and Structure

HA has a hexagonal crystal structure of calcium (Ca^{+2}) and phosphate (PO_4^{3-}) ions around monovalent hydroxyl (OH^-) ions as shown in Figure 3.1. There are two different calcium positions within the structure: column and hexagonal [75]. Four calcium ions in the unit cell are called as columnar calcium and they lie perpendicular to the basal plane. Other six calcium ions in the unit cell are coordinated with hydroxyl ions and found to parallel to the basal plane. Phosphate groups are also located on these planes. The $(OH)^-$ groups are located in the columns parallel to *c* axes at the corners of unit cell [75].

The hexagonal structure contains two triangles of calcium atoms on two different planes at each corner [75]. The hydroxyl channels in the unit cell define this structure as hydroxyapatite and these groups give hydroxyapatite significant properties such as high surface area and good adsorption characteristics [75]. Additionally, the OH^- groups enable ions to easily incorporate into the apatite structure.

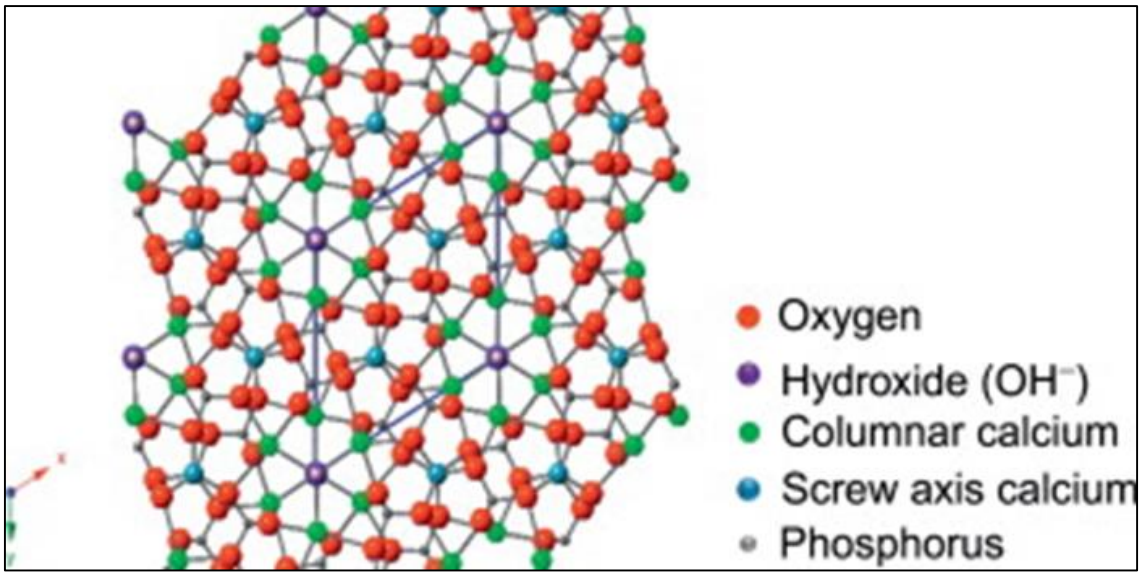

Figure 3.1 Schematic representation of the hydroxyapatite structure [75]

The composition of biological apatites and synthetic HA greatly differs from each other due to ion substitutions, crystallinity and stoichiometry [76]. Natural bone mineral consists minor cations (e.g., Na^{+}, K^{+}, Sr^{+2}, Ba^{+2}, Cu^{+2}, Zn^{+2}, Mg^{+2} or Fe^{+2}) and anions (e.g., HCO_3^{-}, HPO_4^{2-}, Cl^{-} and F^{-}) [76]. These amounts vary according to tissue type which is related to its properties and bioactivity.

The other important aspect is the Ca/P value of HA that the closer value to 1.67 denotes better material stability inside human body and decreased value denotes better bioactivity [74]. Another aspect that influences the properties of HA is its crystallinity degree. As an example, the crystallinity degree of HA is very high in tooth but very low for bone.

As reported above, the differences in structure such as composition, particle size and morphology influence the features of HA significantly and these differences mostly depend on the synthesizing techniques. Therefore, aiming better and more effective biomedical application, several methods have been studied for the preparation of HA with optimum properties that closer to living hard tissues like bone and teeth [77].

3.1.2 Thermal Stability of HA

The thermal instability of HA takes place in a 4 step process that involves dehydroxylation and decomposition (Table 3.1) [78].

Table 3.1 The thermal instability of HA in a 4 step process [78]

Step 1:	$Ca_{10}(PO_4)_6(OH)_2 \rightarrow Ca_{10}(PO_4)_6(OH)_{2-2x}O_x\propto_x + xH_2O$ (Eq. 3.1) (hydroxyapatite) (oxyhydroxyapatite)
Step 2:	$Ca_{10}(PO_4)_6(OH)_{2-2x}O_x\propto_x \rightarrow Ca_{10}(PO_4)_6O + (1-x)H_2O$ (Eq. 3.2) (oxyhydroxyapatite) (oxyapatite)
Step 3:	$Ca_{10}(PO_4)_6O \rightarrow 2Ca_3(PO_4)_2 + Ca_4(PO_4)_2O$ (Eq. 3.3) (oxyapatite) (tricalciumphosphate) (tetracalciumphosphate)
Step 4:	$Ca_4(PO_4)_2O \rightarrow 4CaO+P_2O_5\uparrow$ or $Ca_3(PO_4)_2O \rightarrow 3CaO+P_2O_5\uparrow$ (Eq. 3.4)

Step 1 and 2 shows the dehydroxylation that involves the water loss which leads to interim formation of oxyhydroxyapatite (OHAP) and then oxyapatite (OHA) where $\propto$ indicates the lattice vacancy in the OH position along the crystallographic c-axis. Step 3 and 4 shows the decomposition where OHA proceeds to secondary phases such as tricalcium phosphate, tetracalcium phosphate and calcium oxide [78].

This transformation process is important for mechanical properties of HA that its decomposition will reduce its mechanical strength. The important factors that believed the control HA decomposition are the synthesis method, sintering atmosphere and sintering temperature and holding time, phase purity and Ca/P ratio [78].

3.1.3 Mechanical Properties of HA

The desirable mechanical property of synthetic HA is to be as much as closed to that of natural bone, to enable bone remodeling at the implant site. While sintering is a typical way to improve the mechanical properties of HA, it is still inferior to natural bone (Table 3.2) [78]. Various composites of HA has been studied to enhance its mechanical properties such as polymers [79], [80], metals [81], [82] and other organics [83], [84].

Researches showed that polymers increase the mechanical stability by decreasing the brittleness of HA. However, the concern is that the osteoconductive property can be embowered since the HA particles may be embedded inside the polymer matrix. Therefore, the search of combining HA with another second phase has been proceeding

and as the second phase, the carbon nanomaterials such as carbon nanotubes and graphenes have gained much interest due to their excellent mechanical properties of them. However, the toxicity and agglomeration tendency of these structures are still a concern and this area of research must be fully investigated.

Table 3.2 Mechanical properties of bone vs. HA [78]

Mechanical properties	**Cortical bone**	**Cancellous bone**	**Dentine**	**Dental enamel**	**Dense HA**	**Porous HA**
Compressive strength (MPa)	100-230	2-12	295	384	120-900	2-100
Young's/Elastic modulus (GPa)	18-22		18-21	74-82	35-120	

3.1.4 Biological Properties of HA

Since HA structures contain only calcium and phosphate ions, there are no reports that show its toxicity. It has been widely used in biomedical applications due to its excellent biological properties which include; biocompatibility, bio-affinity, bioactivity, osteoconduction, osteointegration and osteoinduction [78].

When implanted, HA exhibits strong bonding to the bone through a carbonated calcium deficient apatite layer at the bone/implant interface. Porous HA surface also supports osteoblastic cell adhesion, growth and differentiation. The pores provide a mechanical interlock leading to a firm fixation of the material and bone tissue grows well into the pores. Minimum pore size for ingrowth of the surrounding bone together with blood supply is about 100-150 μm for macropores [85].

When used as a scaffold material, it is very crucial to match the osteoconductive properties of porous HA scaffold in one side with the osteoinductive or osteogenic properties of living bone cells in other side. Therefore, the scaffold material needs to be appropriate micro- and macroscopic structural morphology involving pore size, pore connectivity, mechanical strength and biodegradability [85].

3.2 Synthesis of Hydroxyapatite

3.2.1 Precipitation Method

This method is also called as wet precipitation or chemical precipitation or aqueous precipitation. This method is the most popular method for synthesis of HA regarding to the low cost of process and large amount production. In this method, different approaches have been studied that depends on starting materials, pH and temperature values.

One approach is using calcium hydroxide [$Ca(OH)_2$] and phosphoric acid (H_3PO_4) as starting materials (Eq. 3.5). The only byproduct of this reaction is water and there is no foreign element involved in reaction.

$$10\ Ca(OH)_2 + H_3PO_4 \rightarrow Ca_{10}(PO_4)_6(OH)_2 + 18\ H_2O \qquad \text{(Eq. 3.5)}$$

In the above reaction, the size, shape and surface area of HA are very sensitive to the addition rate of orthophosphoric acid as this rate strongly linked to the pH value of the reaction. Another important parameter is the reaction temperature because temperature determines its morphology as monocrystalline or polycrystalline. The low temperatures (< 60 °C) yield to monocrystalline structure of HA [77].

Another approach consists two reactions for HA synthesis (Eq. 3.6 and 3.7). One reaction involves ammonium phosphate [$(NH_4)_2HPO_4$] and $Ca(OH)_2$ as starting materials and other reaction involves calcium hydrogen phosphate [$Ca(H_2PO_4)_2.2H_2O$] and $Ca(OH)_2$ as starting materials.

$$10\ Ca(OH)_2 + 6\ (NH_4)_2.HPO_4 \rightarrow Ca_{10}(PO_4)_6(OH)_2 + 6\ H_2O + 12\ NH_4OH \qquad \text{(Eq. 3.6)}$$

$$7\ Ca(OH)_2 + 3\ Ca(H_2PO_4)_2.H_2O \rightarrow Ca_{10}(PO_4)_6(OH)_2 + 15\ H_2O \qquad \text{(Eq. 3.7)}$$

Higher temperatures can be used to enhance the reaction kinetics and $Ca(OH)_2$ dissolution but the reaction also take place in room temperature. The pH value can be adjusted by ammonium hydroxide (NH_4OH) addition to maintain stability of HA [86].

Other potential precipitation method is the reaction of calcium nitrate [$Ca(NO_3)_2.4H_2O$] with $(NH_4)_2HPO_4$. The grain size of the particles can be controlled by reaction time and temperature [77].

3.2.2 Sol-gel Method

A sol is a two-phase, solid-liquid system that a suspension of colloidal particles in a liquid. The gravitational forces on these particles are negligible and interactions are dominated by Van der Waals forces and surface charges. Thus, the low energy arrangement leads to stability within the system. This stability can be modified by reducing the surface charges of the particles. When the surface charge is reduced sufficiently, gelation is induced and the product is able to maintain its shape without any assistance. The product can be in different forms such as powders, coatings, fibers and etc.

Sol-gel synthesis of HA provides uniform fine-grained structures and offers a molecular-level mixing of the calcium and phosphorus precursors which improves the chemical homogeneity of resulting HA structure [87]. The range of precursors includes; calcium acetate, calcium alkoxide, calcium chloride, calcium nitrate calcium hydroxide and dicalcium phosphate dehydrate. The chemical activity and the temperature required to form the apatite structure mostly depend on the chemical nature of the precursors [77].

The sol-gel process is also suitable for the preparation of HA thin films on metal substrates that the process is simple and could be an alternative to thermal spraying which is currently used for biomedical applications [88].

3.2.3 Hydrothermal Method

A hydrothermal process is a non-conventional method to obtain nanocrystalline inorganic materials and this process consists a direct precursor-product correlation. This method uses the solubility of inorganic substances in water under high pressures and temperatures [89]. This method identifies a heterogeneous chemical reaction in the presence of a solvent above the room temperature and at pressure greater than 1 atm in a closed system [89].

For hydroxyapatite synthesis, the widely used solvent is water and substances are calcium and phosphorus precursors. The reaction takes place in a Teflon-lined autoclave at mild conditions [90]. Hydrothermal processing of hydroxyapatite provides high product purity, homogeneity, crystal symmetry and narrow particle size distributions [89].

3.2.4 Solid-State Method

Although this method has been studied less than others, it is relatively simple and inexpensive compared to other wet treatment methods [78]. This method involves combining β-tricalciumphospate and $Ca(OH)_2$ powders in specific ratios (3:0-3.8), mixing dry powders in water, wet milling, casting the mixture into bodies, drying and sintering (eq. 3.8) [78].

$$3\ Ca_3(PO_4)_2(\beta\text{-TCP}) + Ca(OH)_2 \rightarrow Ca_{10}(PO_4)_6(OH)_2 \qquad \text{(Eq. 3.8)}$$

To obtain pure HA with high crystallinity, high sintering temperature is required and the sintering temperature is a critical parameter for pure HA formation. Also the pH value is important parameter for this reaction since not-controlled pH value can cause HA agglomeration [78].

3.2.5 Biomimetic Deposition Method

Metastable synthetic body fluid (SBF) with an organic salt composition is similar to human body fluid and facilitates the spontaneous nucleation and growth of HA at physiological pH and temperature [77]. Biomimetic deposition of HA imitates the natural remineralization process of HA but in the absence of cellular and organic species [91].

The important factors for this process are the surface chemistry of the substrate materials as the formation of negatively charged surface induces hydroxyapatite growth in SBF [91]. The SBF is prepared according to the chemical compositions of human body fluid, with an ion concentration close to that of human blood plasma, kept under mild conditions of pH and identical physiological temperature [77].

The formation of hydroxyapatite by this process results a bioactive biomimetic apatite coating with better similarity to natural bone mineral. However it has slow deposition rates and the coatings are porous that results low mechanical strength.

3.3 Applications of Hydroxyapatite

3.3.1 Tissue Engineering

The bioactive ceramics have drawn many interests with the growth of tissue engineering researches. In tissue engineering applications, a scaffold is used to deliver cells to a particular clinical treatment site. Therefore, the scaffolds must have very high porosity (greater than 70-80%) with full interconnectivity. To enable the movement of cells into the scaffold, large fenestrations between pores are required that allows vascularization [92].

To date, several scaffold materials have been investigated that provides a suitable platform for cell attachment, proliferation and cell migration. As one of the bioactive material, HA has a great ability of bond formation with the host tissue over most other bone substitutes, such as allograft or metallic implants [93]. Particle size, shape and surface roughness are important parameters for HA scaffolds that affects cellular adhesion, proliferation and phenotype.

Figure 3.2 represents a macroporous hydroxyapatite scaffold with interconnected oval shaped pores of 100-300 μm. The pore size distribution and homogeneous distribution of oval shaped pores of scaffold provides favorable topographical substratum for cell attachment and ingrowth. For the repair and regeneration of hard tissue such as bone, scaffolds also need to have a high elastic modulus in order to be retained in the space they were designated for.

If the scaffold is used as a temporary load-bearing device, it needs to maintain required mechanical strength without showing symptoms of fatigue and failure. Therefore, the basic problem for a scaffold is that to achieve significant strength that the scaffold material must have sufficiently interatomic and intermolecular bonding but also permits hydrolytic attach and breakdown [94].

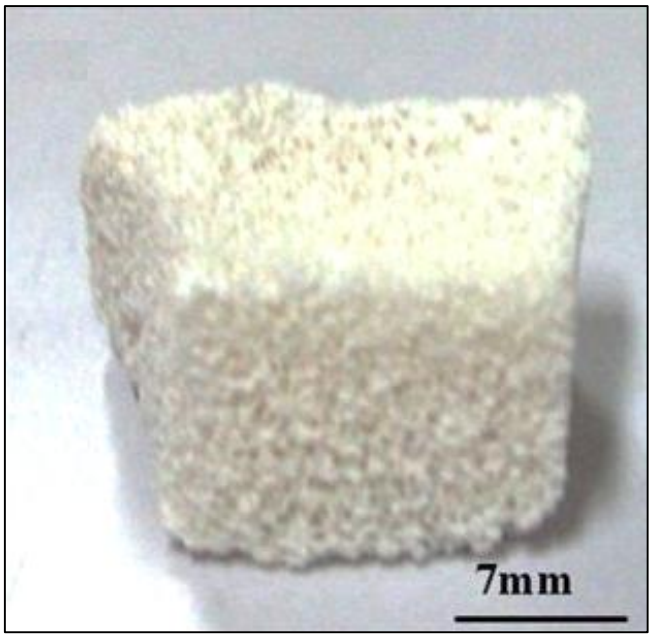

Figure 3.2 Porous hydroxyapatite body of rectangular shape produced via polymeric sponge method using sol–gel derived HA powder and polymer slurry [93]

3.3.2 Implants

Metals are extensively used for load-bearing implant applications such as artificial hip joints, knee joints, bone plates and dental implants. The important properties of an implant for load-bearing applications are high tensile strength and toughness, resistance to fatigue and resistance to time-dependent deformation or creep characteristics. The implants must also be biocompatible and bioinert. Although metal implants show these characteristics, wear-induced osteolysis, corrosion and aseptic loosening can arise due to a weak interfacial bond between host tissue and the implant materials [95].

Ceramic materials are also used as biomaterials that comprise calcium phosphates, silica, alumina, zirconia and titanium dioxide. Among all, hydroxyapatite as one of the calcium phosphate family is most widely used in orthopedics and dentistry regarding to its similar composition to bone mineral [95]. It also shows osteogenic property and able to form strong bonds with host bone tissues. Its bioactivity and degradation behavior can be controlled by changing Ca/P ratio, crystallinity and phase purity [95]. However, considering its low mechanical properties such as stiffness and brittleness, its load-bearing applications are limited. An example for HA implant is shown in Figure 3.3.

Therefore, today's solution is coating metallic implants with nanostructured calcium phosphates (mainly hydroxyapatite) (Figure 3.3). Calcium phosphates are used to impart surface bioactivity and the metallic part provides good mechanical strength for implant.

As a consequence, these composites become capable in bone formation and promoting direct osseointegration with high mechanical strength.

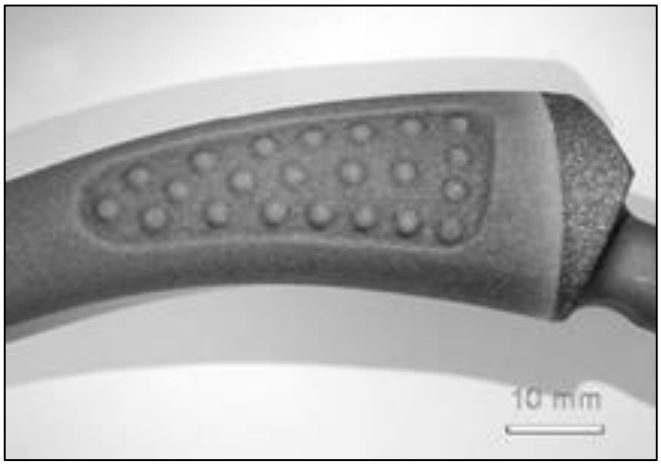

Figure 3.3 A photo of a titanium implant coated with electrochemically deposited HA at 37 ºC [96]

3.3.3 Drug Delivery

In drug delivery applications, small (< 10 μm) and interconnected pores are the key requirements for the preparation of effective drug delivery systems. These pores could carry pharmaceutical substances and release them relatively slowly. The size, amount and interconnectivity of pores are mainly responsible for the drug release and lower porosity means a larger initial burst release of drugs. The pore sizes also need to be in accordance with the size of drug molecules [97].

The use of HA as biomaterials began in dense form but later porous form is produced which makes HA a possible drug delivery carrier. The porosity consisting of small-diameter pores are the determinant in drug delivery system [97]. The porous HA structures are favorable as drug carriers due to its chemical resemblance to natural human bone.

Compared to other drug carriers, HA has better biodegradability and biocompatibility [98]. Additionally, the bioactive property of HA enables it as a drug carrier for bone tissue. Its degradation level is less toxic than silica, quantum dots, carbon nanomaterials or magnetic particles [98]. A schematic setup of a calcium phosphate matrix as a drug carrier was shown in Figure 3.4. After loading with genes or drugs, nano-sized HA provides a protective environment which guards them from degradation and in the meantime ensures a convenient pathway for cell membrane penetration and controlled

drug or gene release [96]. Large specific surface area of HA can hold larger load amounts of drugs than coarser particles. All these features make it a potential candidate for drug delivery systems.

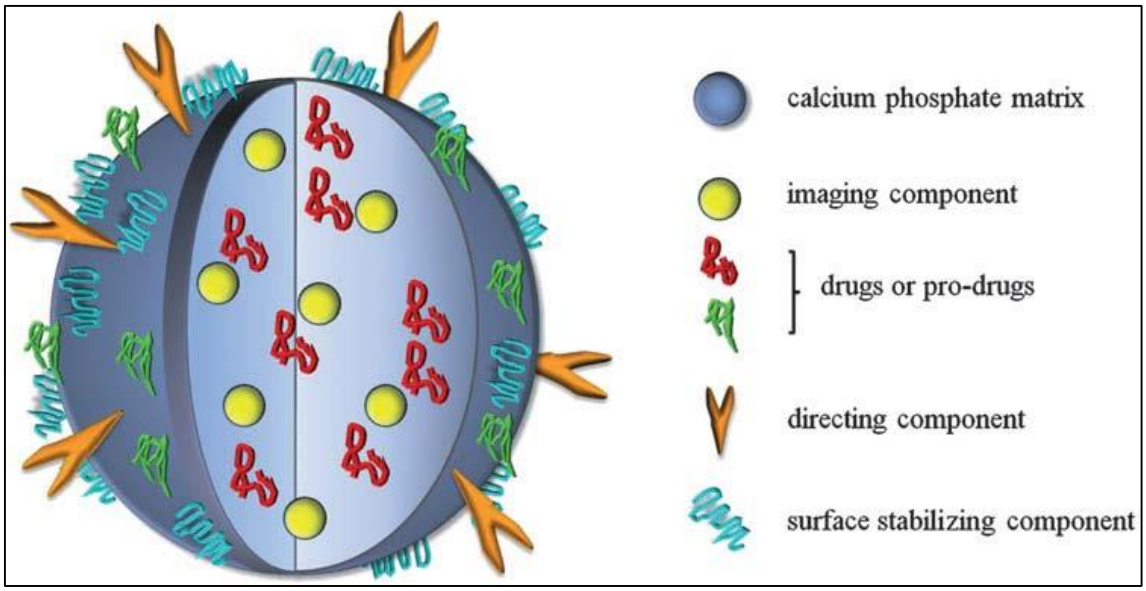

Figure 3.4 A generalized schematic setup of a nanodimensional particle of a calcium orthophosphate suitable for both imaging and drug delivery purposes[96]

CHAPTER 4

LITERATURE SURVEY

4.1 Literature Survey on Graphene Oxide Reduction

Graphene synthesis via reduction of graphene oxide is the most popular procedure regarding to its favorable advantages as reported in Section 2.4.1.2. In that way, several reports have been presented including a number of reducing agents such as hydrazine hydrate [99], hydroquinone [100], sodium borohydride [33], aluminum powder [101], sodium hydrosulfite [102], vanadium (III) [103], thiourea dioxide [104], metallic zinc [105], and ethylenediamine [106].

Despite the distinct advantages of the chemical reduction method, most of the reducing agents (hydrazine, hydroquinone, sodium borohydride etc.) have been known with their high toxic nature which could exhibit harmful effects in bio-related sciences. Therefore, to eliminate negative aspects of toxic agents, green methods have been studied in recent years including biomolecules, microbes and phytoextracts reduction. In bio-reduction process, biomolecules such as proteins, polyphenols, amino acids, alkaloids, alcoholic derivatives, enzymes, flavonoids and vitamins are used as reducing agent. The phytochemicals includes which are obtained from different parts of plants such as leaves, peels and etc. discovered as the potential reducing agents.

In this section, the studies demonstrated in the literature about the graphene oxide reduction were summarized.

Suresh et al. (2015) [107] reported a facile green method for the effective reduction of graphene oxide using Cloves (*Syzygium aromaticum*) extract by a reflux method at 100°C for 30 min. They obtained extractions in reflux conditions at 100°C for 5 h. They confirmed the formation of few layered reduced graphene oxide by using Transmission electron microscope (TEM), X-ray diffractometer (XRD) and ultraviolet-visible (UV-

Vis) studies. They evaluated carcinogenic dye degradation and antioxidant properties of the RGO and as a result, they found that Methylene blue (MB) and Malachite green (MG) eliminated completely within 20 min in dark condition in the presence of 20 mg of RGO.

Suresh et al. (2015) [108] reported the preparation of reduced graphene oxide from graphene oxide using Cinnamon (*Cinnamomum zeylanicum*) extract. They prepared cinnamon extract at 100°C under reflux conditions with constant stirring for 5 h. They mixed GO suspension with cinnamon extract and refluxed for 45 min. They demonstrated the efficient reduction and formation of few layered graphene from GO and also showed that the RGO possess significantly high dye removal property of MG and MB dyes in the absence of UV or Sun light. They suggested cinnamon extract as an environment friendly green method for efficient reduction of GO regarding to its antioxidant content.

Gurunathan et al. (2014) [109] explored the possibility of using *Ginkgo biloba* leaf extract as an alternative reducing agent for the synthesis of graphene. The extracts were prepared by boiling leaves for 5 min and then added to GO aqueous solution. The reduction reaction was carried out at 30°C for 12 and 24 hours. For extract preparation, the leaves were boiled for 5 min. They confirmed the formation of graphene by ultraviolet-visible spectrometer (UV-Vis), Fourier transform infrared spectroscopy (FTIR), XRD, Raman spectrometer, Dynamic light scattering (DLS), Scanning electron microscope (SEM) and AFM. They obtained graphene around 1400 nm in size.

Jana et al. (2014) [110] reported the green reduction of GO using drained water from soaked mung beans (*Phaseolus aureus L.).* They presented the drained water from soaked mung beans as a completely green reducing agent regarding to its biocatalyst and phytic acid contents. They soaked mung beans for overnight and decanted drained water. They mixed drained water with GO suspension and performed reaction under continuously stirring conditions for 24 h at room temperature (30±2°C) They confirmed the efficient reduction of GO and observed good electrochemical charge-discharge cyclic stability.

Barua et al. (2013) [111] prepared graphene oxide-silver nanohybrid (Ag-RGO) by simultaneous reduction of graphene oxide and silver ions using the aqueous extract of the *Colocasia esculenta* leaf. The extract was prepared by adding leaves into water and stirring for 20 min at 45°C. 10 mL of aqueous extract was added to GO dispersion with constant stirring. The reaction was performed with $AgNO_3$ addition by constant stirring for 8 h at room temperature. They confirmed the formation of the RGO-silver nanohybrid

by characterization tools [UV-Vis, FTIR, XRD, Transmission electron microscope (TEM) and Raman]. They reported that the nanohybrid shows better antimicrobial activity than the individual nanomaterials.

Firdhouse and Lalita (2013) [112] established eco-friendly reduction of graphene oxide using aqueous extract of *Amaranthus dubius* as reducing agent. The extract was prepared by stirring for 30 min at 50°C. The reduction reaction was performed under reflux conditions until the brown color solution changes to black. They confirmed the reduction by characterization tools (UV-Vis, FTIR, Raman, SEM-EDAX, XRD and Zeta potential). As a result, they obtained nanographene around 5 nm in size.

Haghighi and Tabrizi (2013) [113] used rose water as green reducing and stabilizing agent for the chemical reduction of exfoliated graphite oxide and the synthesis of reduced graphene oxide nanosheets (RGONs). They performed the reduction reaction in a Teflon-lined autoclave and heated for 5 h at 95°C. They showed the removal of oxygen containing functional groups by XRD analysis and indicated monolayer RGONs formation by AFM and Raman spectroscopy.

Lee and Kim (2013) [114] compared the abilities of seven plant leaf extracts (Cherry: *Prunus serrulata,* Magnolia: *Magnolia Kobus,* Platanus: *Platanus orientalis,* Persimmon: *Diopyros kaki,* Pine: *Pinus desiflora,* Maple: *Acer palmatum,* Ginkgo: *Ginkgo biloba)* for graphene oxide reduction. They obtained plant extracts by boiling plants in water for 5 min and optimized reaction conditions. The optimized reaction conditions were determined as follows. Type of plant: *Prunus serrulata,* reaction time: 12 h, composition of the reaction mixture: 16.7% v/v of plant leaf extract in total suspension and temperature: 95°C. They analyzed the degree of reaction by elemental analysis and XPS. They also confirmed the reduction of graphene oxide by UV-Vis, FTIR, Raman, XRD, TEM and Thermogravimetric analysis.

Kuila et al. (2012) [115] reported the simple reduction of GO sheets by using carrots in aqueous solution. Aqueous solution of carrot root was prepared with sliced carrot at room temperature (25°C) and solution was mixed with GO dispersion and stirred for 48 h. They confirmed the formation of few layer graphene by TEM and AFM and provided evidence for the elimination of labile oxygen functionality from the surface of GO by FTIR and X-Ray Photoelectron Spectroscopy (XPS).

Thakur and Karak (2012) [116] investigated the reduction of graphene oxide by phytochemicals using aqueous leaf extracts of *Colocasia esculenta* and *Mesua ferrea* Linn. and an aqueous peel extract of orange (*Citrus sinensis)*. The extracts were prepared by stirring for 20 min at 50°C. The reduction reactions were carried out by stirring or under reflux until the reduction was completed. They observed the removal of oxygen containing groups from the GO and the formation of RGO by UV-Vis, FTIR and Raman spectroscopy. They also determined the extent of reduction by elemental analysis and formation of few layers of graphene by TEM. As a result, they obtained the RGO with good specific capacitance, high electrical conductivity and high carbon to oxygen ratio.

Wang et al. (2011) [117] reported the reduction of exfoliated GO in green tea solution by making use of the reducing capability and aromatic rings of tea polyphenol (TP) that contained in tea solution. Green tea powder was boiled at 100°C for 20 min and added to GO suspension. For reduction reaction, the mixture was sonicated for 30 min and refluxed at 90°C in a nitrogen atmosphere. They found that the TP in the tea solution acts as both reducing agents and stabilizer and enables the resultant graphene good solubility in both aqueous and a variety of organic solvents.

The main findings and the experimental conditions of the studies mentioned above about the graphene oxide reduction were summarized in Table 4.1.

Table 4.1 The demonstration of the studies about plant-based reduction methods of graphene oxide

Reference	Plant Name	Plant parts/ extracts	Extraction conditions			Reduction reaction parameters		
			Reaction Type	Temp. (°C)	Time (h)	Reaction Type	Temp. (°C)	Time (h)
Suresh et al. (2015) [107]	*Syzygium aromaticum* (cloves)	Powdered cloves	Reflux	100	5	Reflux	100	0.5
Suresh et al. (2015) [108]	*Cinnamomum zeylanicum* (Cinnamon)	Powdered bark	Reflux	100	5	Stirring + Reflux	Room temperature	0.75
Gurunathan et al. (2014) [109]	*Ginkgo biloba*	Leaf	Boiling	100	5 min	Stirring	30	12 and 24
Jana et al. (2014) [110]	*Phaseolus aureus L.*	Plant	Soaking	Room temperature	Overnight	Stirring	Room temperature	24
Barua et al. (2013) [111]	*Colocasia esculenta*	Leaf	Stirring	45	20 min	Stirring	Room temperature	8
Firdhouse and Lalita (2013) [112]	*Amaranthus dubius*	Plant	Stirring	50	30 min	Stirring + Reflux	Room temperature	Until the colour changes

Table 4.1 The demonstration of the studies about plant-based reduction methods of graphene oxide (continues)

Reference	Plant Name	Plant parts/ extracts	Extraction conditions			Reduction reaction parameters		
			Reaction Type	Temp. (°C)	Time (h)	Reaction Type	Temp. (°C)	Time (h)
Haghighi and Tabrizi (2013) [113]	*Rosa sp.*	Rose water	Rose water 12% (wt) used			Sonication	95	5
Lee and Kim (2013) [114]	*Prunus serrulata*	Leaf	Boiling	100	5 min	Stirring	95	12
	Magnolia kobus	Leaf						
	Platanus orientalis	Leaf						
	Diopyros kaki	Leaf						
	Pinus desiflora	Leaf						
	Acer palmatum	Leaf						
	Ginkgo biloba	Leaf						

Table 4.1 The demonstration of the studies about plant-based reduction methods of graphene oxide (continues)

Reference	Plant Name	Plant parts/ extracts	Extraction conditions			Reduction reaction parameters		
			Reaction Type	Temp. (°C)	Time (h)	Reaction Type	Temp. (°C)	Time (h)
Kuila et al. (2012) [115]	*Daucus carrota*	Root	Stirring	25	48	Stirring	Room temperature	48
Thakur and Karak (2012) [116]	*Colocasia esculenta*	Leaf	Stirring	50	20 min	Stirring or Reflux	Room temperature	8
	Mesua ferrea	Leaf						10
	Citrus sinensis	Leaf						10
Wang et al. (2011) [117]	*Camelia sinensis*	Leaf (powder)	Boiling	100	20 min	Sonication+ Reflux	90	0.5

4.2 Literature Survey on Graphene-Hydroxyapatite Composites

Hydroxyapatite is a promising biomaterial with its significant properties such as bioactivity, osteoconductivity and etc. (detailed in Section 3.1). However, the brittleness and low strength restricts its applications under load-bearing applications. One of the suitable solutions to overcome these negative features is reinforcement of a second phase material. To date, researchers have been studied on polymers [79], [118-120], metals [121], [122], hard ceramics [123], [124] for secondary constituent material to hydroxyapatite. In the recent decade, carbon nanotubes and graphenes are gaining increasing interest as a reinforcement for hydroxyapatite with improved mechanical properties.

In this section, the studies demonstrated in the literature about the graphene-hydroxyapatite composites were summarized.

Azhari et al. (2015) [125] manufactured graphene/hydroxyapatite nanocomposite 3D structures by a powder-bed class of additive manufacturing (AM). They synthesized the nanocomposites through a dispersion-based/wet-mixing process of graphene oxide and hydroxyapatite particles (HAp). The nanocomposites prepared at different GO to HAp percentage (wt), including 0.2% and 0.4% to develop printable powder. To fabricate 3D structures of graphene/HAp nanocomposite, they utilized powders in a power-bed AM system and developed cylindrical 3D model of the structures. They printed samples at different layer thickness and binder saturation levels as process parameters of AM process. They found that at the layer thickness of 125 μm and core binder saturation level of 400%, the compressive mechanical strength of the samples were improved significantly. They also reported that 0.4% (wt) GO to HAp percentage exhibited 70 times higher mechanical strength than pure HAp structure.

Baradaran et al. (2014) [126] prepared reduced graphene oxide (RGO) reinforced hydroxyapatite nano-tube (nHA) composites. They synthesized composites in situ using a simple hydrothermal method in a mixed solvent system of ethylene glycol (EG), N,N-dimethlyformamide (DMF) and water. They synthesized GO using Hummers method and for HA synthesis, they used ammonium dihydrogen phosphate ($NH_4H_2PO_4$) and calcium chloride ($CaCl_2$) as starting materials and ethylene glycol (EG) as aqueous media. After GO addition to this mixture, they used a 50 mL Teflon-lined stainless steel autoclave for hydrothermal reaction at 200°C for 24 h. They prepared RGO-HA composites in different

concentrations of RGO in HA; 0.0, 0.5, 1 and 1.5% (wt). At the end, they performed a consolidation process by hot isostatic pressing (HIP) at 1150°C and 160 MPa to prepare composite discs. They analyzed the mechanical properties of composite discs by using indentation method. They also investigated the *in vitro* biocompatibility of RGO-HA composites. Results showed that the elastic modulus and fracture toughness of the sintered samples increased with the increase of RGO content when compared to the pure HA by 86% and 40%, respectively. Cell culture and viability test results showed that the addition of RGO promotes osteoblast adhesion that leads to the increase in biocompatibility of the RGO-HA composite.

Fan et al. (2014) [127] studied on a convenient one-pot hydrothermal strategy for the synthesis of graphene nanosheet (GNS)/hydroxyapatite (HA) nanorod composites (GNS/HA). They prepared GO colloid solution from graphite according to the modified Hummers method. For HA synthesis, they used calcium nitrate tetrahydrate [$Ca(NO_3)_2.4H_2O$] and di-ammonium hydrogen phosphate [$(NH_4)_2HPO_4$] as starting materials, cetyltrimethylammonium bromide as soft template and trisodium citrate as calcium ion (Ca^{2+}) chelator and reducing agent for GO. For one-pot hydrothermal synthesis of composite, a Teflon-lined stainless steel autoclave was used at 180°C for 24 h. The GNS/HA nanorod composites prepared with three different HA concentrations; 20, 40 and 60% (wt). The mechanical properties of HA and GNS/HA coatings were performed by nano-indentation test and the osseointegration of materials were evaluated by biomimetic mineralization method. As a result, they reported that 40% (wt) GNS/HA nanorod showed twice high value of hardness and Young's modulus values compared to HA. They demonstrated that the introduction of GNS improved the mechanical property of HA effectively and supported osseointegration ability with surrounding tissues and bone cellular proliferation.

Li et al. (2014) [128] firstly employed graphene oxide as nanoscale reinforcement fillers in hydroxyapatite coatings by a cathodic electrophoretic deposition (EPD) process and fabricated GO/HA coatings on pure Ti substrate. They prepared GO/HA coatings with three different concentrations of GO including 0, 2 and 5% (wt). The deposition process was conducted at a constant voltage of 30 V and deposition times of 1-5 min, with a stainless steel electrode (anode) and a Ti substrate (cathode) 2 cm apart. They evaluated corrosion resistance of the samples by open circuit potential (OCP)- time measurements, anodic polarization experiments and electrochemical impedance analysis. They tested the

adhesion strength of the sintered samples using a universal testing machine and evaluated the *in vitro* biocompatibility of the GO/HA coated Ti sheets to L929 murine fibroblast cell lines and MG63 human osteoblast-like cell lines using cell counting kit 8 and direct contact method. Results showed that the addition of GO into HA coatings reduced the surface cracks and increase the coating adhesion strength. They also indicated that GO/HA composite coatings exhibited higher corrosion resistance and superior in vitro biocompatibility compared to pure HA coated and uncoated Ti substrate.

Li et al. (2014) [129] synthesized a graphene oxide-ultrathin plate-like hydroxyapatite (HAp) hybrid via *in situ* mineralization. They directly used GO as a mineralization substrate and reinforced component to produce the biomimetic GO-HAp composites. They prepared GO from graphite by a modified Hummers method. For HAp synthesis, they used disodium hydrogen phosphate and calcium chloride as starting materials in ethylene glycol-water mixture solvent. They performed reaction at 85±1°C for 12 h to accelerate the mineralization process. After mineralization process, the GO surfaces were covered by the formed nanoplates. They performed stress-strain test and in vitro cytotoxicity tests to GO-HAp material. They reported that GO-HAp paper was significantly stiffer (223% higher) than that of unmodified GO paper and the tensile strength was 78% higher than the GO paper. They also showed that after modified by HAp crystals, the toxicity of GO was reduced and the biocompatibility of GO had been significantly enhanced.

Nunez et al. (2014) [130] studied on the growth of non-stoichiometric nanocrystalline hydroxyapatite (nHAp) with a composition similar to natural bone by a wet-chemical-in-situ precipitation route on carbon nanotubes with different degrees of oxygen functionalities and on graphene oxide. They prepared oxidized carbon nanotubes (oCNTs) with higher and lower oxidation degree by refluxing pristine CNTs and prepared graphene oxide using a modified Hummers method. For nHAp preparation, they used calcium carbonate ($CaCO_3$) and phosphoric acid (H_3PO_4) as starting materials and performed precipitation reaction at pH above 10 to avoid hydroxyapatite dissolution. After that, composites were prepared by dispersing the carbon nanomaterial in the ammonia solution before addition of precursor solution. They analyzed morphology, crystalline size, composition and interfacial bonding of the nHAp to the respective nanocarbon support surface. They also studied the in vitro bioactivity of the nanocomposites.

As a result, they demonstrated that functionalization degree and morphology of CNTs and GO are critical parameters controlling the shape and crystallinity of the nHAp nanoparticles in the corresponding composite materials. They achieved crystalline nHAp nanoparticles with rod-like morphology for moderately oxidized CNTs and for GO. In vitro bioactivity of the prepared composites exhibited a fast apatite biomineralization process, induced by the presence of nHAp. For all that reason, they suggested GO as a valuable bioceramic support material.

Oyefusi et al. (2014) [131] successfully grafted hydroxyapatite to carboxylated CNTs and graphene nanosheets (GNS). They used functionalized CNTs by acid treatment and graphenes which was prepared from graphite powder according to Hummers method and reduced by ethylenediamine (EDA). Calcium hydroxide [$Ca(OH)_2$] and H_3PO_4 were used as starting materials for HA synthesis and pH of the suspension was adjusted to ≈ 9. The composites were prepared using precipitation method by mixing HA and CNTs or graphenes in aqueous media. They reported the fabrication of CNTs-HA and GNS-HA and characterization, including the proliferation and differentiation of bone cells in the media containing these nanocomposites. The results showed that bone cells proliferate and differentiate well in treatment media containing CNTs-HA and GNS-HA.

Liu et al. (2013) [132] reported HA-reduced graphite oxide nanocomposites synthesized by a liquid precipitation approach followed by spark plasma sintering (SPS) consolidation. They synthesized RGO from graphite using Hummers method followed by thermal reduction process. For HA synthesis, $Ca(NO_3)_2.4H_2O$ and $(NH_4)_2HPO_4$ were used as starting materials and reaction performed at pH value of 11. They prepared RGO-HA composite powders with different contents of RGO; 0, 0.1 and 1% (wt.). The composites were further consolidated by SPS at temperature of 950°C and pressure of 30 MPa for 3 min. They evaluated mechanical and biological properties of composites. They reported that rod-like HA grains with the dimensions of ~9 nm in diameter and 20-45 nm in length exhibited oriented nucleation and epitaxial growth on graphene flakes. The fracture toughness of the RGO-HA composites reached to 3.94 MPa $m^{1/2}$, showing a 203% increase compared to pure HA. The composites also showed enhanced in vitro cell behavior.

Liu et al. (2013) [133] produced hydroxyapatite-graphene nanosheet (HA-GNS) composites by liquid precipitation approach and following coating deposition by vacuum cold spraying. They synthesized graphene from graphite and prepared HA using

stoichiometric reaction between $(NH_4)_2HPO_4$, $Ca(NO_3)_2$ and NH_3H_2O. HA with the size of ~20-45 nm in length and ~10 nm in diameter was produced and HA-GNS composites were obtained by addition of GNS solution to HA. HA coatings vacuum cold sprayed onto Ti substrates at room temperature. Composites were prepared at different GNS contents; 0, 0.1 and 1% (wt).The study concluded that the coatings are showed competitive adhesive strength and fracture toughness (0.109±0.012 MPa $m^{1/2}$ for pure HA, 0.175±0.006 MPa $m^{1/2}$ for the HA-0.1% (wt) GN, 0.421±0.011 MPa $m^{1/2}$ for the HA-1% (wt) GNS). They also reported that the GNS-containing HA coatings markedly enhanced attachment and proliferation of the osteoblast cells.

Neelgund et al. (2013) [134] functionalized GNS by in situ deposition of hydroxyapatite through a facile chemical precipitation method. Prior to grafting of hydroxyapatite, they synthesized graphene oxide using Hummers method and obtained GNS by the reduction of graphene oxide with ethylenediamine. For hydroxyapatite deposition, they used $Ca(OH)_2$ and H_3PO_4 as starting materials and adjusted pH to ≈ 9. They reported that the hydroxyapatite successfully grafted over well exfoliated graphene nanosheets without destroying the structure.

Zanin et al. (2013) [135] presented a method for the direct electrodeposition of globular nano-hydroxyapatite (nHAp) onto reduced graphene oxide. They prepared RGO samples on Ti substrates by a hot filament chemical deposition vapor system (HFCVD). After that, they functionalized RGO samples using a pulsed-direct current plasma reactor with oxygen flow to change RGO surface hydrophobicity. They performed the electrodeposition of nHAp crystals onto superhydrophilic-RGO films using $Ca(NO_3)_2.4H_2O$ and $(NH_4).2HPO_4$ electrolytes at 4.7 pH. The characterization test results showed that homogenous, high crystalline, stoichiometric nHAp crystals formed without any thermal treatment. The nHAp/RGO composites were reported as an appropriate surface for mesenchymal stem cell adhesion with active formation of membrane projections.

Gonçalves et al. (2012) [136] investigated graphene oxide and functionalized carbon nanotubes (F-CNTs) as the reinforcing agent in a poly(methyl methacrylate) (PMMA)/hydroxyapatite bone cement. They synthesized graphene oxide from graphite by Hummers method and functionalized CNTs by acid treatments. They prepared a PMMA/high-load HA/nanofiller (GO or F-CNTs) cement powder mixture in different concentrations; 0.01, 0.1, 0.5 and 1% (wt) of GO or CNTs. They obtained mixed results

for the changes in the mechanical properties (storage modulus, bending strength and elastic modulus) for the reinforced cement relative to the unreinforced counterpart. They postulated that each of the nanofillers hampered the polymerization process in the cement. They also compared the nanofillers according to mechanical properties and concluded that GO-reinforcement cements showed higher values of some of the mechanical properties compared to the unreinforced cements.

The main findings and the experimental conditions of the studies mentioned above about graphene-hydroxyapatite composites were summarized in Table 4.2.

Table 4.2 The demonstration of the studies about graphene-HA composites

Reference	Graphene type	Graphene concentration in composite (wt%)	HA synthesize conditions			Synthesis method of composites	Mechanical improvements compared to pure HA
			Starting materials	Reaction Type	pH		
Azhari et al. 2015 [125]	Graphene oxide	0.2, 0.4	Purchased			Powder bed class of additive manufacturing	70 times higher mechanical strength
Baradaran et al. 2014 [126]	Reduced graphene oxide	0.5, 1, 1.5	$NH_4H_2PO_4$, $CaCl_2$	Hydrothermal	-	In situ hydrothermal method	86% higher elastic modulus and 40% higher fracture toughness
Fan et al. 2014 [127]	Graphene nanosheet	40, 60, 80	$Ca(NO_3)_2.4H_2O$ $(NH_4)2HPO_4$	Hydrothermal	-	One pot hydrothermal method	Twice high value of hardness and Young's modulus values
Li et al. 2014 [128]	Graphene oxide	0.2, 5	Purchased			Cathodic electrophoretic deposition	Reduced the surface cracks and increase the coating adhesion strength
Li et al. 2014 [129]	Graphene oxide	32.1	$NH_4H_2PO_4$, $CaCl_2$	Mineralization	-	In situ mineralization	223% higher stiffness, 78% higher tensile strength

Table 4.2 The demonstration of the studies about graphene-HA composites (continues)

Reference	Graphene type	Graphene concentration in composite (wt%)	HA synthesize conditions			Synthesis method of composites	Mechanical improvements compared to pure HA
			Starting materials	Reaction Type	pH		
Nunez et al. 2014 [130]	Graphene oxide	15	$CaCO_3$ H_3PO_4	Precipitation	10	Dispersion	-
Oyefusi et al. 2014 [131]	Graphene nanosheet	-	$Ca(OH)_2$ H_3PO_4	Precipitation	9	Mixing	-
Liu et al. 2013 [132]	Graphene nanosheet	0.1, 1	$Ca(NO_3)_2.4H_2O$ $(NH_4)_2HPO_4$	Precipitation	11	Spark plasma sintering	203% increase in fracture toughness
Liu et al. 2013 [133]	Graphene nanosheet	0.1, 1	$(NH_4)_2HPO4$ $Ca(NO_3)_2$	Precipitation	-	Vacuum cold spraying	386% increase in fracture toughness
Neelgund et al. 2013 [134]	Graphene nanosheet	0.1, 1	$CaCO_3$ H_3PO_4	Precipitation	9	In situ deposition	-

Table 4.2 The demonstration of the studies about graphene-HA composites (continues)

Reference	Graphene type	Graphene concentration in composite (wt%)	HA synthesize conditions			Synthesis method of composites	Mechanical improvements compared to pure HA
			Starting materials	Reaction Type	pH		
Zanin et al. 2013 [135]	Reduced graphene oxide	-	$Ca(NO_3)_2.4H_2O$ $(NH_4).2HPO_4$	Electrodeposition	4.7	Direct electrodeposition	-
Gonçalves et al. 2012 [136]	Graphene oxide	0, 0.1, 0.5, 1	Purchased			Freeze-granulation technique	Higher bending strength and elastic modulus

CHAPTER 5

MATERIALS AND METHODS

5.1 Materials

5.1.1 Chemicals

High purity (99.9995%) graphite rods were purchased from Alfa Aesar. Potassium permanganate ($KMnO_4$), hydrochloric acid (37%) (HCl), acetone, hydrogen peroxide solution (35%) (H_2O_2), ortho-Phosphoric acid (85%) (o-H_3PO_4), sulfuric acid (95-98%) (H_2SO_4), and ammonia solution (25%) (NH_4OH) were purchased from Merck. Calcium hydroxide [$Ca(OH)_2$] were purchased from Sigma-Aldrich.

5.1.2 Plants

Six different natural products were used in this study: *Achillea nobilis L.* (Yarrow), *Laurus nobilis L.* (Daphne), *Lavandula agnustifolia Miller* (Lavandula), *Melissa officinalis L.* (Melissa), *Rosae caninae fructus* (Rosehip) and *Salvia officinalis L.* (Salvia). These plants were purchased in dried form from Zeytinburnu Medical Plants Garden located in İstanbul. Digital images of the plants can be seen in Figure 5.1.

Figure 5.1 The digital images of the plants

5.1.3 Apparatus

- **Filters**

For filtration of the samples, filter papers and syringe filters were used. Filter papers were Macherey-Nagel MN 640 with 110 mm diameter and syringe filters were 33 mm diameter sterile Sartorius filters by a 0.45 μm pore size hydrophilic Polyvinylidene fluoride (PVDF) membrane.

- **Magnetic Stirrer**

During the experiments, IKA-RCT standard magnetic stirrer was used to stir the mixtures in various temperatures and rpms. It can be used in speed range of 0-1500 rpm and temperature range of 0-310°C.

- **Analytical Balance**

During the experiments, OHAUS Explorer EX324 analytical balance was used. It has 320 g capacity with 0.1 mg readibility.

- **Vortex**

Benchmixer BV1000 Vortex was used for rapid vortexing of samples. It includes full 50 mL tubes at a variable speed of 200 to 3200 rpm. The operating temperatures for vortex is 4-65°C and it can be operated by touching or in continuous mode.

- **Oven**

MMM Vacucell 22 Vacuum Drying Oven was used for vacuum drying of samples. It has 22 liter capacity and can be operated from ambient temperature to 200°C with the sensitivity of ±0.4°C.

Heratherm OGS60 Lab Oven was used for drying of samples in atmospheric pressure. It has 65 liter capacity and can be operated at temperatures from 50 to 250°C with the sensitivity of ±0.4°C.

- **Ultrapure Water System**

Milli-Q Reference Ultrapure Water Purification System was used for water purification. It has 18.2 MΩ.cm at 25°C and the Total Organic Carbon (TOC) value of the system is smaller than 5 µg/L.

- **Blender**

Waring 8011EB Commercial Blender was used to cut plants into small pieces. The blender has 1 liter capacity and can be operated at 18000 rpm for low-speed mode and at 22000 rpm for high-speed mode.

- **pH Meter**

During the experiments, for measuring pH values, Mettler Toledo Seven Compact S220 pH meter was used. Its pH range is -2.000 to 20.000 with ±0.002 relative accuracy. It can be operated in temperatures of -5.0 to 130.0°C with the temperature accuracy of ±0.1°C.

- **Ultrasonic Bath**

During the experiments, Bandelin Sonorex Digitec Ultrasonic Bath was used for sonication in various temperatures. It has 9 L capacity and the temperature of the bath can be controlled in the range of 20-80°C. It has automatic frequency control at 35 kHz and ultrasonic peak output is 860 W. The ultrasonic bath was shown in Figure 5.2.

- **Centrifuge**

HERMLE Z206A Compact Research Centrifuge was used for centrifugations. Operation of the centrifuge can be timed from 10 seconds to 99 hours (or continuous) and speed can be set and viewed in both rpm and rcf (up to 6,000 rpm/ 4.427 x g). The speed range is 200 rpm to 6,000 rpm. It holds six rotor with 50 mL capacity per one. The centrifuge was shown in Figure 5.3.

Figure 5.2 Bandelin Ultrasonic Bath

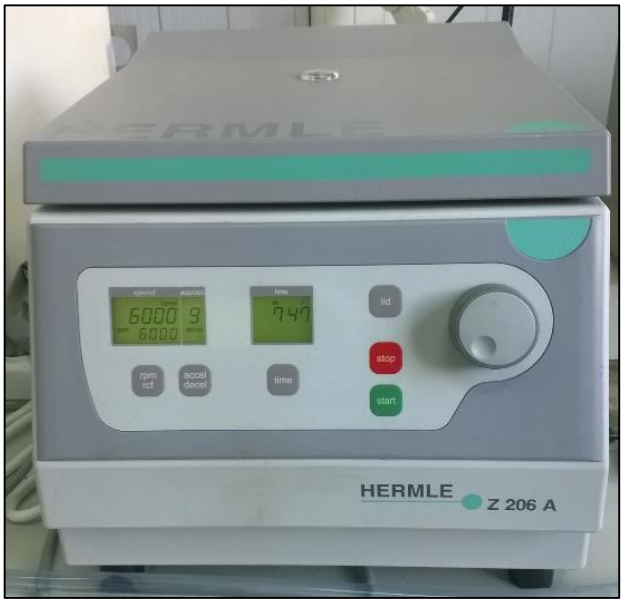

Figure 5.3 Hermle Centrifuge

- **Tube Furnace**

Protherm PTF15/50/610 Tube Furnace was used for sintering of the samples in argon atmosphere. The maximum operating temperature of the furnace is 1500°C. It has 510 mm heated length and 200 mm stable zone length with ±5°C sensitivity. Figure 5.4 indicates the Protherm Tube Furnace.

Figure 5.4 Protherm Tube Furnace

- **Press**

During the experiments, MANFREDI OL57 Hydraulic Press was used to make samples in cylindrical pellet forms with 13 mm diameter and 3 mm height. The maximum working pressure is 200 atm. It was shown in Figure 5.5.

Figure 5.5 Manfredi Hydraulic Press

5.2 Experimental Study

5.2.1 Preparation of Graphene Oxide

Graphene oxide was prepared from powdered graphite nanorods by using Hummers' method. 2 g graphite powder was added to 46 mL of concentrated 98% H_2SO_4 and the mixture was stirred for 1 h. 6 g of $KMnO_4$ was added gradually to maintain the reaction temperature below 20°C. The resulting mixture was stirred at 35 °C for 2 h and then, 92 mL of ultrapure water was added slowly. The mixture was stirred for an additional 1 h and diluted further with 280 mL ultrapure water. Then, 10 mL of H_2O_2 (35%) was added drop wise and the suspension dark brown colour turned to yellow. The resulting GO suspension was left overnight, and the clear supernatant was decanted. The remaining GO suspension was washed by centrifugation first with HCl (5%v/v) and acetone to remove excess of manganese salt and followed by ultrapure water three times. Before all the centrifugation steps, the mixtures were vortexed. The supernatant was decanted and the precipitation of purified GO was dried in vacuum oven at 60°C for 24 h.

5.2.2 Preparation of Plant Extracts

2 g of dried plants were cut into pieces by a commercial blender and added to 50 mL of ultrapure water. To optimize the extraction conditions, the extraction reactions were carried out under sonication at temperatures of 50±5°C and 80±3°C, respectively. The mixtures were sonicated for 2 h. The extracts were first filtered by a filter paper followed by repeat filtration with a 0.45 μm syringe membrane filter.

5.2.3 Reduction of Graphene Oxide

For the reduction of graphene oxide, 50 mg of GO was dispersed in 100 mL ultrapure water by sonication for 30 min. 20 mL of plant extract added to GO suspension, and the mixtures were stirred in a magnetic stirrer at 1000 rpm for 1 h and 600 rpm for additional 12 h at room temperature. The resulting black dispersions were centrifuged at 6000 rpm with ultrapure water several times including vortex mixing before all centrifugation steps. The supernatant were decanted, and the precipitate of purified reduced graphene oxide was dried in an oven at 80°C for 24 h. The nominations given to the reduced graphene oxides were presented at Table 5.1.

Table 5.1 The nominations given to the reduced graphene oxides

ARGO	: presents the reduced graphene oxide by *Achillea nobilis* extract
LNRGO	: presents the reduced graphene oxide by *Laurus nobilis* extract
LARGO	: presents the reduced graphene oxide by *Lavandula agnustifolia* extract
MRGO	: presents the reduced graphene oxide by *Melissa officinalis* extract
RRGO	: presents the reduced graphene oxide by *Rosae caninae* extract
SRGO	: presents the reduced graphene oxide by *Salvia officinalis* extract

5.2.4 Synthesis of RGO-HA Composites

As the optimum reduction efficiency was seen for *Melissa officinalis* extracts reactions after evaluation of the characterization tests (Figure 6.2), the reduced graphene oxide by *Melissa officinalis* (MRGO) was chosen for RGO-HA composites synthesis. These composites were synthesized at four different concentrations of RGO in HA; 0, 0.25, 0.5, 1 and 2% (wt). For HA synthesis, $Ca(OH)_2$ and o-H_3PO_4 were used as starting materials.

Firstly, 2.5, 5, 10 and 20 mg of MRGO (which corresponding to the concentrations of RGO in HA; 0.25, 0.5, 1 and 2% (wt), respectively) were dispersed in 100 mL of ultrapure water, and then these dispersed solutions were sonicated for 30 min.

Secondly, MRGO dispersions (100 mL) were added in Erlenmeyers containing 0.1 M of 100 mL $Ca(OH)_2$ solution which beforehand prepared by stirring at 750 rpm with a magnetic stirrer for 1 h at room temperature. In the meantime, another solution (for pure HA) was prepared without adding any MRGO dispersion for comparison.

After, as-prepared mixtures were stirred at 750 rpm and 40°C for additional 1 h. 0.06 M (404 μL) of o-H_3PO_4 was added to mixtures for achieving the ratio of 1.67 Ca/P, and pH values of these mixtures were adjusted to ≈ 9 with NH_4OH addition [134], [137], [138]. Then, these mixtures were stirred vigorously at 40°C and 1400 rpm for 2 h.

Finally, the resulting mixtures were washed with ultrapure water three times and centrifuged 15 minutes at 6000 rpm after each washing. The supernatants were decanted and the precipitates were dried at 80°C for 24 h.

5.2.5 Sintering of RGO-HA composites

Before sintering, as-prepared four powders of RGO-HA composites at various concentrations and pure HA sample were loaded into hydraulic press and these samples were pressed at 100 atm for 2 minutes. After pressing, the powder samples were obtained in cylindrical pellet forms in a diameter of 13 mm and a height of 3 mm. The RGO-HA pellets and pure HA pellet were placed in a tube furnace for sintering process. Pellets were sintered at 800°C in argon atmosphere for 1 h [137], [139]. The heating and cooling rate for tube furnace was 5°C/min. During sintering process, the flow rate of argon gas was 5 mL/min. The digital images of sintered pellets were given in Figure 5.6.

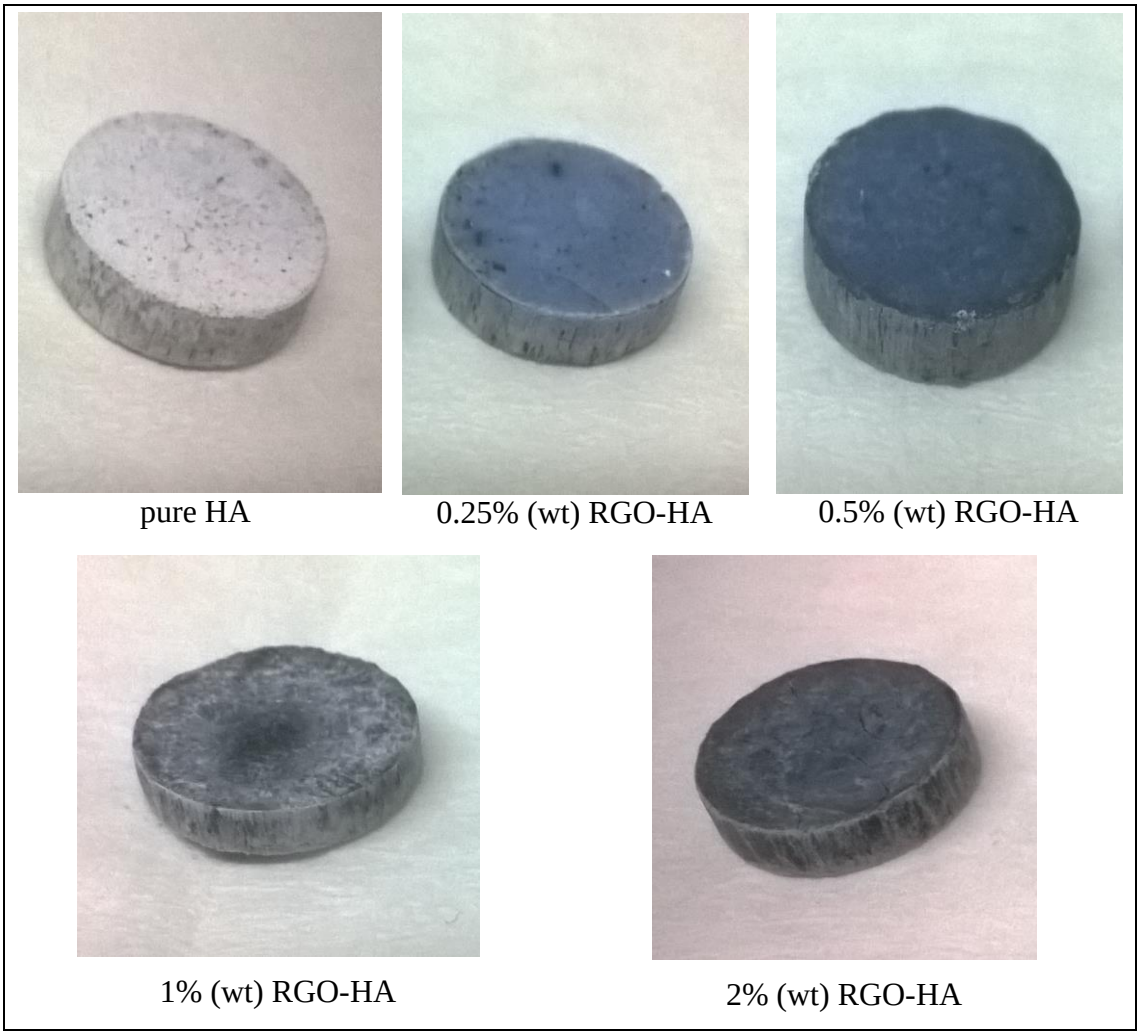

Figure 5.6 Digital images of sintered pellets of pure HA pellet and RGO-HA composite pellets

5.3 The Characterization Studies

The characterization studies were carried out by UV-Vis, FTIR, TGA, XRD, SEM and TEM analysis. UV-Vis spectrums were used to confirm the reduction reaction and FTIR spectrums were used to confirm the removal of oxygen containing groups of graphene oxide. FTIR analysis were also used for confirmation of HA formation and the RGO presence in composite. Thermogravimetric analysis were used to observe the mass change of samples as a function of increasing temperature. XRD analysis were used to evaluation of the phase composition of pure HA sample and RGO-HA composites. SEM and TEM images were carried out to determine morphology of the samples. The mechanical properties of samples were evaluated by Universal Testing Machine.

5.3.1 UV-Visible Spectrophotometer

UV-Visible spectrums of aqueous graphene oxide dispersion and reduced graphene oxide in ultrapure water were recorded by a T80+ UV/Vis Spectrophotometer (PG Instruments Ltd.) (wavelength range of 200-800 nm) (Figure 5.7). It is a high double beam spectrophotometer available with a fixed (2 nm) or variable (0.5, 1, 2, 5 nm) spectral bandwidth. It has a 190-1100 nm spectral range and the wavelength accuracy is ±0.3 nm.

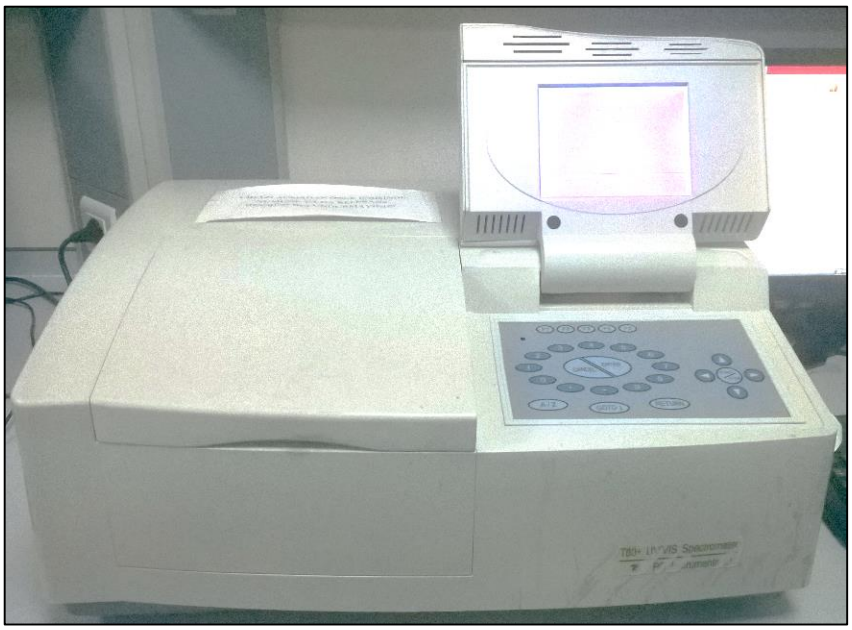

Figure 5.7 PG Instruments T80+ UV/Vis Spectrophotometer

5.3.2 Fourier Transform Infrared (FT-IR) Spectrometer

The functional groups of samples were analyzed with FT-IR spectroscopy measurements which were mounted by using a Bruker Tensor 27 Attenuated Total Reflection (ATR) FT-IR Spectrometer at room temperature in 450-4000 cm^{-1} range (Figure 5.8). It also has 370-7500 cm^{-1} spectral range with standard KBr beamsplitter. The wavenumber accuracy is ±0.01 cm^{-1} and photometric accuracy is ±0.1% T.

Figure 5.8 Bruker Tensor 27 ATR/FT-IR Spectrometer

5.3.3 Thermogravimetric/Differential Thermal Analyzer (TG/DTA)

Thermogravimetric (TG) analysis of samples were performed using an EXSTAR SII TG/DTA6300 instrument (Figure 5.9). It can be operated from ambient temperature to 1500°C. The TG measurement range is 200 mg with ±0.2 μg accuracy. It can work in air or inert atmosphere. In the present study, each measurement was carried out from room temperature to 800°C at a heating rate of 10°C/min under nitrogen atmosphere with a flow rate of 200 ml/min.

5.3.4 Mechanical Testing Instrument

The sintered composite pellets were mechanically tested by a Universal Instron Mechanical Testing System (Instron 5982) (Figure 5.10). The maximum work load of the system is 100 kN and workload accuracy is ±0.5%. It has a speed range from 0.0001 to 1016 mm per minute.

In the present study, the cylindrical samples with a diameter of 13 mm and a high of 3 mm were produced for mechanical testing. The mechanical testing analysis were performed under room temperature. The cross-head speed was set to 0.5 mm/min [140], [141]. Each measurement was repeated three times and the average of the compressive strength values were calculated.

Figure 5.9 EXSTAR SII TG/DTA6300 Analyzer

Figure 5.10 Instron 5982 Universal Testing Machine

5.3.5 X-Ray Powder Diffraction

PANalytical X'Pert Pro analyzer was used to study on X-Ray diffraction patterns of the sintered samples (Figure 5.11). XRD analyzer was equipped with Cu-Kα radiation source. The scanning angle 2θ ranged between 2° and 90° with a step scanning rate of $3°min^{-1}$ at 45 kV and 40 mA.

Figure 5.11 PANalytical X'Pert Pro Analyzer

5.3.6 Scanning Electron Microscope

Zeiss EVO LS10 operating in beam mode at 20 kV with secondary electron detector was used to acquire SEM images (Figure 5.12). The solid samples transferred to a carbon tape held onto a SEM sample holder for analysis. The powders were coated by gold for 45 seconds in argon plasma with Quorum SC7620 Sputter Coater shown in Figure 5.13. The analysis of the samples were carried out at an average working distance of 12.5 mm.

Figure 5.12 Zeiss EVO LS10 Scanning Electron Microscope

Figure 5.13 Quorum SC7620 Sputter Coater

5.3.7 Transmission Electron Microscope

JEOL 2100 HRTEM (High Resolution Transmission Electron Microscope) was used to acquire TEM images (Figure 5.14). The TEM images were taken in TUBİTAK Marmara Research Center.

Figure 5.14 JEOL 2100 HRTEM

CHAPTER 6

RESULTS AND DISCUSSION

In the present study, graphene which is the strongest material ever known was chosen as the second material to HA. As one of the member of graphene family, reduced graphene oxide was used as reinforcement material regarding to its low-cost production. Reduced graphene oxide was synthesized with a plant-based and environmentally friendly process. Six different plants were used for reduction process and their reduction performances were compared. As the *Melissa officinalis* extract showed highest reduction efficiency, the MRGO sample was chosen as second material to HA. The details of the experiments performed were given in the following sections.

6.1 FTIR Analysis of Reduced Graphene Oxide Samples

Firstly, the plant extraction experiments were performed under sonication at 50°C for 2 h [142]. Then, the plant extracts obtained were used for graphene oxide reduction process. Secondly, the graphene reduction experiments were performed by mixing extracts with graphene oxide at room temperature for 13 h. After plant reduction process, the RGO samples obtained were analyzed by FTIR spectroscopy.

According to the data obtained for graphene samples reduced by plant extracts obtained at 50°C, as shown in FTIR spectrum of graphene oxide in Figure 6.1, the broad peak at 3,318 cm^{-1} originates from the stretching vibrations of –OH groups and the peak observed at 1,715 cm^{-1} arising from the C=O stretching vibrations of carbonyl and carboxyl groups. The spectrum of graphene oxide also exhibits peak at 1,610 cm^{-1} for C=C skeletal vibrations and at 1,045 cm^{-1} for C-O (epoxy or alkoxy). As can be seen in Figure 6.1, the peak intensities of oxygen containing moties did not show relative decrease after reduction reactions with plant extracts. Therefore, to obtain more concentrated plant extracts, the temperature during the extraction process was increased from 50 to 80°C. In

the studies demonstrated by Suresh et al. (2015) [113] and Wang et al. (2011) [117], the plant extraction process was also performed at high temperature such as 100ºC under reflux and boiling treatments, respectively.

According to the data obtained for graphene samples reduced by plant extracts obtained at 80°C, the FTIR spectrums of RGOs can be seen in Figures 6.2-6.4. In the spectrums of RRGO and LARGO presented in Figure 6.3, the peak intensities decreased more than ARGO and LNRGO presented in Figure 6.2 but less than MRGO and SRGO presented in Figure 6.4. In Figure 6.4, after the plant-based reduction process, the peak at 1,715 cm^{-1} was disappeared and at 1,610 cm^{-1} and 1,045 cm^{-1} peak intensities decreased significantly in MRGO spectrum regarding to removal of oxygen containing groups. Additionally, the intensity of the broad band at 3,318 cm^{-1} showed relative decrease in SRGO and MRGO spectrum. Therefore, the rest of plant extraction processes were carried out at 80°C for 2 h.

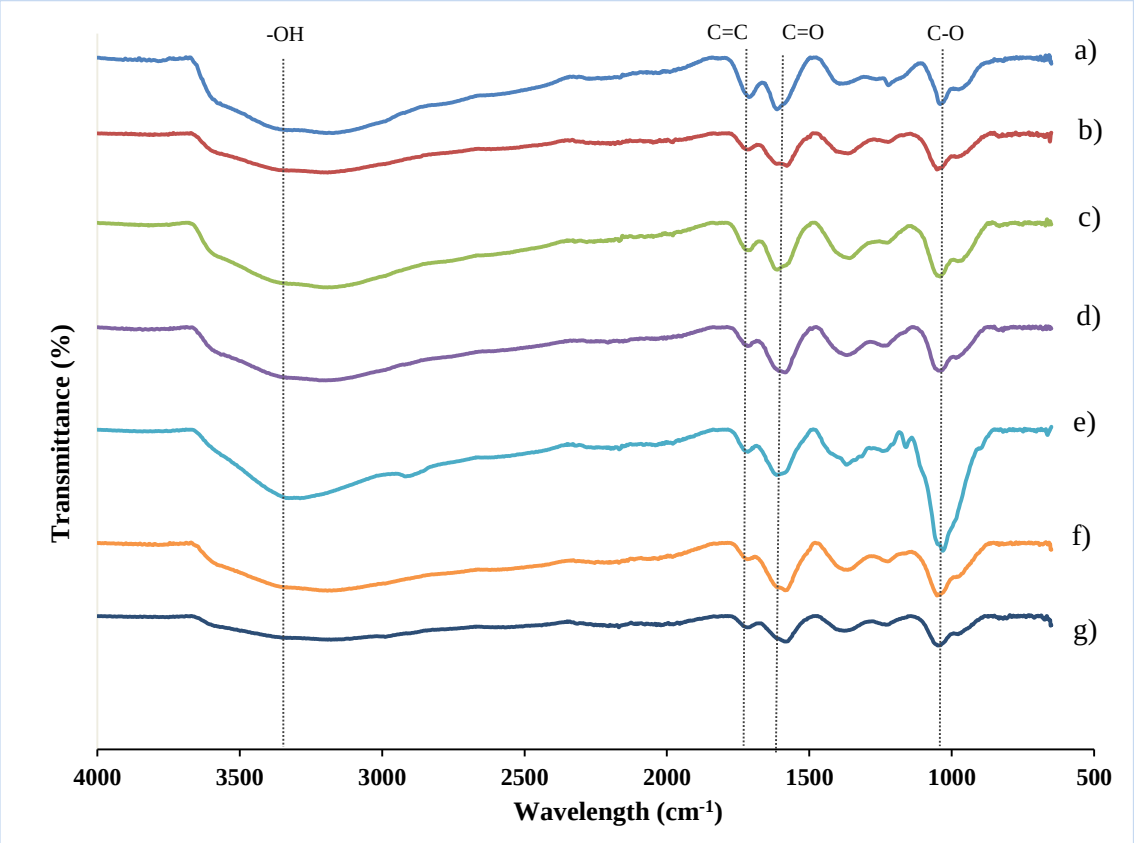

Figure 6.1 FTIR spectrums a) GO, b) ARGO, c) LNRGO, d) LARGO, e) RRGO, f) MRGO and g) SRGO for the plant extraction at 50°C

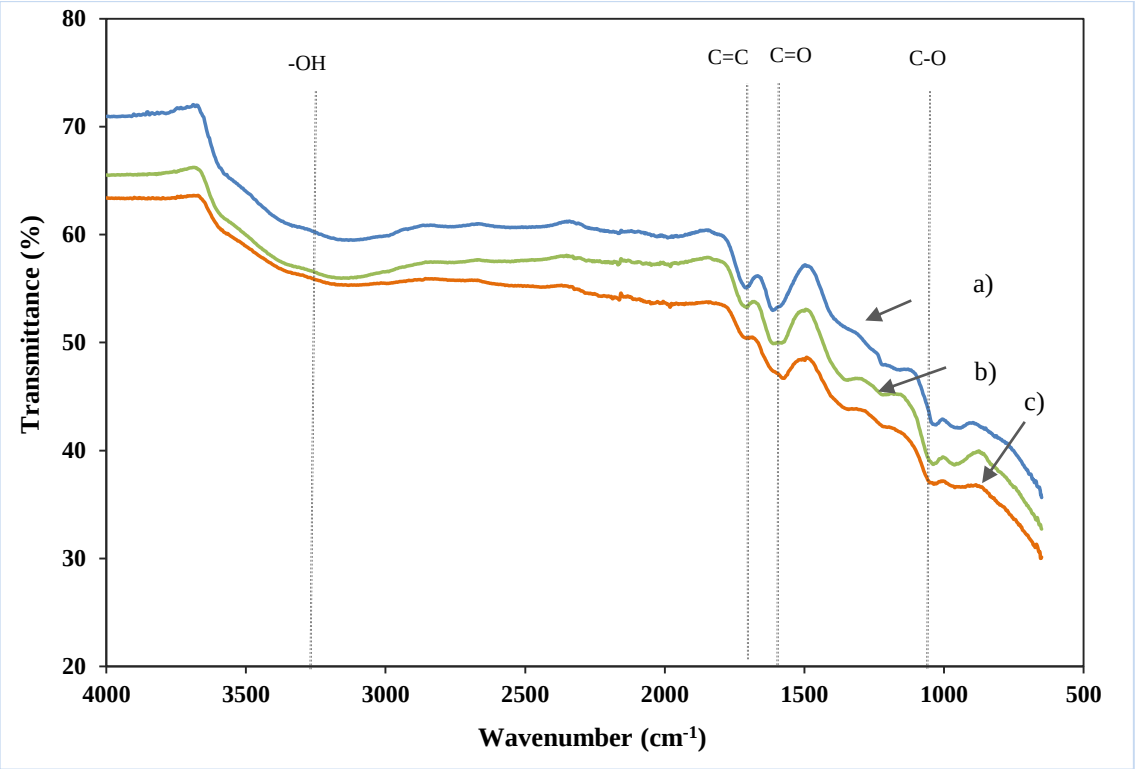

Figure 6.2 FT-IR spectrums of a) GO, b) ARGO and c) LNRGO for the plant extraction at 80°C

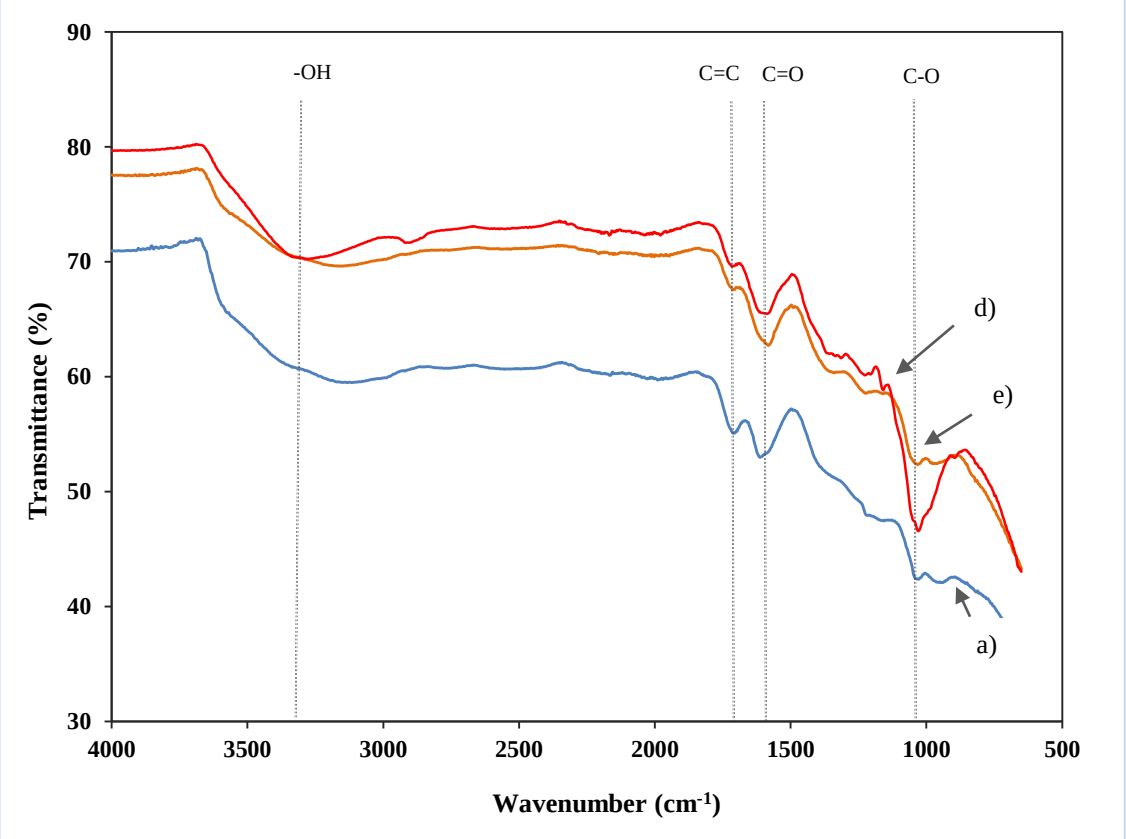

Figure 6.3 FT-IR spectrums of a) GO, d) LARGO and e) RRGO for the plant extraction at 80°C

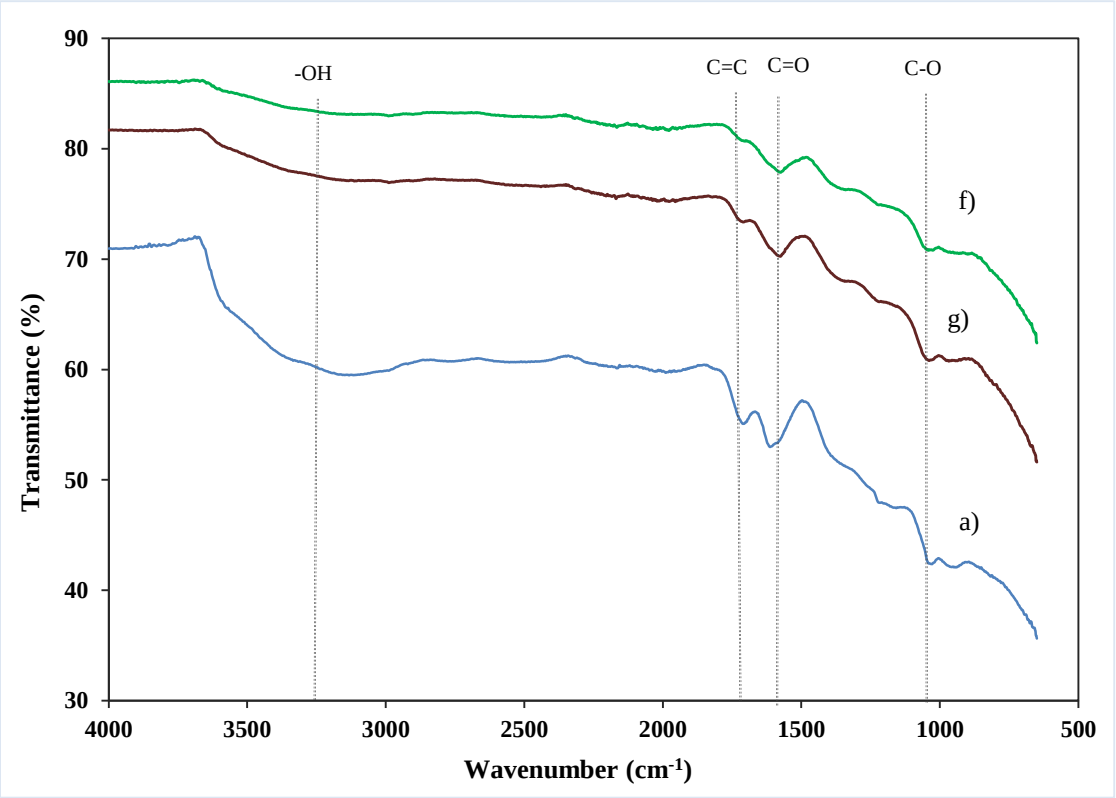

Figure 6.4 FT-IR spectrums of a) GO, f) MRGO and g) SRGO for the plant extraction at 80°C

6.2 Reduction experiments of GO by Plant Extracts

Reduction of GO was performed at room temperature with 20 mL of plant extract and on completion of reduction process a visible change on the reaction colour (as shown in Figure 6.5) observed which can be an obvious indication for reduction process. This change probably resulted from decreasing of the oxygen-containing moties present in GO.

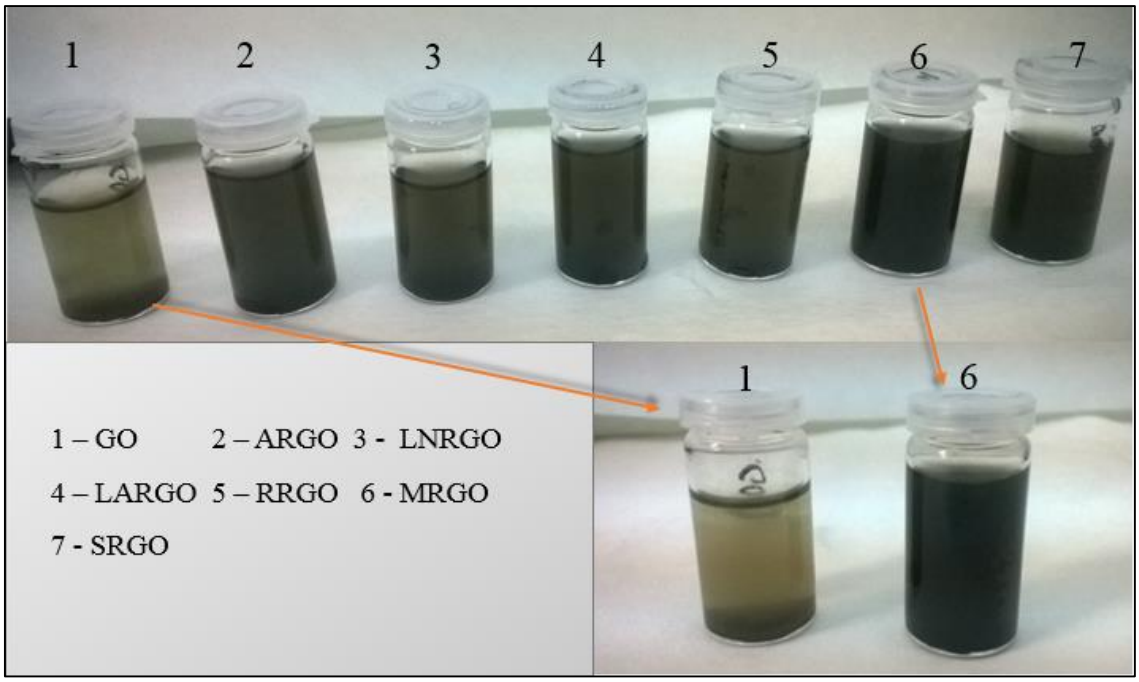

Figure 6.5 Digital images of GO dispersion and RGO dispersions

6.3 UV-Visible Analysis of Reduced Graphene Oxide Dispersions

The UV-Visible spectrums of aqueous GO and plant reduced aqueous GO dispersions were measured in 200-800 nm wavelength range (Figures 6.6-6.8).

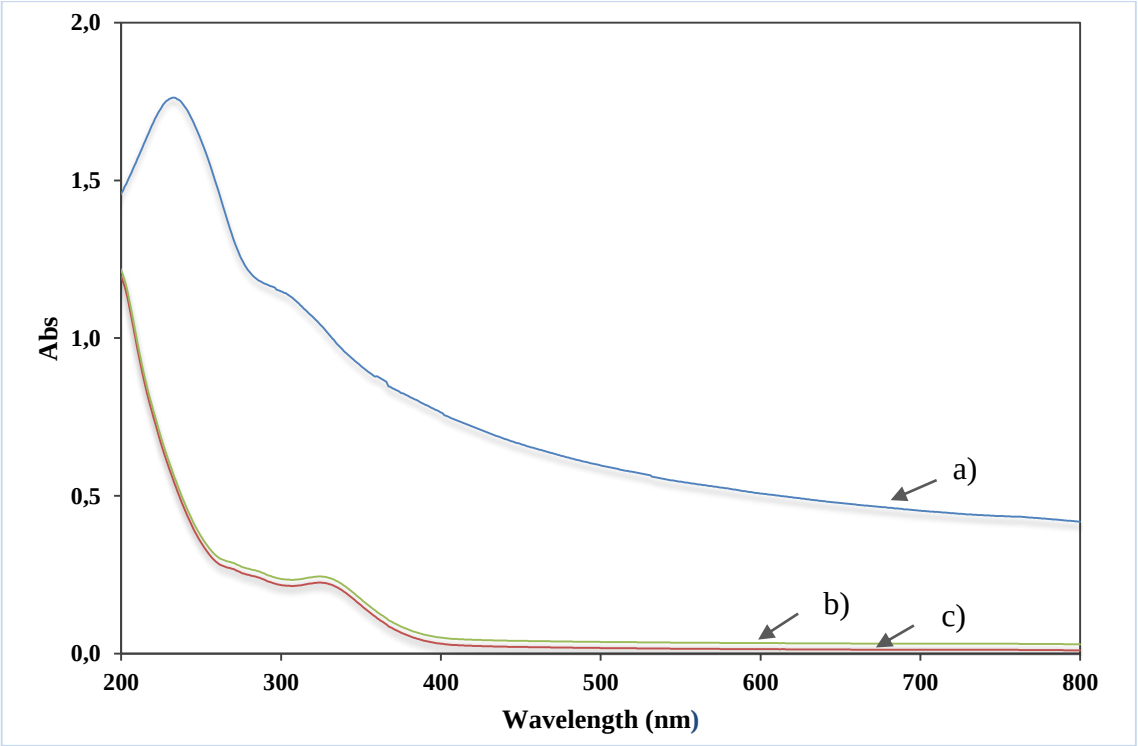

Figure 6.6 UV-Visible Spectrums of a) GO, b) ARGO and c) LNRGO

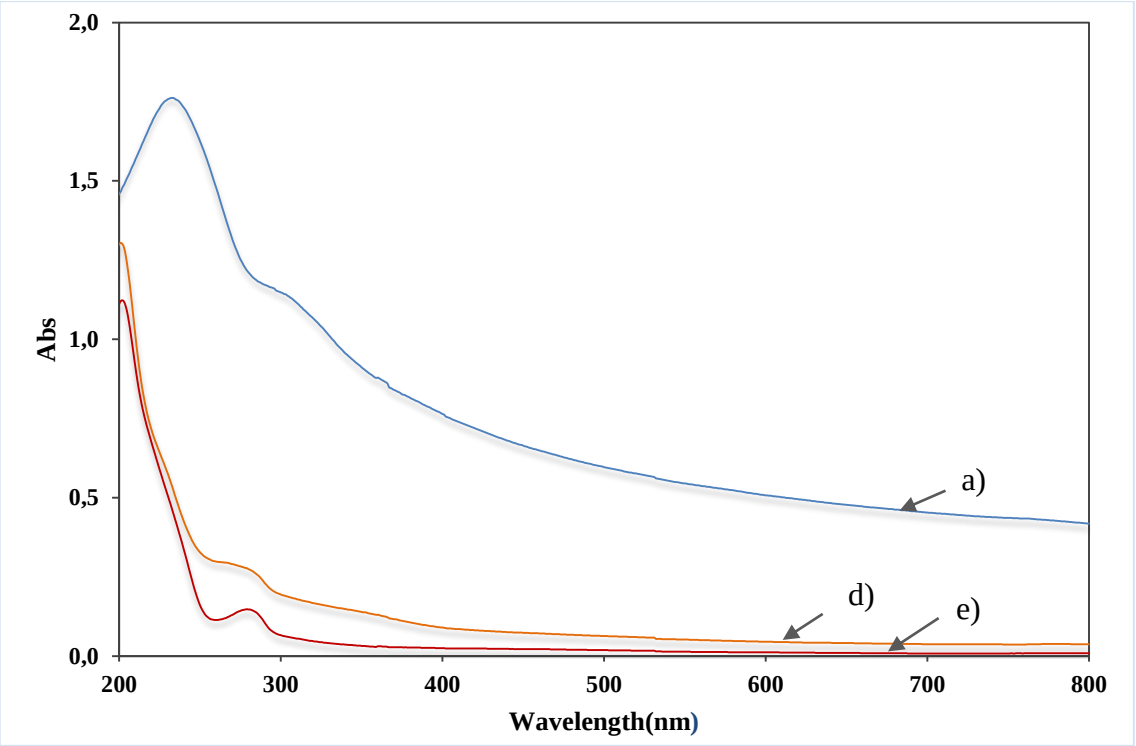

Figure 6.7 UV-Visible Spectrums of a) GO, d) LARGO and e) RRGO

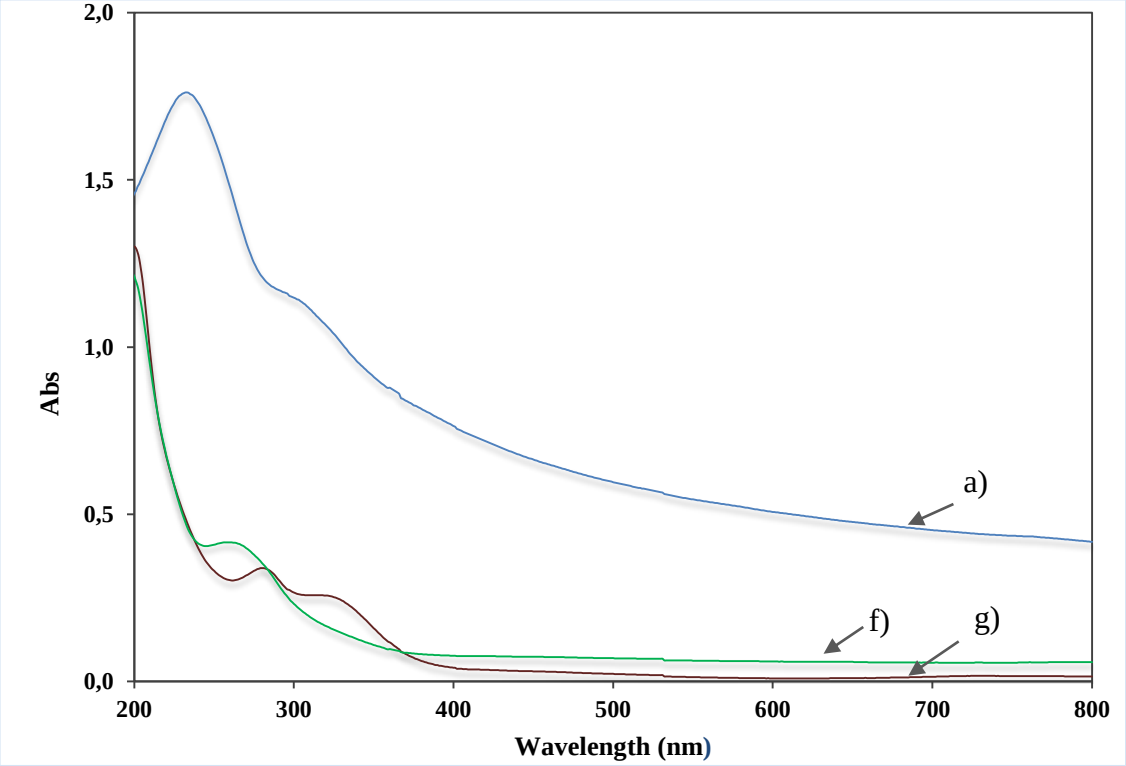

Figure 6.8 UV-Visible Spectrums of a) GO, f) MRGO and g) SRGO

As can be seen in Figures 6.6-6.8, aqueous dispersion of GO (a) shows a maximum absorption peak at 232 nm which was attributed to π-π* transitions of the aromatic C-C bonds and a weak shoulder at 300 nm regarding to n- π* transitions of C=O bonds. After plant-based reduction reactions, the characteristic peak at 232 nm shifts to 290 nm for RRGO (e) and LARGO (d), 268 nm for MRGO (f) and SRGO (g), 335 nm for ARGO (b) and LNRGO (c) as can be seen from Figures 6.6-6.8. These observed peak shifts were attributed to graphene oxide reduction that means electronic conjugations within the sheets of reduced graphene oxide was restored.

6.4 Thermal Analysis of Reduced Graphene Oxide Samples

The thermal profiles of graphite, graphene oxide and reduced graphene oxides by different plants were shown in Figure 6.9. As can be seen in Figure 6.9, pristine graphite did not exhibit any weight loss during the temperature profile. Under nitrogen gas flow, graphene oxide exhibited a weight loss about 12% below 100°C and 28% below 250°C due to loss of hydroxyl, epoxy functional groups and remaining water molecules.

On the other hand, there is no significant difference between graphene oxide and its plant-based reduced forms except MRGO as can be seen in Figure 6.9. MRGO exhibited increased thermal stability due to the absence of thermally unstable oxygen functionalities. 4% of weight loss below 100°C and 11% of weight loss below 250°C were observed for MRGO sample under nitrogen flow which indicated that decrease in amount of oxygen functionalities.

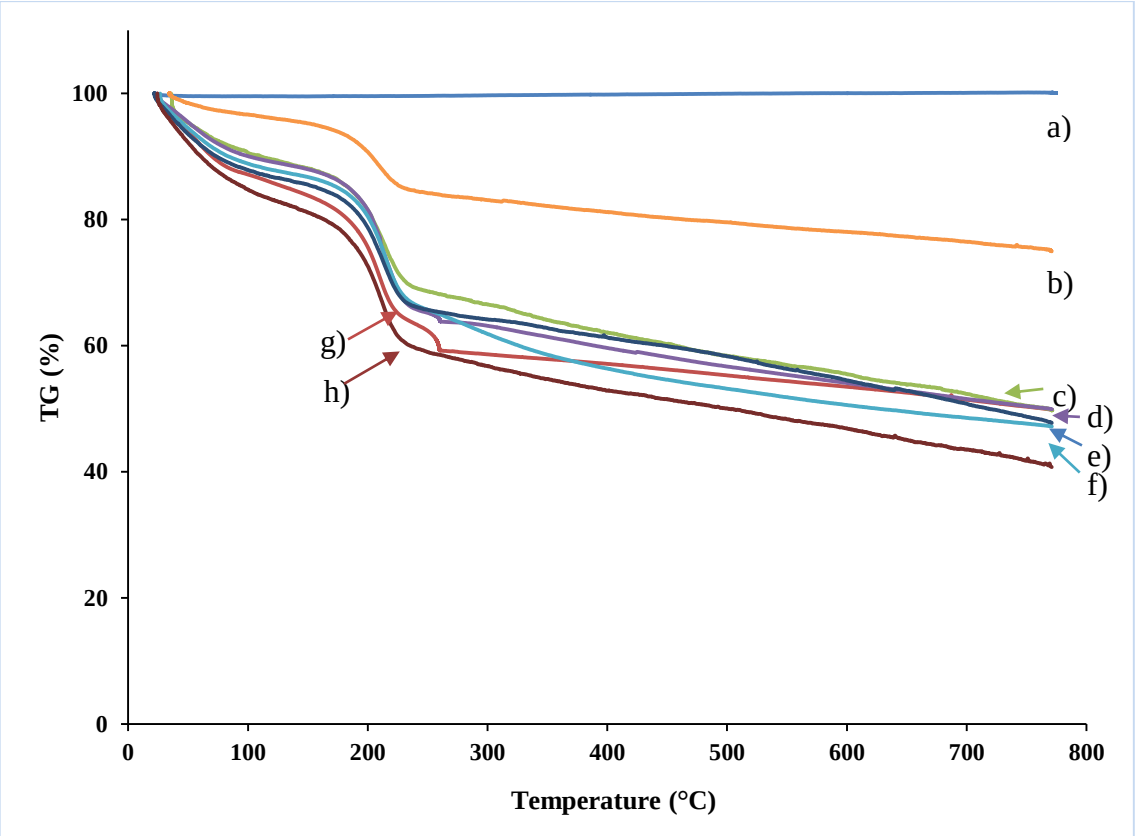

Figure 6.9 TGA profiles of a) graphite, b) MRGO, c) ARGO, d) LNRGO, e) SRGO, f) RRGO, g) LARGO and h) GO

As a result, knowing that the plant based method for reduction of graphene oxide is a green, cheap and non-toxic method, it was proved that the extract of *Melissa officinalis* has important potential on graphene oxide reduction. The characterization results on reduction efficiency of six different plant extracts showed that MRGO has the optimum reduction efficiency among other plant extracts examined. Therefore, the graphene reduction process was performed by using the extract of *Melissa officinalis* for the production of RGO-HA composites.

6.5 FTIR Analysis of RGO-HA Composites

The FTIR spectrums of RGO-HA composites and pure HA sample were shown in Figure 6.10. The spectrums of RGO-HA composites displayed the characteristic absorption bands of pure HA, at 560 and 599 cm^{-1} attributed to P-O bending of phosphate group while the band at 1,019 cm^{-1} was assigned to the vibrations of O-P-O carbonate ions of hydroxyl sites. The bands at 1,453 and 1,419 cm^{-1} were attributed to the vibration mode of carbonate ions and the band at 2,350 cm^{-1} was attributed to P-H stretching absorptions. The bands at 1,456 cm^{-1} corresponds to the aromatic C-C stretching in RGO which

confirms that the obtained composite comprises RGO and pure HA. The spectrums of RGO-HA composites were similar to pure HA spectrum which suggests that pure HA retained the essential feature of its native structure in its composites with graphene as reported by Neelgund et al. [134] in their study.

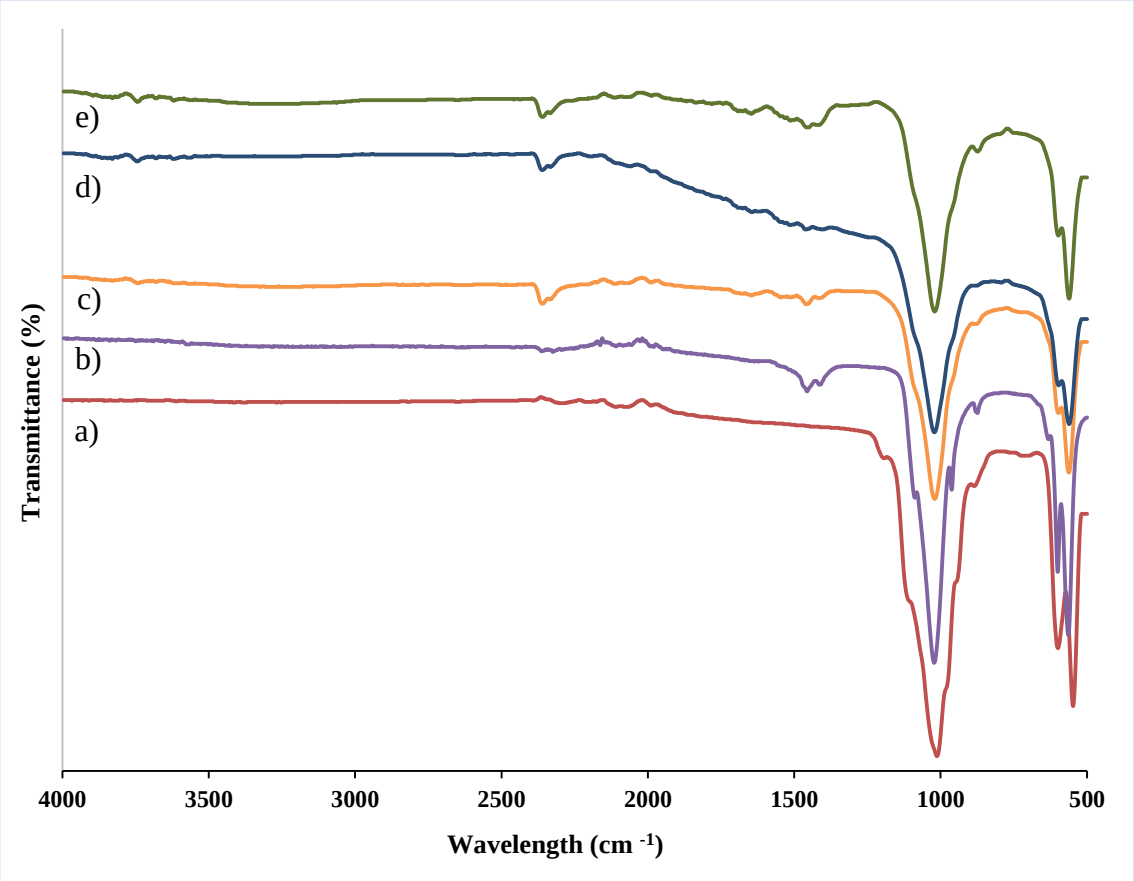

Figure 6.10 FTIR spectrums of a) HA, b) 0.25% RGO-HA, c) 0.5% RGO-HA, d) 1% RGO-HA and e) 2% RGO-HA

6.6 Thermal Analysis of RGO-HA Composites

As can be seen in Figure 6.11, a weight loss about 5% was observed for pure HA which was assumed to be resulted gradual dehydroxyllin in hydroxyapatite powder. This can be explained by the Equation 3.1. 0.25% of RGO-HA exhibited a weight loss about 9% and this value is about 12% for other RGO contents. The difference in weight loss could be related to the residual oxygen containing functional groups on RGO sheets. Therefore, the deposition of HA over RGO samples provided high thermal stability to RGO-HA structure.

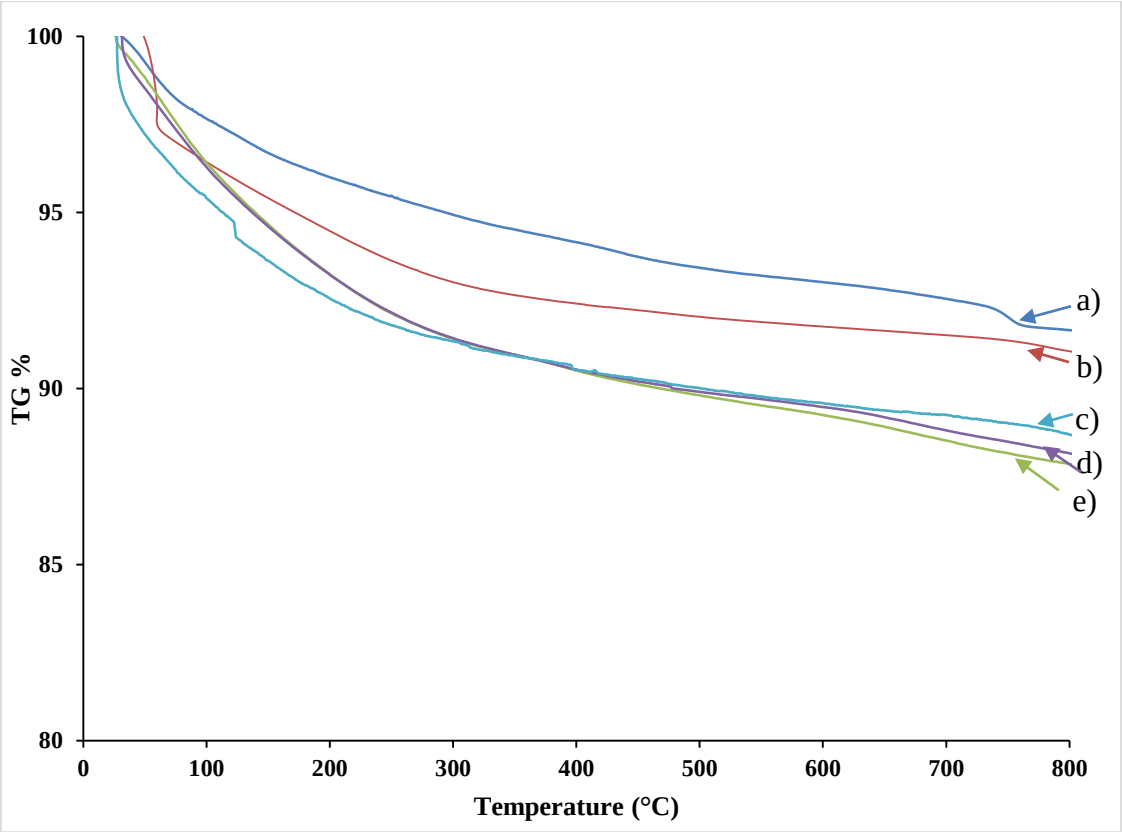

Figure 6.11 TGA profiles of a) pure HA, b) 0.25% RGO-HA, c) 0.5% RGO-HA, d) 1% RGO-HA and e) 2% RGO-HA

6.7 Mechanical Testing Analysis of RGO-HA Composites

The compressive strength values of the sintered pure HA and RGO-HA composites were measured for mechanical testing analysis, and the average of the three measurements were given in Table 6.1. Compared to pure HA, the increase in compressive strength values for RGO-HA composites (0.25, 0.5, 1, 2 % (wt) RGO in HA) were calculated as 77.44%, 156.05%, 220.25% and 231.51%, respectively (Figure 6.12). Although the maximum increase was observed for 2% (wt) RGO-HA composite, its increase was relatively close to the increase value of 1% (wt) RGO-HA composite. Considering the RGO amount and compressive strength values, 1% (wt) RGO-HA composite showed the optimum mechanical behavior compared to other composites.

Table 6.1 The compressive strength values measured for sintered pure HA and RGO-HA composites

Compressive strength (MPa)					
Repeat Number	**pure HA**	**RGO-HA 0.25 % (wt)**	**RGO-HA 0.5 % (wt)**	**RGO-HA 1% (wt)**	**RGO-HA 2% (wt)**
1	81.60	141.91	237.90	283.05	291.02
2	72.33	153.92	219.32	272.85	287.38
3	103.44	160.8	201.78	268.34	274.81
Average	85.79±15	152.21±9.5	219.67±18.06	274.75±7.53	284.4±8.5

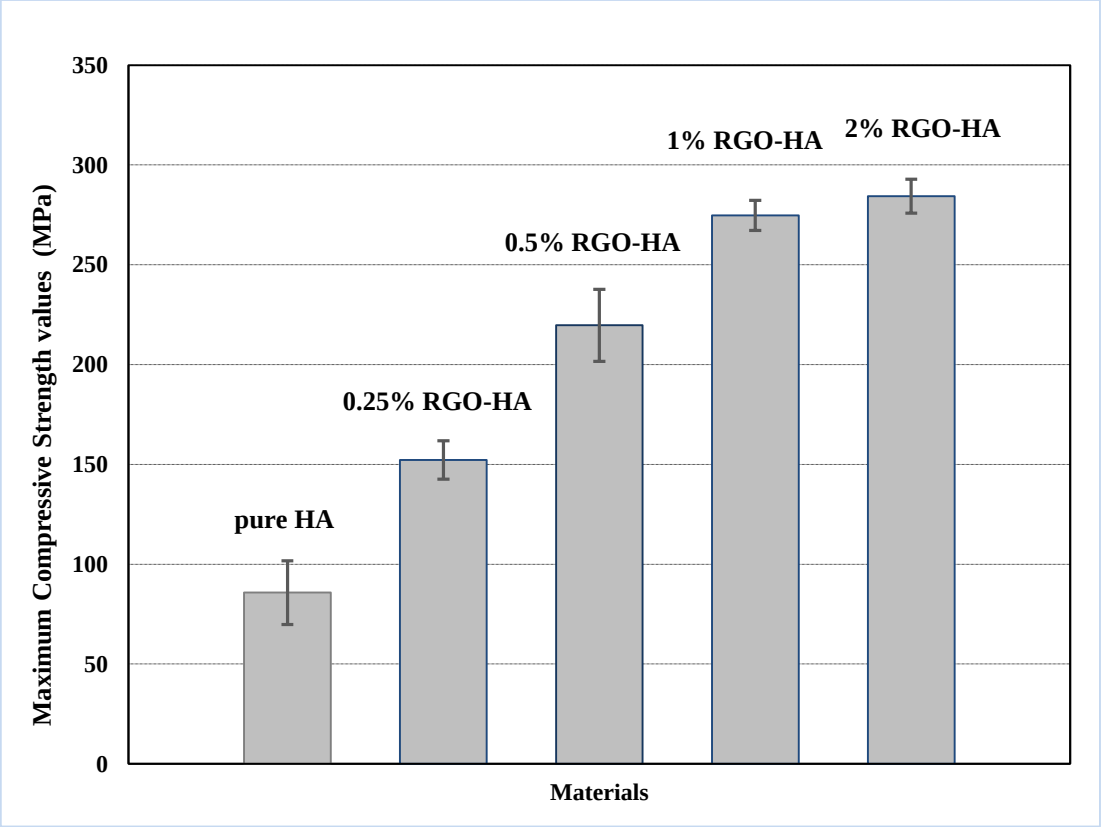

Figure 6.12 The compressive strength values measured for sintered pure HA and RGO-HA composites

6.8 Microstructural Characterization of RGO-HA Composites

The phases of the sintered pure HA and 1% (wt) RGO-HA powders were studied by X-ray diffraction. As can be seen in Figure 6.13, XRD analysis suggested that the presence of crystalline HA. Two principal diffraction peaks were displayed at 2θ values of 26.2° and 32° which were attributed to (002) and (211) reflections of pure HA, respectively. The remaining peaks at 39.9°, 46.9°, 49.5°, 53.2° and 64° were assigned to (310), (222), (213), (004) and (304) reflections of pure HA, respectively.

The XRD diffraction peaks for RGO were not seen, most likely due to the damage of their crystallographic order and irregular arrays of atoms in three dimensions as reported by Li et al. (2014) [128] in their study or presence of strong pure HA peaks and the small content of RGO as reported by Baradaran et al. (2014) [126] in their study. However, the presence of RGO in composite structure was confirmed by FTIR, TGA and TEM analysis which demonstrated that the RGO incorporation had no influence on the stability of HA.

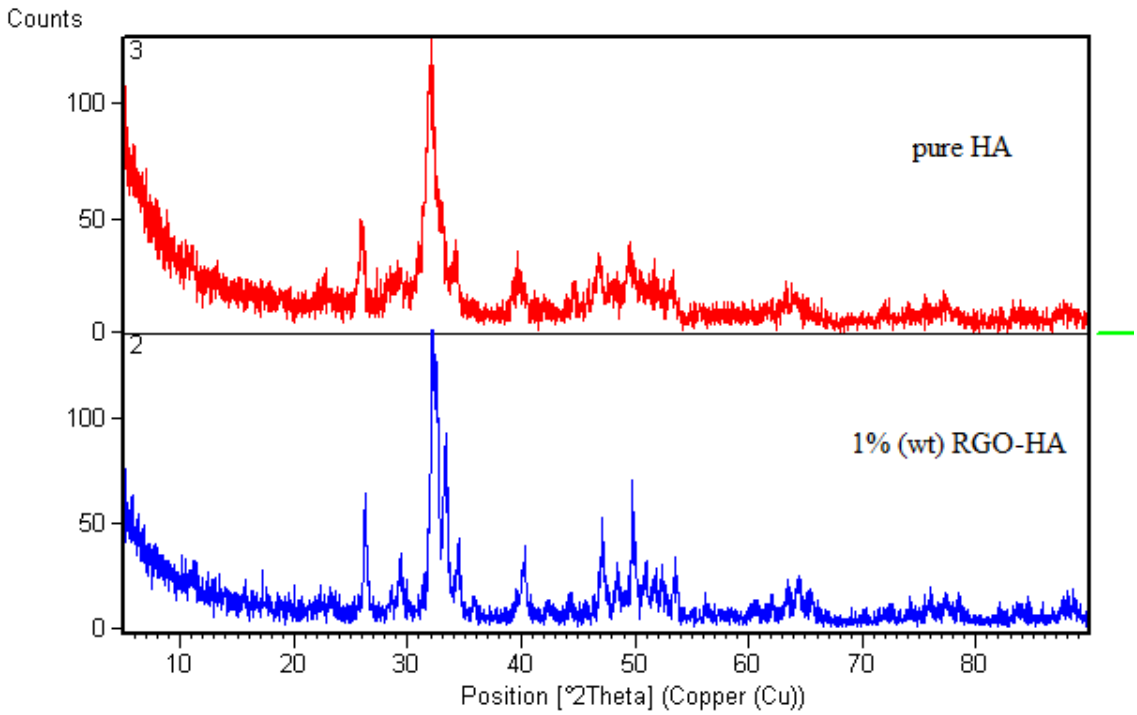

Figure 6.13 XRD patterns of sintered pure HA and 1% (wt) RGO-HA samples

6.9 Morphological Study

SEM and TEM measurements were taken for the morphological evaluation of the samples. For better comparison, MRGO due to optimum reduction efficiency and 1% (wt) RGO-HA composite due to maximum RGO content were evaluated. Also, GO and pure HA samples were evaluated by SEM images. The images can be seen in Figures 6.14 and 6.15.

Figure 6.14 shows the SEM and TEM images of graphene oxide and reduced graphene oxide by *Melissa officinalis* extract at different magnifications. The observed corrugations and scrollings on the edge of reduced graphene oxide are similar to previous reports presented by Zhu et al. (2010) [17] and Lee and Kim (2014) [114] in their study.

In Figure 6.15, the SEM and TEM micrographs shows the presence of porous network structure for pure HA and the HA grain is well bonded to wrinkled graphene structure for 1% (wt) RGO-HA composite sample as reported by Liu et al. (2014) [133] and Saranya et al. (2010) [143] in their stuy. Darker areas are considered to be the inorganic part of the composite and lighter areas assumed to be organic component.

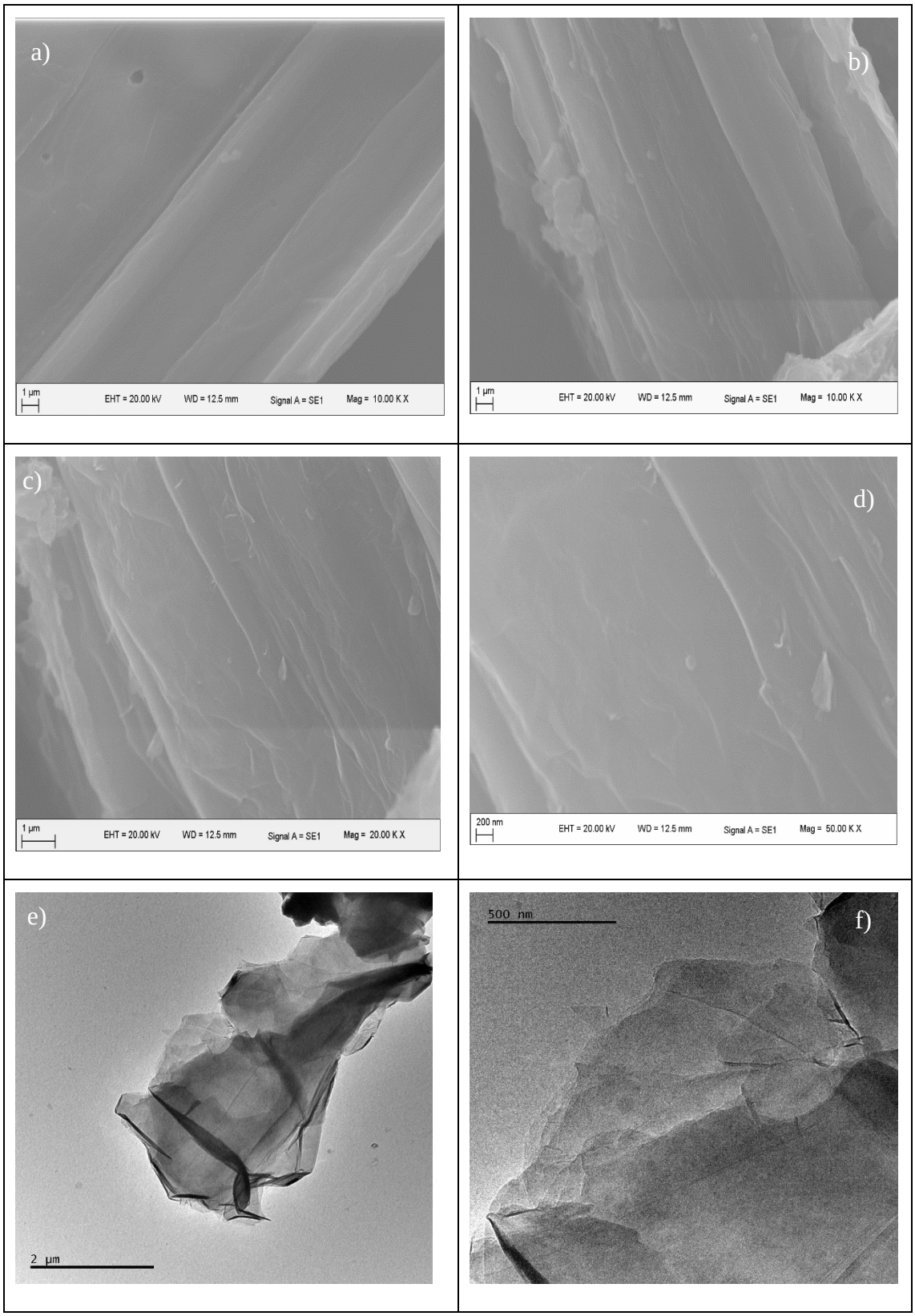

Figure 6.14 SEM images of a) GO, (b-d) MRGO and (e-f) TEM images of MRGO

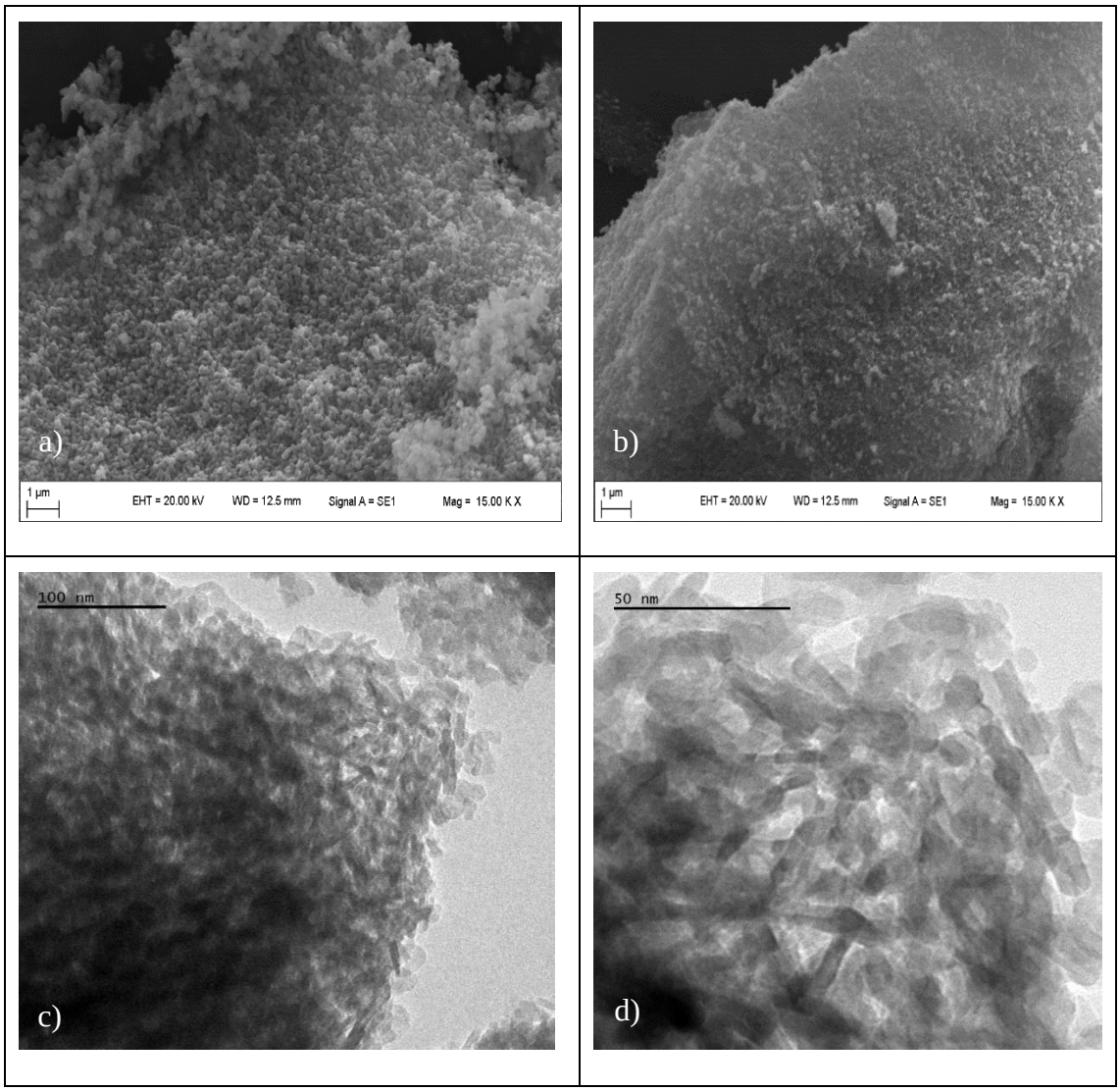

Figure 6.15 SEM images of a) HA,b) 1% (wt) RGO-HA, (c-d) TEM images of 1% (wt) RGO-HA

The main findings and the experimental conditions of the present study compared to other studies demonstrated in the literature about plant-based reduction methods of graphene oxide were summarized in Table 6.2.

Moreover, in Table 6.3, the main findings and the experimental conditions of the present study compared to other studies demonstrated in the literature about graphene-HA composites were summarized.

Table 6.2 The comparison of the present study to other studies in the literature about plant-based reduction methods of graphene oxide

Reference	Plant Name	Plant parts/ extracts	Extraction conditions			Reduction reaction parameters		
			Reaction Type	Temp. (°C)	Time (h)	Reaction Type	Temp. (°C)	Time (h)
The present study (2015)	*Achillea nobilis L.* (Yarrow)	Leaf	Sonication	80	2	Stirring	Room temperature	13
	Laurus nobilis L. (Daphne)	Leaf						
	Lavandula agnustifolia Miller (Lavandula)	Leaf						
	Melissa officinalis L. (Melissa)	Leaf						
	Rosae caninae fructus (Rosehip)	Fruit						
	Salvia officinalis L. (Salvia)	Leaf						

Table 6.2 continues

Reference	Plant Name	Plant parts/ extracts	Extraction conditions			Reduction reaction parameters		
			Reaction Type	Temp. (°C)	Time (h)	Reaction Type	Temp. (°C)	Time (h)
Suresh et al. (2015) [107]	*Syzygium aromaticum* (cloves)	Powdered cloves	Reflux	100	5	Reflux	100	0.5
Suresh et al. (2015) [108]	*Cinnamomum zeylanicum* (Cinnamon)	Powdered bark	Reflux	100	5	Stirring + Reflux	Room temperature	0.75
Gurunathan et al. (2014)[109]	*Ginkgo biloba*	Leaf	Boiling	100	5 min	Stirring	30	12 and 24
Jana et al. (2014) [110]	*Phaseolus aureus L.*	Plant	Soaking	Room temperature	Overnight	Stirring	Room temperature	24
Barua et al. (2013)[111]	*Colocasia esculenta*	Leaf	Stirring	45	20 min	Stirring	Room temperature	8
Firdhouse and Lalita (2013) [112]	*Amaranthus dubius*	Plant	Stirring	50	30 min	Stirring + Reflux	Room temperature	Until the color changes

Table 6.2 continues

Reference	Plant Name	Plant parts/ extracts	Extraction conditions			Reduction reaction parameters		
			Reaction Type	Temp. (°C)	Time (h)	Reaction Type	Temp. (°C)	Time (h)
Haghighi and Tabrizi (2013) [113]	*Rosa sp.*	Rose water	Rose water 12% (wt.) used			Sonication	95	5
Lee and Kim (2013) [114]	*Prunus serrulata*	Leaf	Boiling	100	5 min	Stirring	95	12
	Magnolia kobus	Leaf						
	Platanus orientalis	Leaf						
	Diopyros kaki	Leaf						
	Pinus desiflora	Leaf						
	Acer palmatum	Leaf						
	Ginkgo biloba	Leaf						

Table 6.2 continues

Reference	Plant Name	Plant parts/ extracts	Extraction conditions			Reduction reaction parameters		
			Reaction Type	Temp. (°C)	Time (h)	Reaction Type	Temp. (°C)	Time (h)
Kuila et al. (2012) [115]	*Daucus carrota*	Root	Stirring	25	48	Stirring	Room temperature	48
Thakur and Karak (2012) [116]	*Colocasia esculenta*	Leaf	Stirring	50	20 min	Stirring or Reflux	Room temperature	8
	Mesua ferrea	Leaf						10
	Citrus sinensis	Leaf						10
Wang et al. (2011) [117]	*Camelia sinensis*	Leaf (powder)	Boiling	100	20 min	Sonication+ Reflux	90	0.5

Table 6.3 The comparison of the studies about graphene-HA composites

Reference	Graphene type	Graphene concentration in composite (wt%)	HA synthesize conditions			Synthesis method of composites	Mechanical improvements compared to pure HA
			Starting materials	Reaction Type	pH		
The present study, 2015	Plant-based reduced graphene oxide	0.25, 0.5, 1, 2	$Ca(OH)_2$, o-H_3PO_4	Precipitation	9	Mixing and sintering	220.25 and 231.5% increase in compressive strength for 1 and 2% RGO-HA composites, respectively
Azhari et al. (2015) [125]	Graphene oxide	0.2, 0.4	Purchased			Powder bed class of additive manufacturing	70 times higher mechanical strength
Baradaran et al. (2014) [126]	Reduced graphene oxide	0.5, 1, 1.5	$NH_4H_2PO_4$, $CaCl_2$	Hydrothermal	-	In situ hydrothermal method	86% higher elastic modulus and 40% higher fracture toughness
Fan et al. (2014) [127]	Graphene nanosheet	40, 60, 80	$Ca(NO_3)_2.4H_2O$ $(NH_4)2HPO_4$	Hydrothermal	-	One pot hydrothermal method	Twice high value of hardness and Young's modulus values
Li et al. (2014) [128]	Graphene oxide	0.2, 5	Purchased			Cathodic electrophoretic deposition	Reduced the surface cracks and increase the coating adhesion strength

Table 6.3 The comparison of the studies about graphene-HA composites (continues)

Reference	Graphene type	Graphene concentration in composite (wt%)	HA synthesize conditions			Synthesis method of composites	Mechanical improvements compared to pure HA
			Starting materials	Reaction Type	pH		
Li et al. (2014) [129]	Graphene oxide	32.1	$NH_4H_2PO_4$, $CaCl_2$	Mineralization	-	In situ mineralization	223% higher stiffness, 78% higher tensile strength
Nunez et al. (2014) [130]	Graphene oxide	15	$CaCO_3$ H_3PO_4	Precipitation	10	Dispersion	-
Oyefusi et al. (2014) [131]	Graphene nanosheet	-	$Ca(OH)_2$ H_3PO_4	Precipitation	9	Mixing	-
Liu et al. (2013) [132]	Graphene nanosheet	0.1, 1	$Ca(NO_3)_2.4H_2O$ $(NH_4)_2HPO_4$	Precipitation	11	Spark plasma sintering	203% increase in fracture toughness
Liu et al. (2013) [133]	Graphene nanosheet	0.1, 1	$(NH_4)_2HPO4$ $Ca(NO_3)_2$	Precipitation	-	Vacuum cold spraying	386% increase in fracture toughness
Neelgund et al. (2013) [134]	Graphene nanosheet	0.1, 1	$CaCO_3$ H_3PO_4	Precipitation	9	In situ deposition	-

Table 6.3 The comparison of the studies about graphene-HA composites (continues)

Reference	Graphene type	Graphene concentration in composite (wt%)	HA synthesize conditions			Synthesis method of composites	Mechanical improvements compared to pure HA
			Starting materials	Reaction Type	pH		
Zanin et al. (2013) [135]	Reduced graphene oxide	-	$Ca(NO_3)_2.4H_2O$ $(NH_4).2HPO_4$	Electrodeposition	4.7	Direct electrodeposition	-
Gonçalves et al. (2012) [136]	Graphene oxide	0, 0.1, 0.5, 1	Purchased			Freeze-granulation technique	Higher bending strength and elastic modulus

CHAPTER 7

CONCLUSIONS

One of the few bioactive materials, hydroxyapatite has wide-reaching applications in bio-related sciences. However, weak mechanical properties of hydroxyapatite are limiting its applications, especially in load-bearing fields. The several studies have been carried out to strengthen hydroxyapatite with a second phase material so far.

In the present study, as the strongest material ever known, graphene was chosen as the second material to HA. As one of the member of graphene family, reduced graphene oxide was used as reinforcement material regarding to its low-cost production. The major findings of the present study were given as follows;

1. The reduced graphene oxide was synthesized with a plant-based and environmentally friendly process. For reduction process, six different plants were used, and their reduction performances were compared according to the data obtained from the characterization studies.

2. As the *Melissa officinalis* extract showed highest reduction efficiency among others examined, the graphene reduction process was performed by using this extract for the production of RGO-HA composites.

3. Then, RGO-HA composites were synthesized by precipitation approach with different concentrations of RGO in HA; 0, 0.25, 0.5, 1 and 2% (wt). After this process, the samples obtained were characterized by using FT-IR, TG analysis. The characterization studies showed that the composites were synthesized successfully. Then, the compressive strength values of sintered pure hydroxyapatite pellets and composites were examined. The compressive strength values of pure HA and RGO-HA composites [0.25, 0.5, 1, 2% (wt) RGO in HA] were measured as 85.79±15, 152.21±9.5, 219.67±18.06, 274.75±7.53 and 284.4±8.5 MPa, respectively. Compared to pure HA, the compressive strength values for RGO-HA composites

(0.25, 0.5, 1, 2% (wt) RGO in HA) increased as 77.44%, 156.05%, 220.25% and 231.51%, respectively.

4. 1% (wt) RGO-HA composite showed similar mechanical behavior compared to 2% (wt) RGO-HA composite. The increment was only about 3.5%.
5. For further confirmation of the pure HA and 1% (wt) RGO-HA composite formation, the XRD, SEM and TEM analysis were carried out. As a result, the SEM and TEM micrographs showed the presence of porous network structure for pure HA and the HA grain was well bonded to wrinkled graphene structure for 1% (wt) RGO-HA composite sample while the XRD results showed the presence of crystalline HA structure.
6. As a result, considering the RGO amount and the compressive strength value, 1% (wt) RGO-HA composite was found as the optimum composite among others.

Consequently, the present study represents an easy and convenient method for synthesizing environmentally safe RGO-HA composites. The synthesized composites showed that even small content of graphene reinforcement significantly enhances the compressive strength of hydroxyapatite sample. These results could pave the way for the fabrication of graphene-hydroxyapatite composites for biological applications with combined improvement in mechanical and biological properties. However, for *in vivo* applications, careful considerations of the cytotoxicity and biocompatibility of the composites are required, which is a part of the future work.

REFERENCES

[1] Li, N. Cao, M. and Hu, C., (2012). "Review on the latest design of graphene-based inorganic materials", Nanoscale, 4: 6205-6218.

[2] Iravani, S., (2011). "Green synthesis of metal nanoparticles using plants", Green Chemistry, 13: 2638-2650.

[3] Novoselov, K. Geim, A.K. Morozov, S. Jiang, D. Katsnelson, M. Grigorieva, I. Dubonos, S. and Firsov, A., (2005). "Two-dimensional gas of massless Dirac fermions in graphene", Nature, 438: 197-200.

[4] Wassei, J.K. and Kaner, R.B., (2013). "Oh, the places you'll go with graphene", Accounts of Chemical Research, 46: 2244-2253.

[5] Singh, V. Joung, D. Zhai, L. Das, S. Khondaker, S.I. and Seal, S., (2011). "Graphene based materials: past, present and future", Progress in Materials Science, 56: 1178-1271.

[6] Kroto, H.W. Heath, J.R. O'Brien, S.C. Curl, R.F. and Smalley, R.E., (1985). "C 60: buckminsterfullerene", Nature, 318: 162-163.

[7] Lijima, S., (1991). "Carbon nanotubes", Nature: 354-356.

[8] Novoselov, K.S. Geim, A.K. Morozov, S. Jiang, D. Zhang, Y. Dubonos, S.A. Grigorieva, I. and Firsov, A., (2004). "Electric field effect in atomically thin carbon films", Science, 306: 666-669.

[9] Feng, L. and Liu, Z., (2011). "Graphene in biomedicine: opportunities and challenges", Nanomedicine, 6: 317-324.

[10] Ubbelohde, A.R. and Lewis, F.A., (1960). Graphite and its crystal compounds: Clarendon Press.

[11] Goenka, S. Sant, V. and Sant, S., (2014). "Graphene-based nanomaterials for drug delivery and tissue engineering", Journal of Controlled Release, 173: 75-88.

[12] Bianco, A., (2013). "Graphene: safe or toxic? The two faces of the medal", Angewandte Chemie International Edition, 52: 4986-4997.

[13] Nguyen, K.T. and Zhao, Y., (2014). "Integrated graphene/nanoparticle hybrids for biological and electronic applications", Nanoscale, 6: 6245-6266.

[14] Chen, L. Hernandez, Y. Feng, X. and Müllen, K., (2012). "From nanographene and graphene nanoribbons to graphene sheets: chemical synthesis", Angewandte Chemie International Edition, 51: 7640-7654.

[15] Biró, L.P. Nemes-Incze, P. and Lambin, P., (2012). "Graphene: nanoscale processing and recent applications", Nanoscale, 4: 1824-1839.

[16] Snook, I. and Barnard, A., (2011). Graphene nano-flakes and nano-dots: Theory, experiment and applications: INTECH Open Access Publisher.

[17] Zhu, Y. Murali, S. Cai, W. Li, X. Suk, J.W. Potts, J.R. amd Ruoff, R.S., (2010). "Graphene and graphene oxide: synthesis, properties, and applications", Advanced Materials, 22: 3906-3924.

[18] Abergel, D. Apalkov, V. Berashevich, J. Ziegler, K. and Chakraborty, T., (2010). "Properties of graphene: a theoretical perspective", Advances in Physics, 59: 261-482.

[19] Soldano, C. Mahmood, A. and Dujardin, E., (2010). "Production, properties and potential of graphene", Carbon, 48: 2127-2150.

[20] Zhao, J. Guo, Y. Li, Z. Guo, Q. Shi, J. Wang, L. and Fan, J., (2012). "An approach for synthesizing graphene with calcium carbonate and magnesium", Carbon, 50: 4939-4944.

[21] Huang, X. Qi, X. Boey, F. and Zhang, H., (2012). "Graphene-based composites", Chemical Society Reviews, 41: 666-686.

[22] Nair, R. Blake, P. Grigorenko, A. Novoselov, K. Booth, T. Stauber, T. Peres, N. and Geim, A., (2008). "Fine structure constant defines visual transparency of graphene", Science, 320: 1308-1308.

[23] Balandin, A.A. Ghosh, S. Bao, W. Calizo, I. Teweldebrhan, D. Miao, F. and Lau, C.N., (2008). "Superior thermal conductivity of single-layer graphene", Nano Letters, 8: 902-907.

[24] Rao, C. Biswas, K. Subrahmanyam, K. and Govindaraj, A., (2009). "Graphene, the new nanocarbon", Journal of Materials Chemistry, 19: 2457-2469.

[25] Edwards, R.S. and Coleman, K.S., (2013). "Graphene synthesis: relationship to applications", Nanoscale, 5: 38-51.

[26] Jiang, L. Niu, T. Lu, X. Dong, H. Chen, W. Liu, Y. Hu, W. and Zhu, D., (2013). "Low-temperature, bottom-up synthesis of graphene via a radical-coupling reaction", Journal of the American Chemical Society, 135: 9050-9054**.**

[27] Geim, A.K. and Novoselov, K.S., (2007). "The rise of graphene", Nature Materials, 6: 183-191.

[28] Chen, J. Duan, M. and Chen, G., (2012). "Continuous mechanical exfoliation of graphene sheets via three-roll mill", Journal of Materials Chemistry, 22: 19625-19628.

[29] Zhang, Y. Tan, Y.-W. Stormer, H.L. and Kim, P., (2005). "Experimental observation of the quantum Hall effect and Berry's phase in graphene", Nature, 438: 201-204.

[30] Guo, S. and Dong, S., (2011). "Graphene nanosheet: synthesis, molecular engineering, thin film, hybrids, and energy and analytical applications", Chemical Society Reviews, 40: 2644-2672.

[31] Allen, M.J. Tung, V.C. and Kaner, R.B., (2009). "Honeycomb carbon: a review of graphene", Chemical Reviews, 110: 132-145.

[32] Stankovich, S. Dikin, D.A. Piner, R.D. Kohlhaas, K.A. Kleinhammes, A. Jia, Y. Wu, Y. Nguyen, S.T. and Ruoff, R.S., (2007). "Synthesis of graphene-based nanosheets via chemical reduction of exfoliated graphite oxide", Carbon, 45: 1558-1565.

[33] Chua, C.K. and Pumera, M., (2013). "Reduction of graphene oxide with substituted borohydrides", Journal of Materials Chemistry A, 1: 1892-1898.

[34] Dreyer, D.R. Park, S. Bielawski, C.W. and Ruoff, R.S., (2010). "The chemistry of graphene oxide", Chemical Society Reviews, 39: 228-240.

[35] Mao, H.Y. Laurent, S. Chen, W. Akhavan, O. Imani, M. Ashkarran, A.A. and Mahmoudi, M., (2013). "Graphene: promises, facts, opportunities, and challenges in nanomedicine", Chemical Reviews, 113: 3407-3424.

[36] Pei, S. and Cheng, H.-M., (2012). "The reduction of graphene oxide", Carbon, 50: 3210-3228.

[37] Wang, C. Ju, J. Yang, Y. Tang, Y. Bi, H. Liao, F. Lin, J. Shi, Z. Huang, F. and Han, R.P., (2013). "Robust and stable intercalated graphene encapsulation of tin nanorods for enhanced cycle and capacity performance for lithium storage", RSC Advances, 3: 21588-21595.

[38] Janowska, I. Ersen, O. Jacob, T. Vennégues, P. Bégin, D. Ledoux, M.-J. and Pham-Huu, C., (2009). "Catalytic unzipping of carbon nanotubes to few-layer graphene sheets under microwaves irradiation", Applied Catalysis A: General, 371: 22-30.

[39] Kozubek, R. Ochedowski, O. Zagoranskiy, I. Karlušić, M. and Schleberger, M., (2014). "Application of HOPG and CVD graphene as ion beam detectors", Nuclear Instruments and Methods in Physics Research Section B: Beam Interactions with Materials and Atoms, 340: 81-84.

[40] Chen, B. Huang, H. Ma, X. Huang, L. Zhang, Z. and Peng, L.M., (2014). "How good can CVD-grown monolayer graphene be?", Nanoscale, 6: 15255-15261.

[41] Kim, J. Ishihara, M. Koga, Y. Tsugawa, K. Hasegawa, M. and Iijima, S., (2011). "Low-temperature synthesis of large-area graphene-based transparent conductive films using surface wave plasma chemical vapor deposition", Applied Physics Letters, 98: 091502.

[42] Muñoz, R. and Gómez-Aleixandre, C., (2013). "Review of CVD synthesis of graphene", Chemical Vapor Deposition, 19: 297-322.

[43] Park, H.J. Meyer, J. Roth, S. and Skákalová, V., (2010). "Growth and properties of few-layer graphene prepared by chemical vapor deposition", Carbon, 48: 1088-1094.

[44] Sutter, P.W. Flege, J.-I. and Sutter, E.A., (2008). "Epitaxial graphene on ruthenium", Nature Materials, 7: 406-411.

[45] Coraux, J. Engler, M. Busse, C. Wall, D. Buckanie, N. Zu Heringdorf, F.-J.M. Van Gastel, R. Poelsema, B. and Michely, T., (2009). "Growth of graphene on Ir (111)", New Journal of Physics, 11: 023006.

[46] Addou, R. Dahal, A. and Batzill, M., (2013). "Growth of a two-dimensional dielectric monolayer on quasi-freestanding graphene", Nature Nanotechnology, 8: 41-45.

[47] Ago, H. Ito, Y. Mizuta, N. Yoshida, K. Hu, B. Orofeo, C.M. Tsuji, M. Ikeda, K.-i. and Mizuno, S., (2010). "Epitaxial chemical vapor deposition growth of single-layer graphene over cobalt film crystallized on sapphire", Acs Nano, 4: 7407-7414.

[48] Oznuluer, T. Pince, E. Polat, E.O. Balci, O. Salihoglu, O. and Kocabas, C., (2011). "Synthesis of graphene on gold", Applied Physics Letters, 98: 183101.

[49] An, X. Liu, F. Jung, Y.J. and Kar, S., (2012). "Large-area synthesis of graphene on palladium and their raman spectroscopy", The Journal of Physical Chemistry C, 116: 16412-16420.

[50] Zhang, Y. Zhang, L. and Zhou, C., (2013). "Review of chemical vapor deposition of graphene and related applications", Accounts Of Chemical Research, 46: 2329-2339.

[51] Reina, A. Thiele, S. Jia, X. Bhaviripudi, S. Dresselhaus, M.S. Schaefer, J.A. and Kong, J., (2009). "Growth of large-area single-and bi-layer graphene by controlled carbon precipitation on polycrystalline Ni surfaces", Nano Research, 2: 509-516.

[52] Bae, S. Kim, H. Lee, Y. Xu, X. Park, J.-S. Zheng, Y. Balakrishnan, J. Lei, T. Kim, H.R. and Song, Y.I., (2010). "Roll-to-roll production of 30-inch graphene films for transparent electrodes", Nature Nanotechnology, 5: 574-578.

[53] Shikin, A. Rybkin, A. Marchenko, D. Popova, A. Varykhalov, A. and Rader, O., (2011). "Graphene: Synthesis and features of electronic structure", Nanotechnologies in Russia, 6: 625-632.

[54] Tetlow, H. De Boer, J.P. Ford, I. Vvedensky, D. Coraux, J. and Kantorovich, L., (2014). "Growth of epitaxial graphene: Theory and experiment", Physics Reports, 542: 195-295.

[55] Whitener, K.E. and Sheehan, P.E., (2014). "Graphene synthesis", Diamond and Related Materials, 46: 25-34.

[56] Chen, D. Feng, H. and Li, J., (2012). "Graphene oxide: preparation, functionalization, and electrochemical applications", Chemical reviews, 112: 6027-6053.

[57] Duan, J. Zhang, X. Yuan, W. Chen, H. Jiang, S. Liu, X. Zhang, Y. Chang, L. Sun, Z. and Du, J., (2015). "Graphene oxide aerogel-supported Pt electrocatalysts for methanol oxidation", Journal of Power Sources, 285: 76-79.

[58] Mohanraju, K. and Cindrella, L., (2015). "Electrocatalytic activity of Mn/Cu doped Fe 2 O 3–PANI–rGO composites for fuel cell applications", RSC Advances, 5: 39455-39463.

[59] Ren, F. Zhai, C. Zhu, M. Wang, C. Wang, H. Bin, D. Guo, J. Yang, P. and Du, Y., (2015). "Facile synthesis of PtAu nanoparticles supported on polydopamine reduced and modified graphene oxide as a highly active catalyst for methanol oxidation", Electrochimica Acta, 153: 175-183.

[60] Li, Y. Gao, W. Ci, L. Wang, C. and Ajayan, P.M., (2010). "Catalytic performance of Pt nanoparticles on reduced graphene oxide for methanol electro-oxidation", Carbon, 48: 1124-1130.

[61] Zhang, Y. Zhao, H. Wu, Z. Xue, Y. Zhang, X. He, Y. Li, X. and Yuan, Z., (2013). "A novel graphene-DNA biosensor for selective detection of mercury ions", Biosensors and Bioelectronics, 48: 180-187.

[62] Gao, L. Lian, C. Zhou, Y. Yan, L. Li, Q. Zhang, C. Chen, L. and Chen, K., (2014). "Graphene oxide–DNA based sensors", Biosensors and Bioelectronics, 60: 22-29.

[63] Liu, J. Xue, Y. Zhang, M. and Dai, L., (2012). "Graphene-based materials for energy applications", MRS Bulletin, 37: 1265-1272.

[64] Sun, Y. Wu, Q. and Shi, G., (2011). "Graphene based new energy materials", Energy & Environmental Science, 4: 1113-1132.

[65] Das, S. Sudhagar, P. Kang, Y.S. and Choi, W., (2014). "Graphene synthesis and application for solar cells", Journal of Materials Research, 29: 299-319.

[66] Chong, Y. Ma, Y. Shen, H. Tu, X. Zhou, X. Xu, J. Dai, J. Fan, S. and Zhang, Z., (2014). "The in vitro and in vivo toxicity of graphene quantum dots", Biomaterials, 35: 5041-5048.

[67] Zhang, S. Yang, K. Feng, L. and Liu, Z., (2011). "In vitro and in vivo behaviors of dextran functionalized graphene", Carbon, 49: 4040-4049.

[68] Shen, H. Zhang, L. Liu, M. and Zhang, Z., (2012). "Biomedical applications of graphene", Theranostics, 2: 283.

[69] Wang, K. Ruan, J. Song, H. Zhang, J. Wo, Y. Guo, S. and Cui, D., (2011). "Biocompatibility of graphene oxide", Nanoscale Res Lett, 6: 1-8.

[70] Liu, Z. Robinson, J.T. Sun, X. and Dai, H., (2008). "PEGylated nanographene oxide for delivery of water-insoluble cancer drugs", Journal of the American Chemical Society, 130: 10876-10877.

[71] Ku, S.H. Lee, M. and Park, C.B., (2013). "Carbon-Based Nanomaterials for Tissue Engineering", Advanced Healthcare Materials, 2: 244-260.

[72] Li, N. Cheng, Y. Song, Q. Jiang, Z. Tang, M. and Cheng, G., (2014). "Graphene meets biology", Chinese Science Bulletin, 59: 1341-1354.

[73] Nayak, T.R. Andersen, H. Makam, V.S. Khaw, C. Bae, S. Xu, X. Ee, P.-L.R. Ahn, J.-H. Hong, B.H. and Pastorin, G., (2011). "Graphene for controlled and accelerated osteogenic differentiation of human mesenchymal stem cells", Acs Nano, 5: 4670-4678.

[74] Rivera-Muñoz, E.M., (2011). Hydroxyapatite-based materials: synthesis and characterization: INTECH Open Access Publisher.

[75] Lee, E.-J. Kim, H.-W. and Knowles, J.C., (2015). Chapter 12 - Ceramic Biomaterials as Tissue Scaffolds, A.V.S.S. Ramalingam, ed. Stem Cell Biology and Tissue Engineering in Dental Sciences. Boston: Academic Press, 163-174.

[76] Jalota, S. Tas, A.C. and Bhaduri, S.B., (2004). "Microwave-assisted synthesis of calcium phosphate nanowhiskers", Journal of Materials Research, 19: 1876-1881.

[77] Nayak, A.K., (2010). "Hydroxyapatite synthesis methodologies: an overview", International Journal of ChemTech Research, 2: 903-907.

[78] Chetty, A. Wepener, I. Marei, M.K. Kamary, Y. and Moussa, R.M., (2012). Chapter 2 - Synthesis, properties, and applications of hydroxyapatite, Hydroxyapatite:Synthesis, properties, and applications. Nova Science Publishers, 91-132.

[79] Kim, S.-S. Park, M.S. Jeon, O. Choi, C.Y. and Kim, B.-S., (2006). "Poly (lactide-co-glycolide)/hydroxyapatite composite scaffolds for bone tissue engineering", Biomaterials, 27: 1399-1409.

[80] Deng, X. Hao, J. and Wang, C., (2001). "Preparation and mechanical properties of nanocomposites of poly (D, L-lactide) with Ca-deficient hydroxyapatite nanocrystals", Biomaterials, 22: 2867-2873.

[81] Eriksson, M. Andersson, M. Adolfsson, E. and Carlström, E., (2006). "Titanium–hydroxyapatite composite biomaterial for dental implants", Powder Metallurgy, 49: 70-77.

[82] Wang, X. Chen, Y. Xu, L. Xiao, S. Kong, F. and Do Woo, K., (2011). "Ti–Nb–Sn–hydroxyapatite composites synthesized by mechanical alloying and high frequency induction heated sintering", Journal of the Mechanical Behavior of Biomedical Materials, 4: 2074-2080.

[83] Pei, X. Wang, J. Wan, Q. Kang, L. Xiao, M. and Bao, H., (2011). "Functionally graded carbon nanotubes/hydroxyapatite composite coating by laser cladding", Surface and Coatings Technology, 205: 4380-4387.

[84] Li, H. Zhao, N. Liu, Y. Liang, C. Shi, C. Du, X. and Li, J., (2008). "Fabrication and properties of carbon nanotubes reinforced Fe/hydroxyapatite composites by in situ chemical vapor deposition", Composites Part A: Applied Science and Manufacturing, 39: 1128-1132.

[85] Sopyan, I. Mel, M. Ramesh, S. and Khalid, K., (2007). "Porous hydroxyapatite for artificial bone applications", Science and Technology of Advanced Materials, 8: 116-123.

[86] Koutsopoulos, S., (2002). "Synthesis and characterization of hydroxyapatite crystals: a review study on the analytical methods", Journal Of Biomedical Materials Research, 62: 600-612.

[87] Liu, D.-M. Troczynski, T. and Tseng, W.J., (2001). "Water-based sol–gel synthesis of hydroxyapatite: process development", Biomaterials, 22: 1721-1730.

[88] Agrawal, K. Singh, G. Puri, D. and Prakash, S., (2011). "Synthesis and characterization of hydroxyapatite powder by sol-gel method for biomedical application", Journal of Minerals & Materials Characterization & Engineering, 10: 727-734.

[89] Byrappa, K. and Adschiri, T., (2007). "Hydrothermal technology for nanotechnology", Progress in Crystal Growth and Characterization of Materials, 53: 117-166.

[90] Jin, X. Zhuang, J. Zhang, Z. Guo, H. and Tan, J., (2015). "Hydrothermal synthesis of hydroxyapatite nanorods in the presence of sodium citrate and its aqueous colloidal stability evaluation in neutral pH", Journal Of Colloid And Interface Science, 443: 125-130.

[91] Xia, W. Lindahl, C. Engqvist, H. and Lausmaa, J., (2011). Biomimetic hydroxyapatite deposition on titanium oxide surfaces for biomedical application: INTECH Open Access Publisher.

[92] Best, S. Porter, A. Thian, E. and Huang, J., (2008). "Bioceramics: past, present and for the future", Journal of the European Ceramic Society, 28: 1319-1327.

[93] Tripathi, G. and Basu, B., (2012). "A porous hydroxyapatite scaffold for bone tissue engineering: Physico-mechanical and biological evaluations", Ceramics International, 38: 341-349.

[94] Hutmacher, D.W., (2000). "Scaffolds in tissue engineering bone and cartilage", Biomaterials, 21: 2529-2543.

[95] Bose, S. Tarafder, S. and Bandyopadhyay, A., (2015). "7 Hydroxyapatite coatings for metallic implants", Hydroxyapatite (HAp) for Biomedical Applications: 143.

[96] Dorozhkin, S.V., (2012). "Nanodimensional and nanocrystalline calcium orthophosphates", American Journal of Biomedical Engineering, 2: 48-97.

[97] Mucalo, M., (2015). Hydroxyapatite (HAp) for Biomedical Applications: Elsevier.

[98] Mohammad, N.F. Othman, R. and Yee-Yeoh, F., (2014). "Nanoporous Hydroxyapatite Preparation Methods for Drug Delivery Applications", Rev. Adv. Mater. Sci, 38: 138-147.

[99] Ren, P.-G. Yan, D.-X. Ji, X. Chen, T. and Li, Z.-M., (2011). "Temperature dependence of graphene oxide reduced by hydrazine hydrate", Nanotechnology, 22: 055705.

[100] Wang, G. Yang, J. Park, J. Gou, X. Wang, B. Liu, H. and Yao, J., (2008). "Facile synthesis and characterization of graphene nanosheets", The Journal of Physical Chemistry C, 112: 8192-8195.

[101] Fan, Z. Wang, K. Wei, T. Yan, J. Song, L. and Shao, B., (2010). "An environmentally friendly and efficient route for the reduction of graphene oxide by aluminum powder", Carbon, 48: 1686-1689.

[102] Zhou, T. Chen, F. Liu, K. Deng, H. Zhang, Q. Feng, J. and Fu, Q., (2011). "A simple and efficient method to prepare graphene by reduction of graphite oxide with sodium hydrosulfite", Nanotechnology, 22: 045704.

[103] Kauppila, J. Lund, L. Laiho, T. Salomäki, M. Kankare, J. and Lukkari, J., (2014). "Effective low temperature reduction of graphene oxide with vanadium (III)", Journal of Materials Chemistry C, 2: 3602-3609.

[104] Chua, C.K. Ambrosi, A. and Pumera, M., (2012). "Graphene oxide reduction by standard industrial reducing agent: thiourea dioxide", Journal of Materials Chemistry, 22: 11054-11061.

[105] Yang, S. Yue, W. Huang, D. Chen, C. Lin, H. and Yang, X., (2012). "A facile green strategy for rapid reduction of graphene oxide by metallic zinc", RSC Advances, 2: 8827-8832.

[106] Ma, H.-L. Zhang, Y. Hu, Q.-H. Yan, D. Yu, Z.-Z. and Zhai, M., (2012). "Chemical reduction and removal of Cr (VI) from acidic aqueous solution by ethylenediamine-reduced graphene oxide", Journal of Materials Chemistry, 22: 5914-5916.

[107] Suresh, D. Udayabhanu Nagabhushana, H. and Sharma, S.C., (2015). "Clove extract mediated facile green reduction of graphene oxide, its dye elimination and antioxidant properties", Materials Letters, 142: 4-6.

[108] Suresh, D. Kumar, M.P. Nagabhushana, H. and Sharma, S., (2015). "Cinnamon supported facile green reduction of graphene oxide, its dye elimination and antioxidant activities", Materials Letters, 151: 93-95.

[109] Gurunathan, S. Han, J.W. Park, J.H. Eppakayala, V. and Kim, J.-H., (2014). "Ginkgo biloba: a natural reducing agent for the synthesis of cytocompatible graphene", International Journal of Nanomedicine, 9: 363.

[110] Jana, M. Saha, S. Khanra, P. Murmu, N.C. Srivastava, S.K. Kuila, T. and Lee, J.H., (2014). "Bio-reduction of graphene oxide using drained water from soaked mung beans (Phaseolus aureus L.) and its application as energy storage electrode material", Materials Science and Engineering: B, 186: 33-40.

[111] Barua, S. Thakur, S. Aidew, L. Buragohain, A.K. Chattopadhyay, P. and Karak, N., (2014). "One step preparation of a biocompatible, antimicrobial reduced graphene oxide–silver nanohybrid as a topical antimicrobial agent", RSC Advances, 4: 9777-9783.

[112] Firdhouse, M.J. and Lalitha, P., (2013). "Eco-friendly synthesis of graphene using aqueous extract of Amaranthus dubius", Carbon–Science and Technology, 5: 253-259.

[113] Haghighi, B. and Tabrizi, M.A., (2013). "Green-synthesis of reduced graphene oxide nanosheets using rose water and a survey on their characteristics and applications", RSC Advances, 3: 13365-13371.

[114] Lee, G. and Kim, B.S., (2014). "Biological reduction of graphene oxide using plant leaf extracts", Biotechnology Progress, 30: 463-469.

[115] Kuila, T. Bose, S. Khanra, P. Mishra, A.K. Kim, N.H. and Lee, J.H., (2012). "A green approach for the reduction of graphene oxide by wild carrot root", Carbon, 50: 914-921.

[116] Thakur, S. and Karak, N., (2012). "Green reduction of graphene oxide by aqueous phytoextracts", Carbon, 50: 5331-5339.

[117] Wang, Y. Shi, Z. and Yin, J., (2011). "Facile synthesis of soluble graphene via a green reduction of graphene oxide in tea solution and its biocomposites", ACS applied materials & interfaces, 3: 1127-1133.

[118] Wei, G. and Ma, P.X., (2004). "Structure and properties of nano-hydroxyapatite/polymer composite scaffolds for bone tissue engineering", Biomaterials, 25: 4749-4757.

[119] Wang, H. Li, Y. Zuo, Y. Li, J. Ma, S. and Cheng, L., (2007). "Biocompatibility and osteogenesis of biomimetic nano-hydroxyapatite/polyamide composite scaffolds for bone tissue engineering", Biomaterials, 28: 3338-3348.

[120] Kim, H.-W. Knowles, J.C. and Kim, H.-E., (2004). "Hydroxyapatite/poly (ε-caprolactone) composite coatings on hydroxyapatite porous bone scaffold for drug delivery", Biomaterials, 25: 1279-1287.

[121] Zheng, X. Huang, M. and Ding, C., (2000). "Bond strength of plasma-sprayed hydroxyapatite/Ti composite coatings", Biomaterials, 21: 841-849.

[122] Witte, F. Feyerabend, F. Maier, P. Fischer, J. Störmer, M. Blawert, C. Dietzel, W. and Hort, N., (2007). "Biodegradable magnesium–hydroxyapatite metal matrix composites", Biomaterials, 28: 2163-2174.

[123] Li, J. Fartash, B. and Hermansson, L., (1995). "Hydroxyapatite—alumina composites and bone-bonding", Biomaterials, 16: 417-422.

[124] Shen, Z. Adolfsson, E. Nygren, M. Gao, L. Kawaoka, H. and Niihara, K., (2001). "Dense hydroxyapatite–zirconia ceramic composites with high strength for biological applications", Advanced Materials, 13: 214-216.

[125] Azhari, A. Toyserkani, E. and Villain, C., (2015). "Additive Manufacturing of Graphene–Hydroxyapatite Nanocomposite Structures", International Journal of Applied Ceramic Technology, 12: 8-17.

[126] Baradaran, S. Moghaddam, E. Basirun, W. Mehrali, M. Sookhakian, M. Hamdi, M. Moghaddam, M.N. and Alias, Y., (2014). "Mechanical properties and biomedical applications of a nanotube hydroxyapatite-reduced graphene oxide composite", Carbon, 69: 32-45.

[127] Fan, Z. Wang, J. Wang, Z. Ran, H. Li, Y. Niu, L. Gong, P. Liu, B. and Yang, S., (2014). "One-pot synthesis of graphene/hydroxyapatite nanorod composite for tissue engineering", Carbon, 66: 407-416.

[128] Li, M. Liu, Q. Jia, Z. Xu, X. Cheng, Y. Zheng, Y. Xi, T. and Wei, S., (2014). "Graphene oxide/hydroxyapatite composite coatings fabricated by electrophoretic nanotechnology for biological applications", Carbon, 67: 185-197.

[129] Li, Y. Liu, C. Zhai, H. Zhu, G. Pan, H. Xu, X. and Tang, R., (2014). "Biomimetic graphene oxide–hydroxyapatite composites via in situ mineralization and hierarchical assembly", RSC Advances, 4: 25398-25403.

[130] Núñez, J.D. Benito, A.M. González, R. Aragón, J. Arenal, R. and Maser, W.K., (2014). "Integration and bioactivity of hydroxyapatite grown on carbon nanotubes and graphene oxide", Carbon, 79: 590-604.

[131] Oyefusi, A. Olanipekun, O. Neelgund, G.M. Peterson, D. Stone, J.M. Williams, E. Carson, L. Regisford, G. and Oki, A., (2014). "Hydroxyapatite grafted carbon nanotubes and graphene nanosheets: Promising bone implant materials", Spectrochimica Acta Part A: Molecular and Biomolecular Spectroscopy, 132: 410-416.

[132] Liu, Y. Huang, J. and Li, H., (2013). "Synthesis of hydroxyapatite–reduced graphite oxide nanocomposites for biomedical applications: oriented nucleation and epitaxial growth of hydroxyapatite", Journal of Materials Chemistry B, 1:1826.

[133] Liu, Y. Dang, Z. Wang, Y. Huang, J. and Li, H., (2014). "Hydroxyapatite/graphene-nanosheet composite coatings deposited by vacuum cold spraying for biomedical applications: Inherited nanostructures and enhanced properties", Carbon, 67: 250-259.

[134] Neelgund, G.M. Oki, A. and Luo, Z., (2013). "In situ deposition of hydroxyapatite on graphene nanosheets", Materials Research Bulletin, 48: 175-179.

[135] Zanin, H. Saito, E. Marciano, F.R. Ceragioli, H.J. Granato, A.E.C. Porcionatto, M. and Lobo, A.O., (2013). "Fast preparation of nano-hydroxyapatite/superhydrophilic reduced graphene oxide composites for bioactive applications", Journal of Materials Chemistry B, 1: 4947-4955.

[136] Gonçalves, G. Cruz, S.M. Ramalho, A. Grácio, J. and Marques, P.A., (2012). "Graphene oxide versus functionalized carbon nanotubes as a reinforcing agent in a PMMA/HA bone cement", Nanoscale, 4: 2937-2945.

[137] Saeri, M. Afshar, A. Ghorbani, M. Ehsani, N. and Sorrell, C., (2003). "The wet precipitation process of hydroxyapatite", Materials Letters, 57: 4064-4069.

[138] Afshar, A. Ghorbani, M. Ehsani, N. Saeri, M. and Sorrell, C., (2003). "Some important factors in the wet precipitation process of hydroxyapatite", Materials & Design, 24: 197-202.

[139] Monmaturapoj, N. and Yatongchai, C., (2010). "Effect of sintering on microstructure and properties of hydroxyapatite produced by different synthesizing methods", Journal of Metals, Materials and Minerals, 20: 53-61.

[140] Batra, U. and Kapoor, S., (2010). "Microstructural and In-Vitro Characterization of Glass-Reinforced Hydroxyapatite Composites", International Journal of Chemical and Biological Engineering 3:45-50.

[141] Mukherjee, S. Kundu, B. Chanda, A. and Sen, S., (2015). "Effect of functionalisation of CNT in the preparation of HAp–CNT biocomposites", Ceramics International, 41: 3766-3774.

[142] Mason, T.J., (1996). Advances in sonochemistry: Elsevier.

CURRICULUM VITAE

PERSONAL INFORMATION

Name Surname : Elif ÖZTÜRK

Date of birth and place : 26/08/1989 - Istanbul

Foreign Languages : English

E-mail : ozturkeliff@gmail.com

EDUCATION

Degree	**Department**	**University**	**Date of Graduation**
Undergraduate	Chemical Engineering	Yıldız Technical University	2007 - 2012
High School		Ahmet Buhan High School	2003 - 2007

WORK EXPERIENCE

Year	Corporation/Institute	Enrollment
2014 -	Yıldız Technical University, Central Science and Technology Application and Research Center	Research Assistant
2013-2014	Gebze Technical University, Chemical Engineering Department	Research Assistant

PUBLISHMENTS

Conference Papers

1.	Öztürk, E., Özbek, B. and Zaman, A.C., (2015), "Production of green reduced graphene oxide–hydroxyapatite composites", *10th European Congress of Chemical Engineering (ECCE10),* Acropolis Convention Center, Nice, France, 27th September-1st October, Submission-1684.
2.	Öztürk, E., Şimşek, S. and Özbek, B., (2015), "Bio-reduction of graphene oxide by natural products", *International Nanotechnology Conference (NANOTECH FRANCE 2015),* 15-17 June 2015, Pole Universitaire Leonard de Vinci, La Defense, Paris, France, pp. 18.

Projects

1.	Özbek, B. and Öztürk, E., (2015), "Reduction of graphene oxide by natural products and production of reduced graphene oxide-hydroxyapatite composites", Yıldız Technical University Scientific Research Projects Coordination Department, Project No: 2015-07-01-YL01.